NASA LEWIS SEMI–ANNUAL STATUS REPORT

NAG 3-67 (12/1/80 – 5/30/81)

PREDICTION OF SOUND RADIATION FROM DIFFERENT PRACTICAL JET ENGINE INLETS

By

Ben T. Zinn

William L. Meyer

GEORGIA INSTITUTE OF TECHNOLOGY

A UNIT OF THE UNIVERSITY SYSTEM OF GEORGIA

SCHOOL OF AEROSPACE ENGINEERING

ATLANTA, GEORGIA 30332

1981

NASA LEWIS SEMI-ANNUAL STATUS REPORT

NAG 3-67 (12/1/80 - 5/30/81)

PREDICTION OF SOUND RADIATION FROM DIFFERENT PRACTICAL JET ENGINE INLETS

BY

Ben T. Zinn

and

William L. Meyer

SCHOOL OF AEROSPACE ENGINEERING

GEORGIA INSTITUTE OF TECHNOLOGY

ATLANTA, GA. 30332

ABSTRACT

This report summarizes the work performed during the second six month period of the NASA Lewis sponsored research program (Contract Number NAG 3-67) entitled "Prediction of Sound Radiation from Different Practical Jet Engine Inlets". During the initial six month period of the contract the computer codes necessary for this study were developed and checked against exact solutions using the NASA Lewis QCSEE inlet geometry. This research is summarized in the Semi-Annual Status Report (6/2/80 - 11/30/80).

During the past six months the developed computer codes were used to predict the acoustic characteristics of the following five inlet configurations: the NASA Langley Bellmouth, the NASA Lewis JT15D-1 Ground Test Nacelle and three hyperbolic inlets of 50, 70 and 90 degrees. Various calculations have been done on each so that comparisons with the results of other experimental and theoretical studies could be made. In this report both reflection coefficients and radiation patterns calculated by the integral solution procedure developed here at Georgia Tech are compared with the results of other experimental and theoretical studies.

TABLE OF CONTENTS

INTRODUCTION

This research program consists of two major tasks. The first task was the upgrading, development and testing of computer codes for the calculations of the radiation patterns associated with various axisymmetric inlet configurations. The idea was to develop computer codes capable of producing accurate results for non-dimensional wave numbers (based on duct radius) of up to 20. The initial computer development work was done on the NASA Lewis QCSEE inlet of Ref. 1. The results of this work are presented in the NASA Lewis Semi-Annual Status Report (6/2/80 - 11/30/80) for Grant Number NAG 3-67.

The second task was to use the computer codes developed during the first six months of the contract to generate results for various other inlet configurations. These results were to be compared with those of theoretical and experimental studies performed elsewhere for the same inlet configurations. The inlet configurations used in the second part of this study were: the NASA Langley Bellmouth[2,3]; the NASA Lewis JT15D-1[4,5] and three of the hyperbolic inlets of the Y.C. Cho[6,7] study of 50, 70 and 90 degrees. Although the main objective of this study was to compare the radiation patterns generated by the integral technique[8-10] with those calculated and measured in other experimental and theoretical studies the reflection coefficients were also calculated and compared for certain specific inlet configurations where other results were available. These comparisons were not expected to yield particularly good agreement as it has been shown by the authors that reflection coefficients (or admittances)

calculated by different methods do not necessarily yield the same values[11] even for the same geometries.

In addition to the above work, the authors have also published a paper[12] during the reporting period. This paper provides comparisons between experimentally measured and theoretically calculated results for the NASA Lewis QCSEE inlet (employed during the first six month reporting period for this contract). The paper shows that very good agreement was obtained between measured and calculated acoustic radiation patterns. This particular study was conducted under AFOSR support and additional results are presented in the final technical report for that agency[13].

THE LANGLEY BELLMOUTH

The geometry for the Langley Bellmouth was obtained directly from R. J. Silcox as the cone angle of 57 degrees given in Ref. 2 is incorrect. The actual cone angle is closer to 56 degrees. Computer runs done for this inlet configuration utilized 102 points on the surface of the body where the acoustic quantities of interest, the acoustic potential and normal acoustic velocity, were calculated. The geometrical input data for this inlet is plotted in Fig.1 where the arrows represent the normals to the body at the various points on the body. The open circles are the points where the acoustic quantities are calculated and the locations denoted by small crosses are those used in the integration procedure. Since the theory requires a closed body, the outer wall of the inlet was approximated by part of a smaller ellipse centered at the same point as the larger inner lip ellipse. Also, the body was terminated by an ellipse.

The choice of these curves is relatively arbitrary as it has been shown by the authors in previous studies that the specific termination given to a body to "close it off" does not significantly affect the acoustic radiation in the forward half plane.

Next, the boundary conditions utilized in this study need to be considered. In all of the investigated cases, the acoustic potential was specified along the driver surface and a zero normal acoustic velocity was specified (i.e., the body is assumed to have acoustically hard walls) along the remaining surfaces. Also, when the acoustic reflection coefficient is calculated it is done at the driver surface (e.g. on the body). The complex

reflection coefficient used in this study is defined as

$$R = \frac{ik\varphi - \frac{\partial\varphi}{\partial n}}{ik\varphi + \frac{\partial\varphi}{\partial n}} \qquad (1)$$

where k is the wave number, φ is the acoustic potential and $\frac{\partial\varphi}{\partial n}$ is the outward normal acoustic velocity.

A list of the computer runs done for this geometry is included in Table I. The right hand column refers to the number of points used in the Gauss-Legendre integration in the tangential direction. A two point integration is always used along the body. For each case run, a standard plot is produced by the computer program of the Sound Pressure Level in decibels (i.e., SPL in dB) at a distance of 20.36a from the exit plane of the inlet where a is the radius at the driver plane. This distance was chosen so that direct comparisons could be made with the results presented in Ref. 3. These plots, for the Langley Bellmouth, are presented in Figs. 2-14. The SPL was calculated at 2 degree intervals from 0 degrees (i.e., the centerline of the inlet) to 90 degrees. In the small table in each figure any dB level that was calculated to be less than -99 dB is printed as a zero.

For the Langley Bellmouth there are 25 points on the driver plane. Since there is no straight duct section connected to the inlet in the theoretical model (See Fig. 1.) the driver plane is where the reflection coefficient is calculated. The boundary condition on the driver plane is specified as the acoustic potential for the transverse mode of interest, and the normal acoustic velocity at this plane is determined by the solution. The reflection coefficient is then calculated using Eqn. 1.

Direct comparisons with the data presented in Ref. 3 for the reflection coefficient is difficult as one value of the reflection coefficient is presented for each tangential mode at each non-dimensional wave number, ka, whereas the integral solution procedure yields a value at each point across the duct. In Figs. 15 and 16 the non-dimensional wave number is held constant and the tangential mode number is varied. When compared to the results presented in Ref. 3 (Fig. 16.) it is noted that the reflection coefficients calculated in the present study have modulii that are uniformly high. This is consistently found to be the case for this inlet. The Cho theory (See Ref. 7.) also predicts the reflection coefficients modulii to be consistently higher than the measured data with the present results being even higher. It should be noted, however, that the present results do predict the correct trend in that as the tangential mode number is increased the modulus of the reflection coefficient increases and the phase angle of the reflection coefficient decreases. It also needs to be pointed out that values close to the centerline of the duct are probably in error for tangential modes greater than zero due to the relatively small values of the acoustic potential there, and values close to the wall probably contain errors due to the proximity of the sharp corners (a common fault with most potential type solution procedures -- leakage at sharp corners).

In Figs. 17 and 18 results are presented for the modulus and phase respectively for a tangential mode number of 4 and a non-dimensional wave number of 5.81. Simularly, in Figs. 19 and 20 results are presented for M = (6,0) and ka = 11.14. Again, the calculated values are higher than either the Cho or experimentally derived values.

In Figs. 21 and 22 the modulus and phase of the reflection coefficient are plotted holding the tangential mode number constant, M = (1,0), and varying the non-dimensional wave number. Although the results of this analysis are high, the values show the correct trends as for increasing non-dimensional wave number the modulus of the reflection coefficient decreases while the phase increases. Similarly, in Figs. 23 and 24, where the tangential mode is M = (2,0), the same trends are observed.

One of the characteristics of the integral solution procedure is that results obtained in the field surrounding a given body are generally better than those obtained on the body itself. This is thought to be due to the fact that an acoustic quantity calculated at a point on the body is actually an average value of the quantity over the integration area associated with that point. Therefore, direct point comparisons, especially where the acoustic quantity of interest varies significantly over the integration area (e.g., near the centerline of the duct for tangential mode numbers greater than zero), usually do not yield extremely good agreement. However, when calculating acoustic quantities in the field surrounding the body at a specific point a simple summation or integral of the acoustic quantities on the surface of the body is performed. In this case better point results are obtained in the field if average, not point, values are known on the body which turns out to be the case. Thus, it is expected that better agreement will be found with the experimental results presented in Ref. 3 for the quantities measured in the field surrounding the body. Also, good agreement between experiment and theory has already been shown in the study of the NASA Lewis QCSEE inlet performed for AFOSR and presented in Ref. 12.

In Fig. 25 the relative SPL in the field on a circle centered at the exit plane of the Langley Bellmouth at a radius of 20.36a is presented for M = (0,0) and ka = 1.39. The points calculated were at 2 degree increments from the centerline to 90°. This plot should be compared with Fig. 17 of Ref. 3. Due to the wavyness of this experimentally derived data it is subject to some interpretation and therefore a range of values shall be presented here when discussing it. If the data is arbitrarily smoothed in Fig. 17 of Ref. 3 it is found that there is approximately a 10-15 dB drop between 0 and 90° whereas the present analysis (See Fig. 25.) yields a 12 dB drop. Figures 26-28 should also be compared with Fig. 17 of Ref. 3. For M = (0,0) and ka = 3.76 it is estimated from the experimental data that there is a 25-30 dB drop from 0 to 90° and it is found that the present analysis yields a 27 dB drop. (It will be noted again here that Figs. 2-14 have small SPL (dB) tables associated with them so that these relative SPL (dB) values may be easily calculated.) Also, the curve flattens towards the horizonital at 90° in Fig. 26 as it does in Fig. 17 of Ref. 3. In Fig. 27 the mode number is M = (1,0) and the non-dimensional wave number is ka = 2.66. It is found that the maximum SPL (dB) for this case occurs at 32° from the centerline and that there is a 12 dB drop from this peak to 90°. From the experimental data it is estimated that the peak lies between 25 and 35° and that there is a 10-15 dB drop from there to 90°. Finally from Fig. 17 of Ref. 3 for M = (1,0) and ka = 5.29 it is estimated that the radiation peak is between 15 and 25° and that there is a 20-25 dB drop from the peak to 90°. In Fig. 28 for the same case it is found that the peak is at 22° and that there is a 22 dB drop from there to 90°.

As can be seen the experimental data of Ref. 3 and the theoretically calculated data of this study compare very well in the field surrounding the body even though there was rather poor comparison between the reflection coefficients. Since the integral technique does not require the calculation of reflection coefficients to generate results in the field this is not considered a significant short-coming of the method.

Figures 29 and 30 are presented for comparison with Fig. 24 of Ref. 3. Experimentally the first peak for the case where M = (2,0) and ka = 3.37 lies very close to 40° and the dB drop for the case is found to be about 10 dB. Theoretically the peak is found to be at 42° and the dB drop from there to 90° is found to be 9 dB. Simularly, the experimental radiation peak for M = (2,0) and ka = 4.40 is found to be between 30 and 40° from the centerline of the duct and from there to 90° the dB drop is measured to be between 10 and 15 dB. In the present study these are found to be 36° and 13 dB respectively; again showing excellent correlation with the experimental results of Ref. 3.

For the higher mode number of M = (4,0) only one plot of the radiation pattern in the field surrounding the Langley Bellmouth is given. This is found in Fig. 24 of Ref. 3 for ka = 5.81. From this experimental data plot it is estimated that the first radiation peak occurs between 40 and 50° from the centerline of the duct and that there is a 10-15 dB drop from this point to 90°. Theoretically, (See Fig. 31.) these are calculated to be 46° and 11 dB respectively.

Figures 32 and 33 are presented for comparison with Fig. 20 of Ref. 3. A summary of the radiation results presented thus far are presented in

Table II. Also, for comparison with the "concept of angular location of predominant acoustic radition" set forth in Ref. 3 the angular location of the 6 dB down points are tabulated for all the cases run in Table III. This table should be compared with Fig. 19 of Ref. 3.

The relative phase of the radiation in the field is plotted for three cases in Figs. 34-36. The term relative phase is used here as the phase was referred to the phase at the maximum SPL (dB) point for the amplitude in the field. This occured at zero degrees in the first plot (See Fig. 34.) as it is for the plane wave, M = (0,0) mode. This figure may be compared with Fig. 21 of Ref. 3. Doing this it is found that the phase variation between the centerline of the duct and 90^{o} is about 90^{o} for the experimental results of Ref. 3 whereas the calculated phase variation is much less. In Fig. 35 the phase is referred to that at 38^{o} degrees from the centerline. If this plot is compared to the experimental data presented in Fig. 25 of Ref. 3 it is again found that the theory predicts much less variation in the phase. Similarly, if Fig. 36 is compared to Fig. 21 of Ref. 3 the theory again predicts less variation than is found experimentally. The phase in Fig. 36 is referenced to that at 32^{o}.

THE LEWIS JT15D-1 GROUND TEST NACELLE

The geometry for the Lewis JT15D-1 was obtained directly from the blue-prints used in its manufacture. The driver plane for the theoretical studies was placed at the junction of the curved inlet section and the straight duct as was done with the Langley Bellmouth. For the computer runs 175 points were used on the body and for the tangential integration a 96 point Gauss-Legendre integration scheme was used in all cases due to the relatively high tangential mode number M = (13,0) that was investigated. The geometrical input data for the computer runs is presented in Fig. 37. The inlet lip geometry consists of 3 circular arcs and is terminated smoothly with an ellipse as with the Langley Bellmouth.

The two non-dimensional wave numbers of interest are ka = 15.51 and ka = 19.42 and results for the SPL in dB radiated into the field are presented in Figs. 38 and 39, respectively. As with the Langley Bellmouth these results are calculated on a circular arc at 2^{o} increments from the centerline to 90^{o} which has a radius of 20.36a and is centered at the inlet lip exit plane. Again, any SPL dB level less than -99 is represented in the small tables in Figs. 38 and 39 as zero. Also, the values are truncated, not rounded, in the tables (e.g., In Fig. 38 at 14^{o} from the centerline the value is 20.9 and thus the visible offset in the plot.).

In Figs. 40-43 the modulus and phase of the reflection coefficient at the driver plane of the duct is presented for both cases run. As can be seen from the input geometry in Fig. 37, there are 50 points on the driver plane where these are calculated. As before, the first few points near the

centerline of the duct must be neglected due to the extremely low dB levels there and very close to the wall (i.e., the sharp corner) they must be neglected also.

In Figs. 44-47 the relative SPL in dB in the field and the relative phase (referred to the maximum SPL point) are presented for the two cases of interest. The SPL peaks show the proper trend as the higher wave number case yields the peak radiation closer to the centerline (See Fig. 19 of Ref. 5.).

THE 50 DEGREE HYPERBOLOIDAL INLET

The geometry used for the following computations is presented in Fig. 48. Since the integral equation technique used in the present study requires a closed, finite body the hyperbolic inner lip of the body had to be terminated at some finite distance. Since the results of the computations will be compared with those of the Y. C. Cho theory[7] this is a very important approximation as the Cho theory considers an infinite hyperbolic horn. The hyperbolic inner lip was terminated with a semi-circle; the outer lip is the same hyperbola as that of the inner lip except that it is shifted, and, the body is again terminated with an ellipse.

A summary of the computer runs done for this geometry is presented in Table IV. Since all the runs for this geometry are for M = (0,0) and all of the non-dimensional wave numbers are relatively small (i.e., less than 5) 32 points were used for the tangential integration in all cases.

For all of the cases run for this geometry the SPL in dB radiation patterns are presented in Figs. 49-54. For these calculations the circle on which the patterns are calculated in the field is centered at the driver plane of the inlet and not at the exit plane as previously done. Also, the radius of the circle is 20a (where a is the radius of the duct at the driver plane) and as before the field quantities are calculated every 2 degrees.

In Fig. 55 the modulus of the reflection coefficient is plotted for all of the cases run for this geometry. Note that a single value of the reflection coefficient is not obtained but rather a series of values across the duct exit plane (i.e., the driver plane for the present study). Since the non-dimensional wave numbers are so low, essentially constant distributions are obtained.

Furthermore, when Fig. 55 is compared with Fig. 4 of Ref. 7 very good agreement is found.

In Fig. 56 the phase of the reflection coefficient is presented for all of the investigated cases. As can be seen, the distributions of the phase of the reflection coefficient do not lend themselves to average values as readily as the modulus did, except for very low values of the non-dimensional wave number (e.g. $ka < 1.0$). For these values good agreement is found between the Cho theory of Ref. 7 (See Fig. 4.) and the present study. For the higher wave number cases no reasonable comparison is possible.

In Fig. 57 the relative SPL in dB in the field, at 20a from the driver plane (exit plane) of the duct is presented. Although direct comparisons cannot , by virtue of its formulation, yield values outside 50^{o} from the duct axis. In Fig. 58 the relative phase of the radiated field is presented for completeness.

THE 70 DEGREE HYPERBOLOIDAL INLET

The geometry used for calculations in this study for the 70^{o} hyperboloidal inlet is presented in Fig. 59. Its makeup is similar to that of the 50^{o} hyperboloidal inlet of the previous section (See Fig. 48.). This inlet is also an approximation of one of the inlets that Y. C. Cho presented in Ref. 7. Three specific cases were run for this configuration; specifically, M = (8,0) and ka = 9.7, 12.0 and 16.0. For all three of these cases a 64 point Gauss-Legendre integration formula was employed for the integration in the tangential direction. The standard computer plots of the SPL in dB in the field on a quarter circle centered at the driver (exit) plane of the duct at a radius of 20a are presented in Figs. 60-62. As before, the quantities of interest in the field were calculated at 2 degree increments from the centerline to 90^{o}.

In Figs. 63 and 64 the modulus and phase of the reflection coefficient at the driver (exit) plane of the 70^{o} hyperboloidal inlet are presented. These figures should be compared with Fig. 5 of Ref. 7 for ka = 9.7 and ka = 12.0. In both cases the modulus of the reflection coefficient as calculated in this study seems to be high when compared to the Cho theory. Similarly, the phase is also high.

In Figs. 65 and 66 the relative SPL and phase in the field are presented. The SPL plot should be compared with Fig. 10 of Ref. 7. In the present study the radiation peaks occur earlier than in the Cho theory for ka = 9.7 and 12.0; however, the peak for ka = 16.0 is very close. The plot of relative phase (See Fig. 66.) is presented for completeness. When analyzing

these phase data, one should bear in mind that the sharp peaks are not actually there as the curves should continue smoothly from -180^{o} to $+180^{o}$ and vice versa near 90^{o} from the centerline of the duct.

THE PLANE BAFFLE

The approximation to the geometry of the plane baffle employed in the present study is presented in Fig. 67. In this figure the non-dimensional length a (the radius of the driver) is shown explicitly. The top edge of the plane baffle is a quarter circle and the body is terminated by an ellipse.

There were 14 separate cases run for this geometry and they are presented in Table V. The standard computer plots for the SPL in dB generated in the field for the first set of cases (i.e., those for which M = (0,0)) are given in Figs. 68-71.

In Figs. 72 and 73 the modulus and phase of the reflection coefficient for the plane baffle for all of the cases run where M = (0,0) are given. This should be compared with Fig. 4 of Ref. 7. The modulus plots compare very well with each other even though in the present study the reflection coefficient is strictly a function of position as the curves generated are almost constant across a large portion of the exit (driver) plane. The phase plots cannot be compared as easily, as in the present study it is found that the phase of the reflection coefficient changes drastically over the exit plane.

For the sake of completeness the relative SPL in dB and phase in degrees of the radiated field are presented for the cases where M = (0,0) in Figs. 74 and 75.

The standard computer plot for SPL in the field is presented in Fig. 76 for the case where M = (0,1) and ka = 3.0. If this is compared with Fig. 12 of Ref. 7 it is found that the present study does not predict the side lobe at 90^{o} to be greater than the principle lobe at 0^{o} (i.e., on the centerline of the

duct). It is felt that this is due in part to the fact that in the present study there is radiation in the backward half plane (i.e., from 90^{o} to 180^{o}) because the body is a finite plane baffle and not an infinite one as in the Cho study.

The modulus and phase of the reflection coefficient is given for this case in Figs. 77 and 78. Also, the modulus and phase of the radiated field at 20.0a from the center of the driver plane is given in Figs. 79 and 80 for this case.

In Figs. 81-85 the standard computer plots for the SPL in the field is presented for the cases where M = (8,0) for the plane baffle.

In Figs. 86 and 87 the modulus and phase of the reflection coefficient for the plane baffle for the cases where the M = (8,0) mode is input at the driver plane are presented. These plots should be compared with Fig. 5 of Ref. 7. Doing this it is found that although the results of the present study do not yield average values directly (i.e., the curves vary significantly across the exit plane) both the modulus and phase of the reflection coefficient do show the same trends.

The relative SPL in the field is presented in Fig. 88 for these cases. If these results are compared with Fig. 14 of Ref. 7 it can be seen that the radiation peaks occur very close to the same angular locations in the field. The relative phase in the field is presented in Fig. 89 for completeness. In viewing this plot, one should recall that the widly varying top to bottom curves actually represent rather smooth curves as they pass from -180^{o} to $+180^{o}$ and vice versa.

The standard computer plots of SPL in the field surrounding the plane baffle for all of the cases run for M = (8,1) are presented in Figs. 90-93. These plots, along with Figs. 82-85 should be compared with Fig. 15 fof Ref. 7. Doing this, it is found that the present study again does not predict the large side lobes that the Cho study does; however, as before, this is thought to be due to the differences in the geometries used for the calculations.

The modulus and phase of the reflection coefficient for the cases where M = (8,1) are presented in Figs. 94 and 95 respectively. Also, the relative SPL and phase in the field are presented for these cases in Figs. 96 and 97. These four plots are merely included for completeness.

CONCLUSIONS

Results of theoretical predictions, based upon the utilization of integral solution techniques, of the radiated sound patterns associated with different engine inlets are presented in this report. The predictions of the present study compare very well with experimental data describing the radiated sound field around the Langley Bellmouth. This observation is consistent with earlier comparisons performed by the authors of the present study for experimental and theoretical results obtained for the QCSEE inlet[12,13]. In contrast, the predicted admittance values (i.e., reflection coefficients) at the duct exit plane for this same inlet did not compare very well with corresponding experimental results. In this case, both sets of data showed the same trends but quantitative agreement was lacking. Such lack of agreement between theoretical admittance data calculated by different methods was also observed by the authors in an earlier study of admittances at a duct termination[11].

The results generated in the present study for comparison with the Cho[6-7] theory only showed a qualitative agreement in most cases. The authors feel that this is probably due to the different geometries used in the two studies more than any inherent errors in either of the solution approaches. In the Cho theory an infinite body is used while in the present study the acoustic characteristics of a finite, closed body is investigated. This is significant as the authors have also shown that seemingly small changes in the geometry of an acoustic radiator can result in large changes in its radiated sound field.[14]

The predictions of the method used in the present study have been shown to compare very favorably with exact solutions generated by the "point source method" for complicated geometries and have also been shown to compare very well with experimental data. The present approach also has the capability of predicting the acoustic properties of geometries which have acoustically soft or lined walls where these can be represented by an acoustic admittance on the body. Thus, the method used in the present study has been shown to be a powerful tool which can be used to predict the effect of changes in either the geometry or acoustic properties of the body on the radiated sound field without having to use the artifice of reflection coefficients at a duct exit plane which may or may not be of value depending upon how they are calulated.

REFERENCES

1) "Effect of Entry-Lip Design on Aerodynamics and Acoustics of High-Throat-Mach-Number Inlets for the Quiet, Clean, Short-Haul Experimental Engine," B. A. Miller, B. J. Dastoli and H. L. Wesoky, NASA TM X-3222, May 1975.

2) "Inlet Contour and Flow Effects on Radiation," J. M. Ville and R. J. Silcox, AIAA Paper Number 80-0966, June 1980.

3) "Experimental Investigation of the Radiation of Sound from an Unflanged Duct and a Bellmouth Including the Flow Effect," J. M. Ville and R. J. Silcox, NASA Technical Paper 1697, August 1980.

4) "Analysis of Radiation Patterns of Interaction Tones Generated by Inlet Rods in the JT15D Engine," M. F. Heidmann, A. V. Saule and J. G. McArdle, AIAA Paper Number 79-0581, March 1979.

5) "Analysis of Radiation Patterns of Interaction Tones Generated by Inlet Rods in the JT15D Engine," M. F. Heidmann, A. V. Saule and J. G. McArdle, NASA TM-79074, March 1979.

6) "Sound Radiation from Hyperboloidal Inlet Ducts," Y. C. Cho, AIAA Paper Number 79-0677, March 1979.

7) "Rigorous Solutions for Sound Radiation from Circular Ducts with Hyperbolic Horns or Infinite Plane Baffle," Y.C. Cho, Journal of Sound and Vibration, Vol 69, No. 3, pp. 405-425, 1980.

8) "Predicting the Acoustics of Arbitrarily Shaped Bodies Using an Integral Approach," W. A. Bell, W. L. Meyer and B. T. Zinn, AIAA Journal, Vol. 15, No. 6, pp. 813-820, June 1977.

9) "Boundary Integral Solutions of Three Dimensional Acoustic Radiation Problems," W. L. Meyer, W. A. Bell, M. P. Stallybrass and B. T. Zinn, Journal of Sound and Vibration, Vol. 59, No. 2, pp. 245-262, July 1978.

10) "Prediction of the Sound Field Radiated from Axisymmetric Surfaces," W. L. Meyer, W. A. Bell, M. P. Stallybrass and B. T. Zinn, Journal of the Acoustical Society of America, Vol. 63, No. 2, pp. 631-638, March 1979.

11) "Sound Radiation from Ducts: A Comparison of Admittance Values," W. L. Meyer, W. A. Bell and B. T. Zinn, TECHNICAL NOTE, AIAA Journal, Vol. 18, No. 12, pp. 1538-1540, December 1980.

12) "Acoustic Radiation from Axisymmetric Ducts: A Comparison of Theory and Experiment," W. L. Meyer, B. R. Daniel and B. T. Zinn, AIAA Journal, Vol. 18, No.3, pp. 317-323, March 1981.

13) "Noise Suppression in Jet Inlets," B. T. Zinn, W. L. Meyer and B. R. Daniel, AFOSR Final Technical Report, AFOSR-TR-80-0452, February 1980.

14) "Sound Radiation from Finite Length Axisymmetric Ducts and Engine Inlets," W. L. Meyer, W. A. Bell and B. T. Zinn, AIAA Paper Number 79-0675, presented at the AIAA 5th Aeroacoustics Conference, Seattle, Washington, March 12-14, 1979.

TABLE I

COMPUTER RUNS DONE FOR LANGLEY BELLMOUTH

MODE (TANGENTIAL, RADIAL)	NON-DIMENSIONAL WAVE NUMBER ka	NUMBER OF POINTS IN TANGENTIAL INTEGRATION
(0,0)	1.39	32
(0,0)	3.76	32
(1,0)	1.91	64
(1,0)	2.03	64
(1,0)	2.66	64
(1,0)	3.76	64
(1,0)	5.29	64
(2,0)	3.37	64
(2,0)	3.76	64
(2,0)	4.40	64
(2,0)	5.29	64
(4,0)	5.81	64
(6,0)	11.14	96

TABLE II

RADIATION RESULTS FOR THE LANGLEY BELLMOUTH

MODE NUMBER	WAVE NUMBER	POSITION OF PRINCIPLE RADIATION LOBE (Deg.)		dB DROP FROM PRINCIPLE LOBE TO 90 DEGREES	
			Present		Present
M	ka	Ref. 3	Study	Ref. 3	Study
(0,0)	1.39	0	0	10-15	12
(0,0)	3.76	0	0	25-30	27
(1,0)	1.91	35-45	38	5-10	7
(1,0)	2.66	25-35	32	10-15	12
(1,0)	3.76	20-30	26	12-17	15
(1,0)	5.29	15-25	22	20-25	22
(2,0)	3.37	35-45	42	8-13	9
(2,0)	3.76	30-40	38	8-13	10
(2,0)	4.40	30-40	36	10-15	13
(2,0)	5.29	25-35	32	13-18	16
(4,0)	5.81	40-50	46	10-15	11

TABLE III

THE CONCEPT OF ANGULAR LOCATION OF PREDOMINANT ACOUSTIC RADIATION FOR THE LANGLEY BELLMOUTH

MODE NUMBER M	WAVE NUMBER ka	f / f_{mn}	Ψ_{MIN} (-6dB) (Degrees)	Ψ_{MAX} (-6dB) (Degrees)
(0,0)	1.39	∞	---	55
(0,0)	3.76	∞	---	29
(1,0)	1.91	1.04	12	87
(1,0)	2.03	1.10	12	82
(1,0)	2.66	1.44	10	68
(1,0)	3.76	2.04	8	55
(1,0)	5.29	2.87	7	44
(2,0)	3.37	1.10	19	79
(2,0)	3.76	1.23	18	72
(2,0)	4.40	1.44	16	65
(2,0)	5.29	1.73	15	58
(4,0)	5.81	1.09	26	54
(6,0)	11.14	1.49	26	59

TABLE IV

COMPUTER RUNS DONE FOR THE 50 DEGREE HYPERBOLOIDAL INELT

MODE (TANGENTIAL, RADIAL)	NON-DIMENSIONAL WAVE NUMBER ka	NUMBER OF POINTS IN TANGENTIAL INTEGRATION
(0,0)	0.1	32
(0,0)	0.5	32
(0,0)	1.0	32
(0,0)	2.5	32
(0,0)	3.83	32
(0,0)	4.5	32

TABLE V

COMPUTER RUNS DONE FOR THE PLANE BAFFLE

MODE (TANGENTIAL, RADIAL)	NON-DIMENSIONAL WAVE NUMBER ka	NUMBER OF POINTS IN TANGENTIAL INTEGRATION
(0,0)	1.0	32
(0,0)	2.0	32
(0,0)	3.0	32
(0,0)	3.83	32
(0,1)	3.0	32
(8,0)	9.7	96
(8,0)	12.0	96
(8,0)	13.5	96
(8,0)	14.5	96
(8,0)	16.0	96
(8,1)	12.0	96
(8,1)	13.5	96
(8,1)	14.5	96
(8,1)	16.0	96

TABLE V

COMPUTER RUNS DONE FOR THE PLANE BAFFLE

MODE (TANGENTIAL, RADIAL)	NON-DIMENSIONAL WAVE NUMBER Ka	NUMBER OF [illegible] IN FREQUENCY INTERPOLATION
(0,0)	1.0	[illegible]
(0,0)	2.0	[illegible]
(0,0)	3.0	[illegible]
(0,0)	3.83	[illegible]
(0,1)	5.0	[illegible]
(3,0)	9.7	[illegible]
(3,0)	12.0	[illegible]
(3,0)	13.5	[illegible]
(3,0)	14.5	[illegible]
(3,0)	16.0	[illegible]
(3,1)	12.0	[illegible]
(3,1)	13.5	[illegible]
(3,1)	14.5	[illegible]
(3,1)	16.0	[illegible]

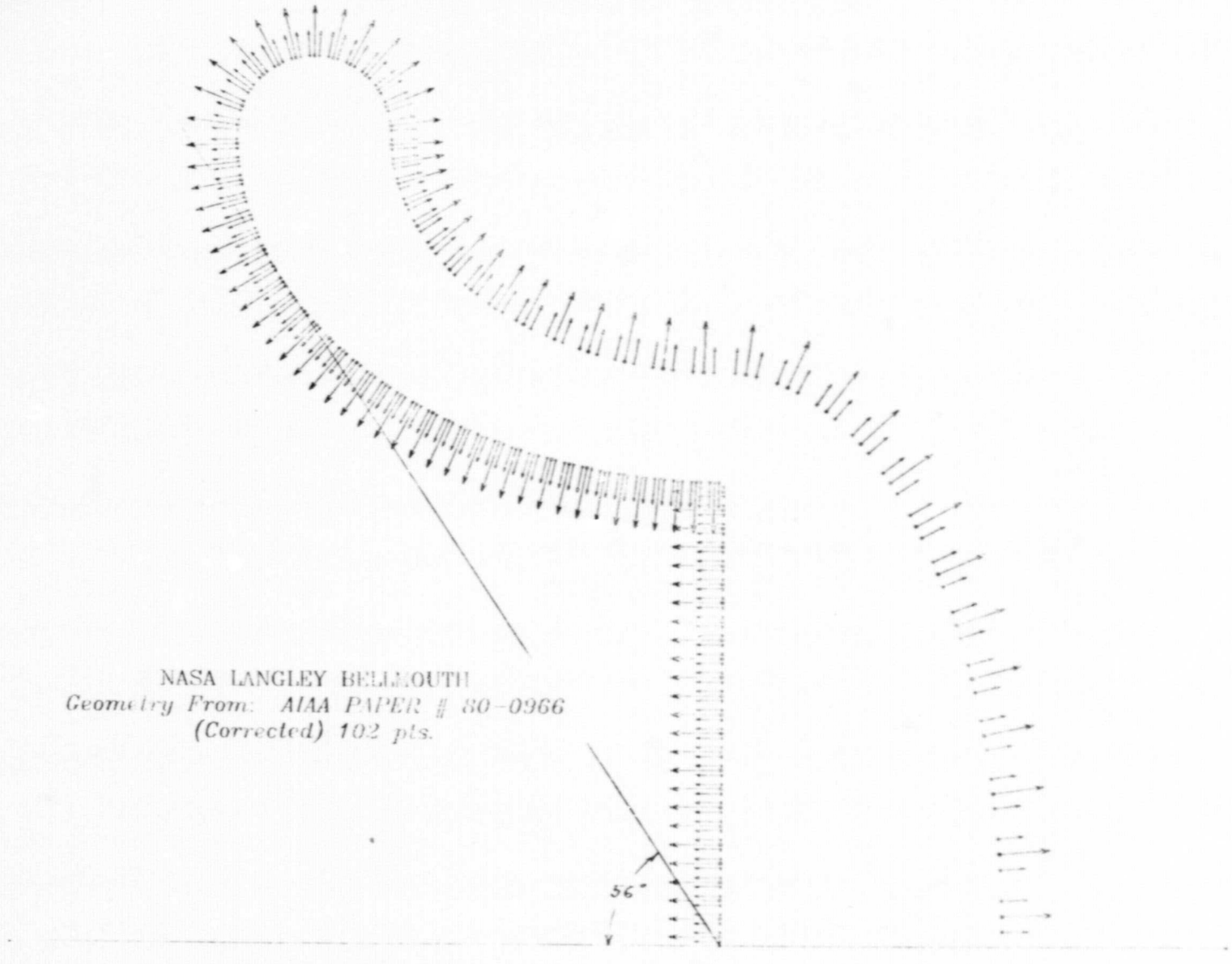

Fig. 1 Langley Bellmouth Geometry used for Computer Calculations.

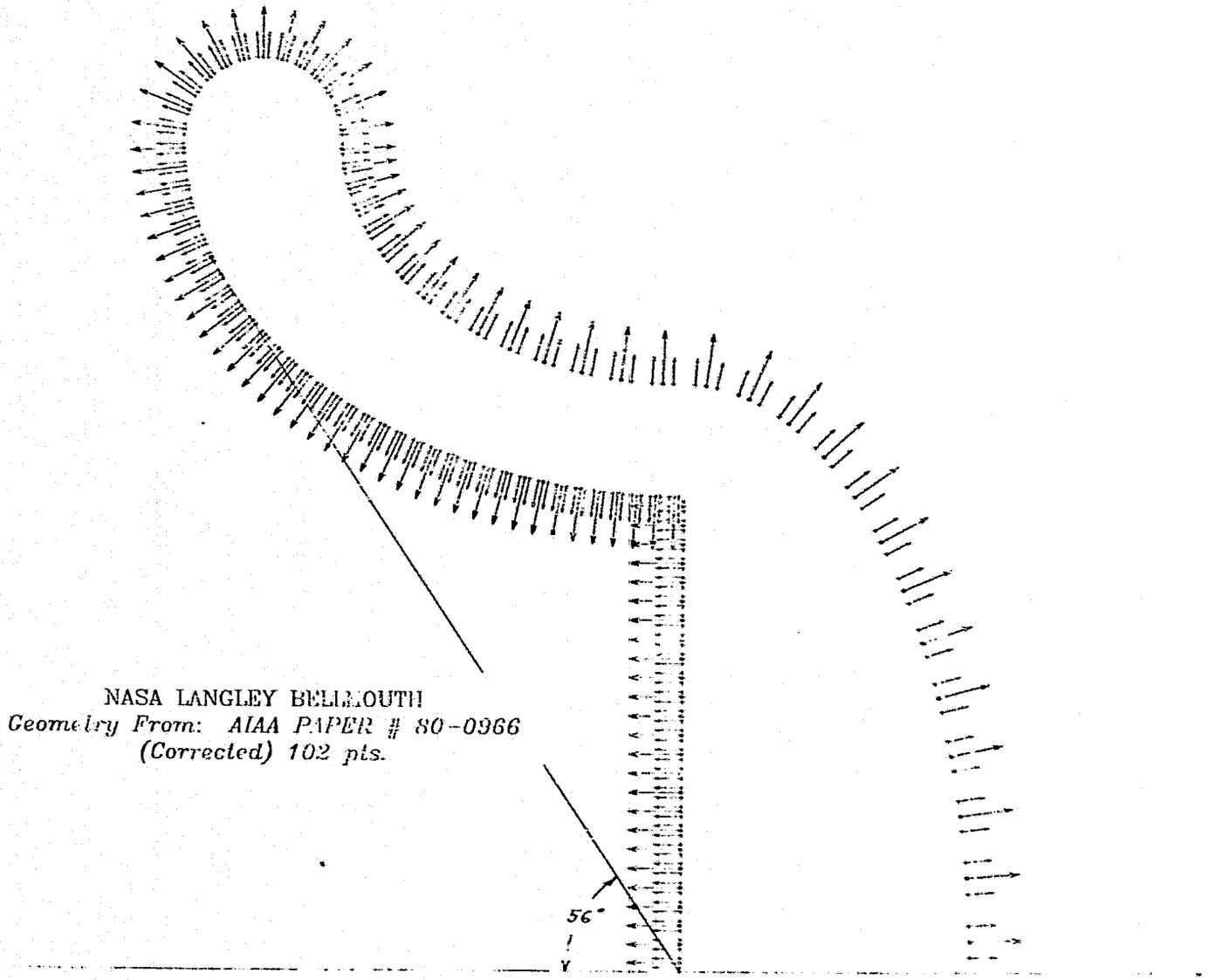

Fig. 1 Langley Bellmouth Geometry used for Computer Calculations.

LANGLEY BELLMOUTH

Deg	SPL	Deg	SPL
0	121	46	116
2	121	48	116
4	121	50	116
6	121	52	115
8	121	54	115
10	121	56	115
12	121	58	114
14	120	60	114
16	120	62	113
18	120	64	113
20	120	66	113
22	120	68	112
24	120	70	112
26	119	72	112
28	119	74	111
30	119	76	111
32	119	78	111
34	118	80	110
36	118	82	110
38	118	84	110
40	117	86	110
42	117	88	109
44	117	90	109

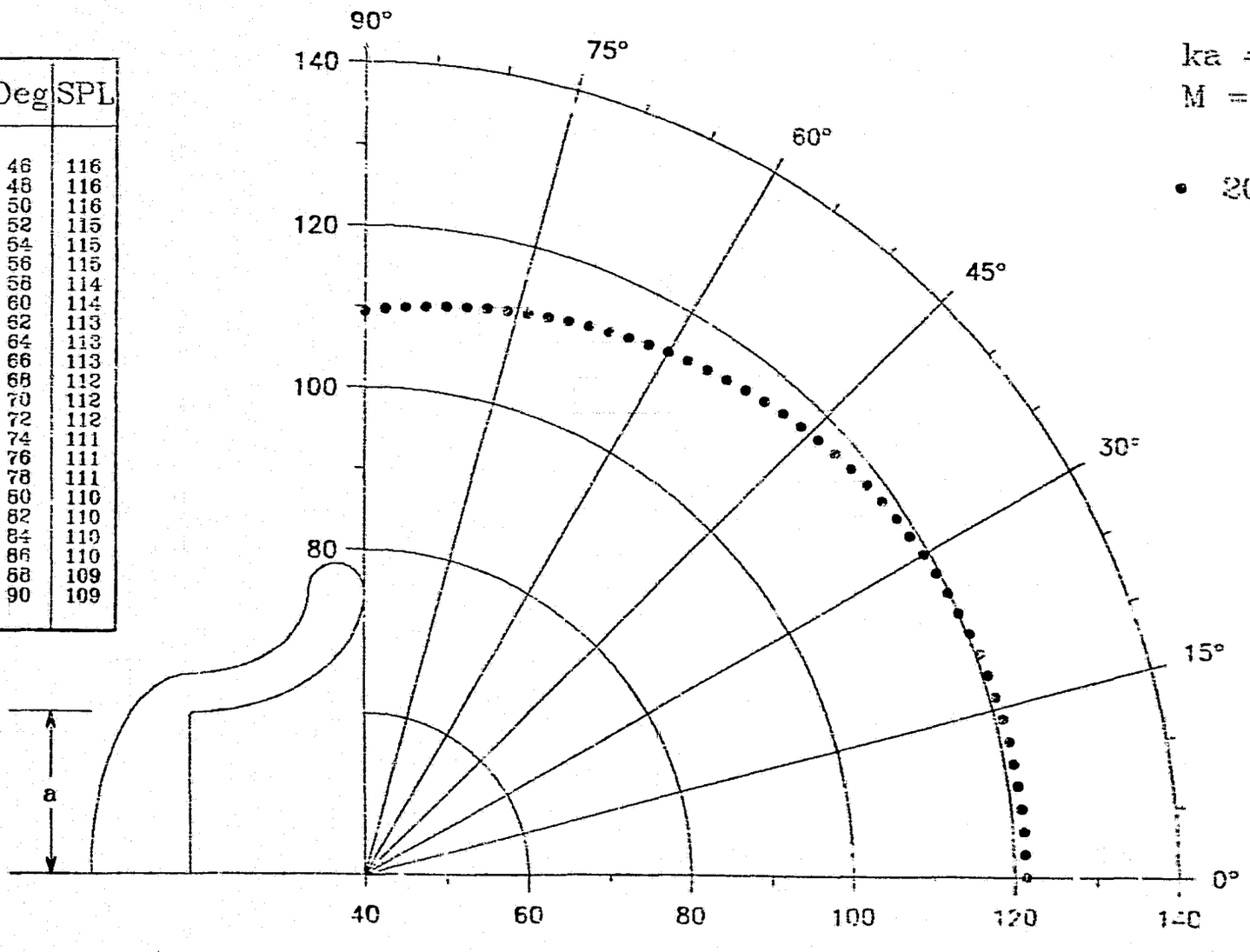

Fig. 2 SPL (dB)

Deg	SPL	Deg	SPL
0	138	46	120
2	136	48	121
4	135	50	120
6	134	52	119
8	135	54	118
10	135	56	117
12	134	58	117
14	134	60	116
16	134	62	115
18	133	64	114
20	133	66	114
22	132	68	113
24	131	70	113
26	131	72	112
28	130	74	112
30	129	76	111
32	129	78	111
34	127	80	111
36	127	82	110
38	126	84	110
40	125	86	110
42	124	88	109
44	123	90	109

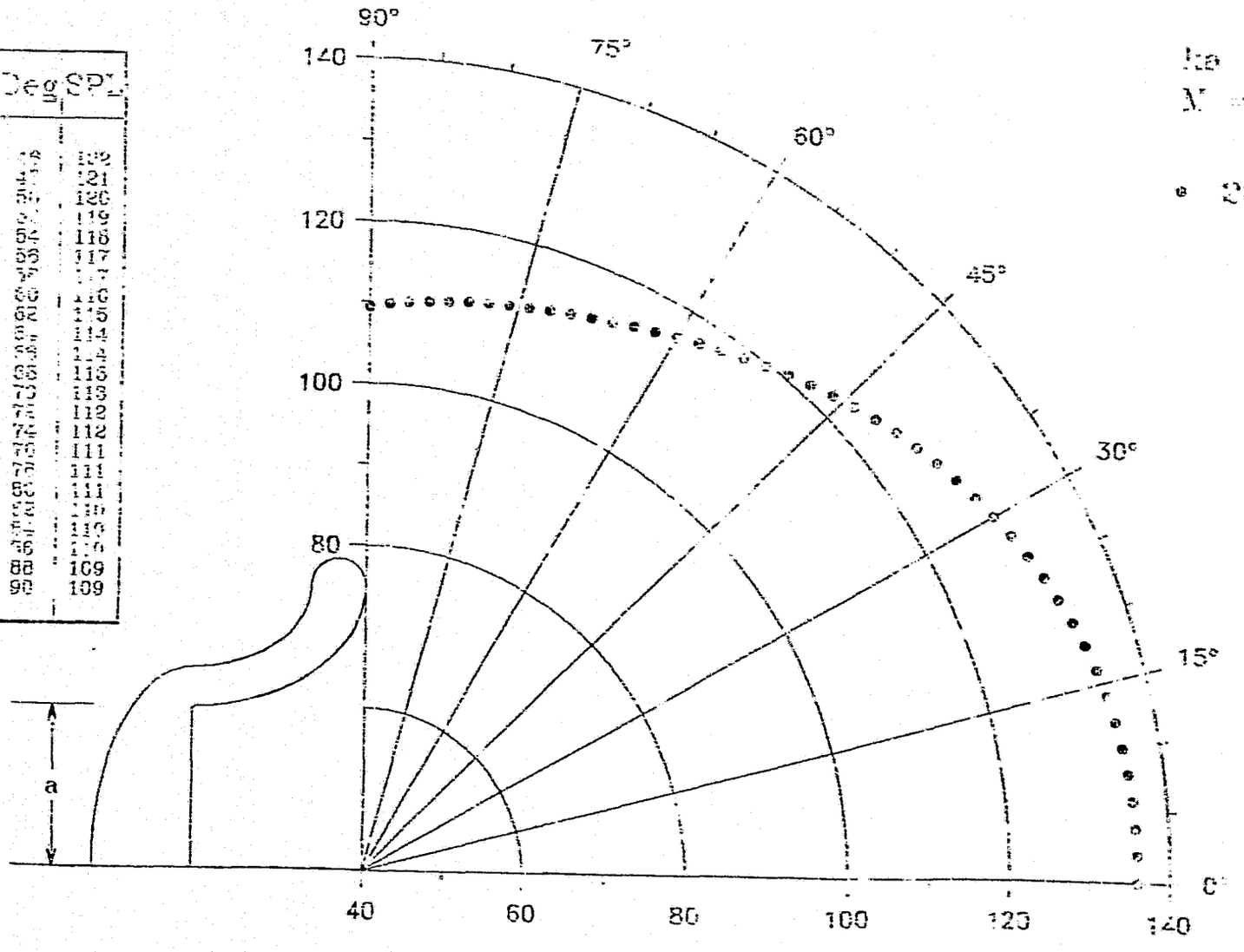

Fig. 3 SPL (dB)

Deg	SPL	Deg	SPL
0	0	46	108
2	87	48	108
4	93	50	107
6	96	52	107
8	99	54	107
10	100	56	107
12	102	58	106
14	103	60	106
16	104	62	106
18	105	64	106
20	106	66	105
22	106	68	105
24	107	70	105
26	107	72	104
28	107	74	104
30	107	76	104
32	108	78	103
34	108	80	103
36	108	82	103
38	108	84	102
40	108	86	102
42	108	88	102
44	108	90	101

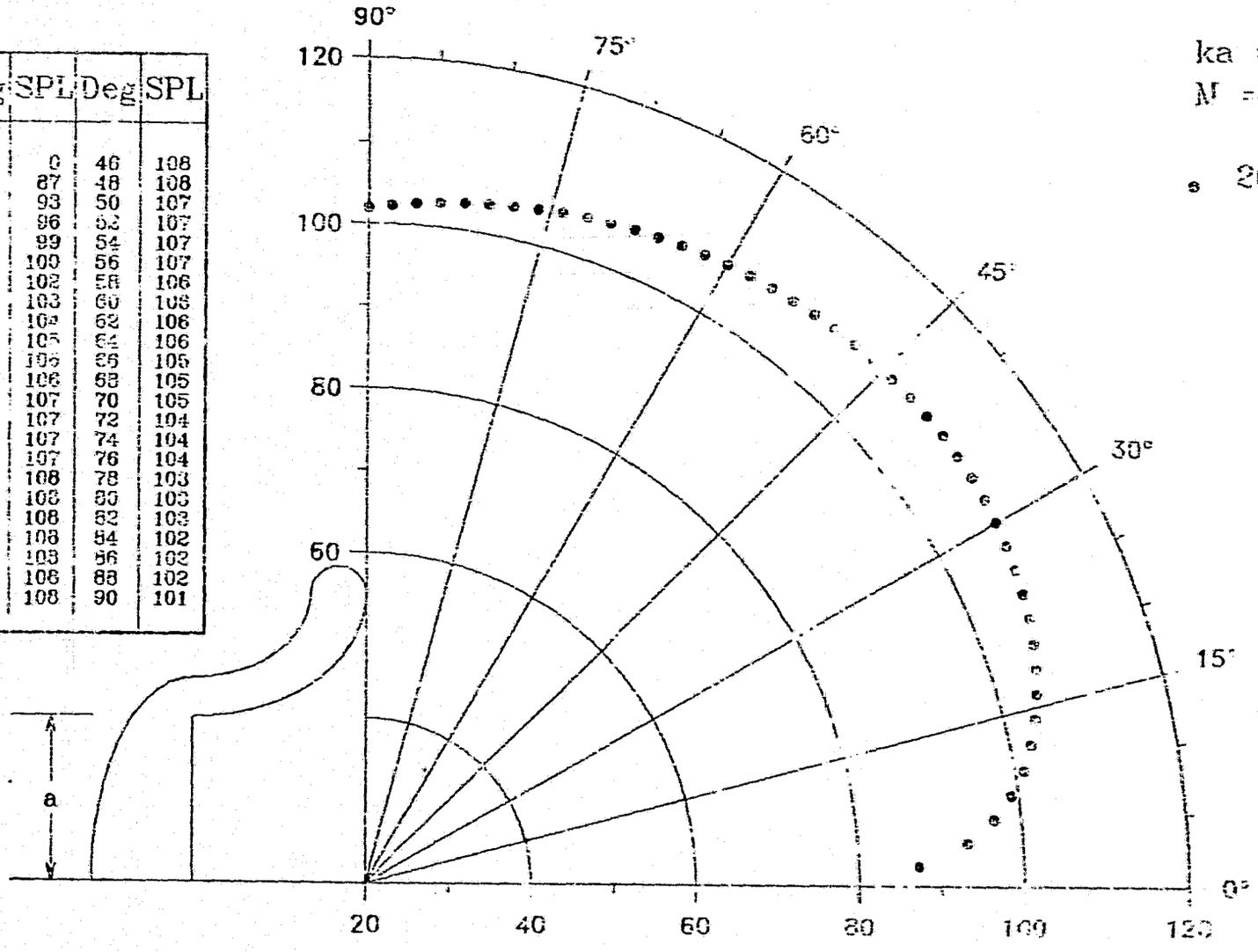

Fig. 4 SPL (dB

LANGLEY BELLMOUTH

Deg	SPL	Deg	SPL
0	0	46	110
2	89	48	110
4	95	50	109
6	99	52	109
8	101	54	109
10	103	56	109
12	104	58	108
14	106	60	106
16	107	62	106
18	107	64	107
20	108	66	107
22	109	68	107
24	109	70	106
26	109	72	106
28	110	74	106
30	110	76	105
32	110	78	105
34	110	80	104
36	110	82	104
38	110	84	104
40	110	86	103
42	110	88	103
44	110	90	103

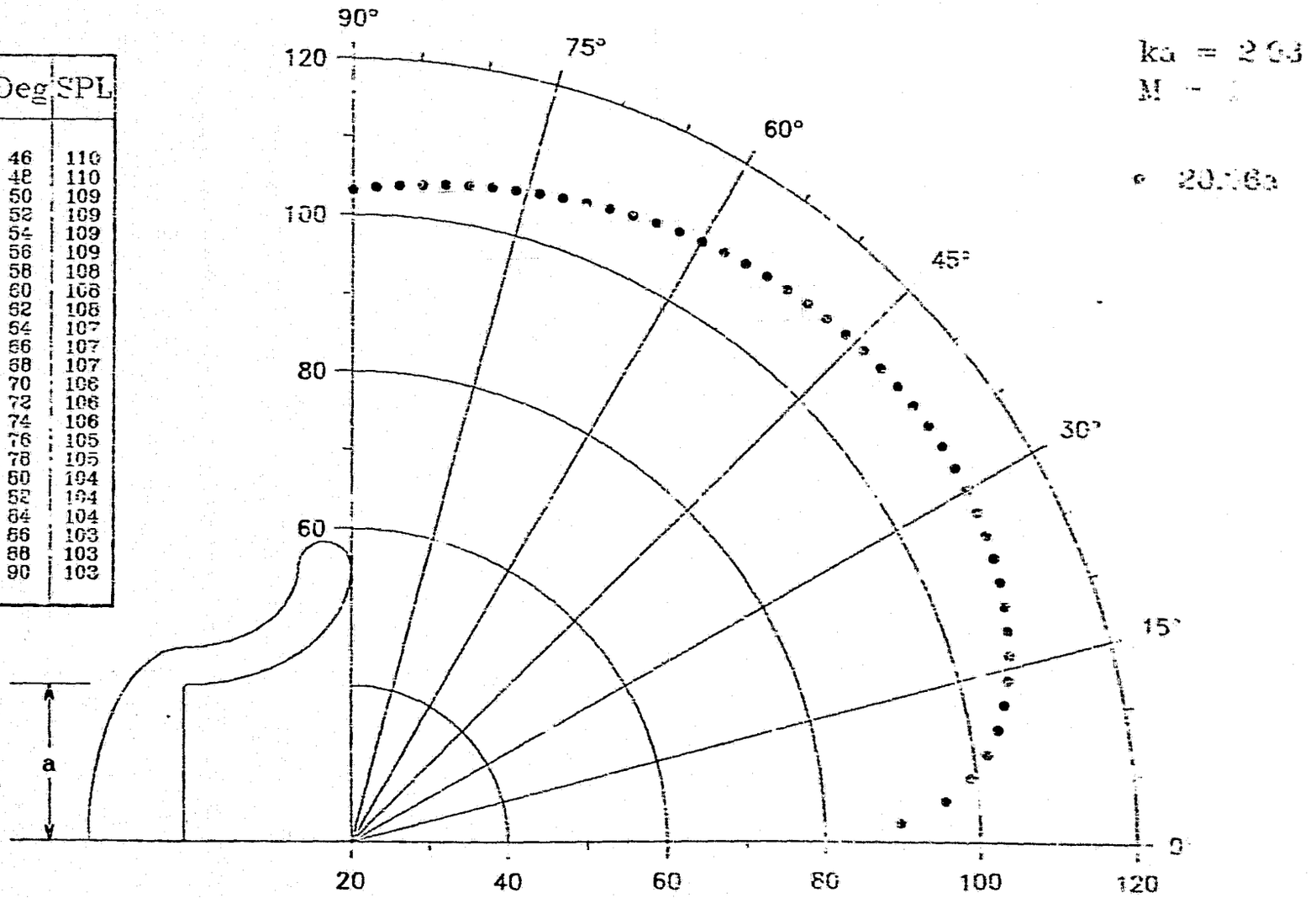

Fig. 5 SPL (dB)

LANGLEY BELLMOUTH

Deg	SPL	Deg	SPL
0	0	46	116
2	97	48	116
4	103	50	115
6	107	52	115
8	109	54	114
10	111	56	114
12	112	58	114
14	114	60	113
16	114	62	113
18	115	64	112
20	116	66	112
22	116	68	111
24	116	70	111
26	117	72	110
28	117	74	110
30	117	76	109
32	117	78	109
34	117	80	108
36	117	82	107
38	117	84	107
40	117	86	106
42	116	88	106
44	116	90	105

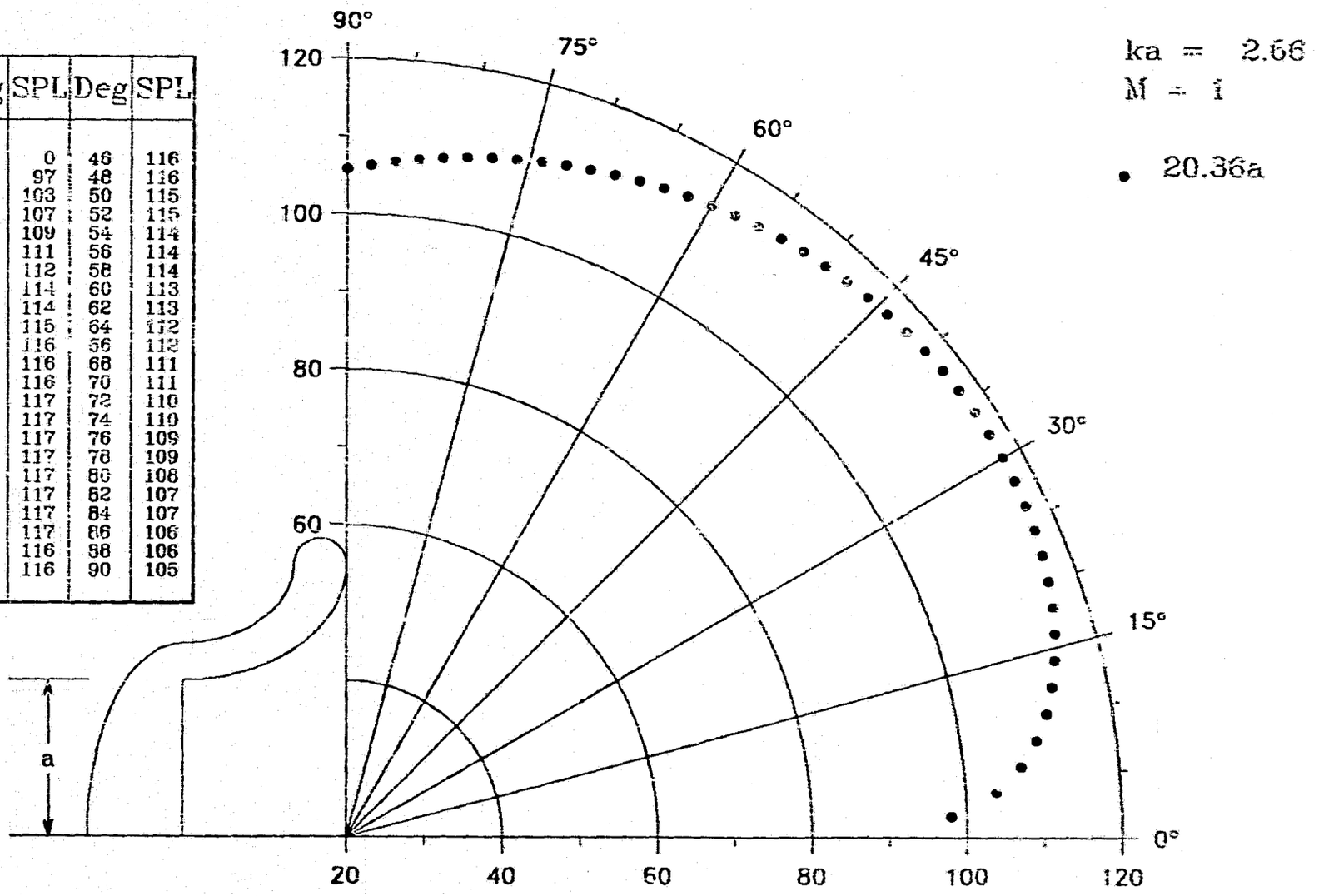

Fig. 6 SPL (dB)

LANGLEY BELLMOUTH

Deg	SPL	Deg	SPL
0	0	46	120
2	106	48	119
4	112	50	119
6	115	52	118
8	117	54	117
10	119	56	117
12	120	58	116
14	121	60	116
16	122	62	115
18	122	64	114
20	123	66	114
22	123	68	113
24	123	70	113
26	123	72	112
28	123	74	112
30	123	76	111
32	123	78	110
34	123	80	110
36	122	82	110
38	122	84	109
40	121	86	109
42	121	88	108
44	120	90	108

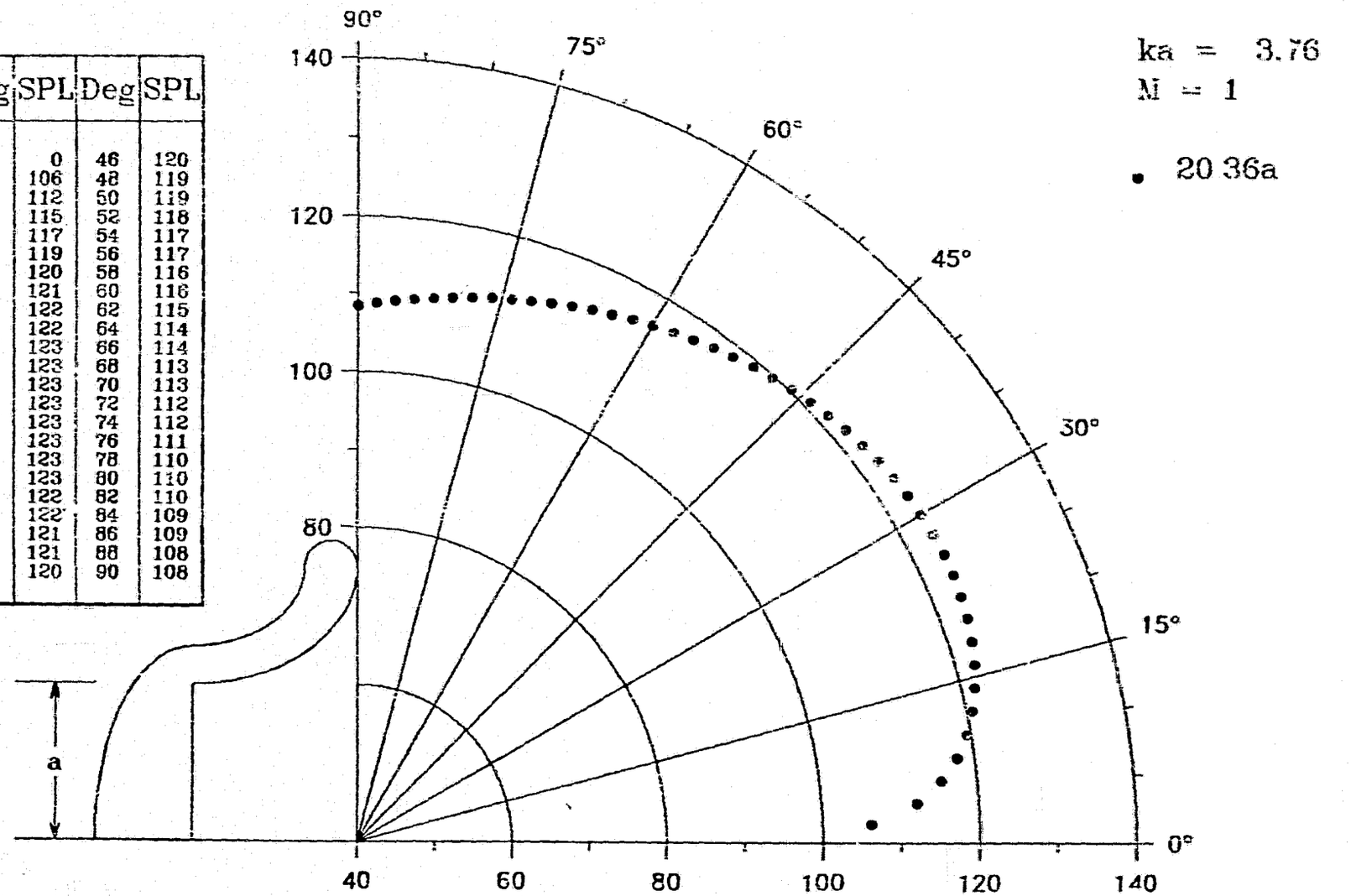

Fig. 7 SPL (dB)

LANGLEY BELLMOUTH

Deg	SPL	Deg	SPL
0	.0	46	122
2	112	48	121
4	116	50	120
6	121	52	119
8	124	54	118
10	125	56	117
12	126	58	116
14	127	60	115
16	128	62	114
18	128	54	113
20	128	56	113
22	128	68	112
24	128	70	112
26	128	72	111
28	126	74	110
30	127	76	110
32	127	78	109
34	126	60	109
36	126	82	108
38	125	84	108
40	124	86	107
42	123	88	107
44	122	90	106

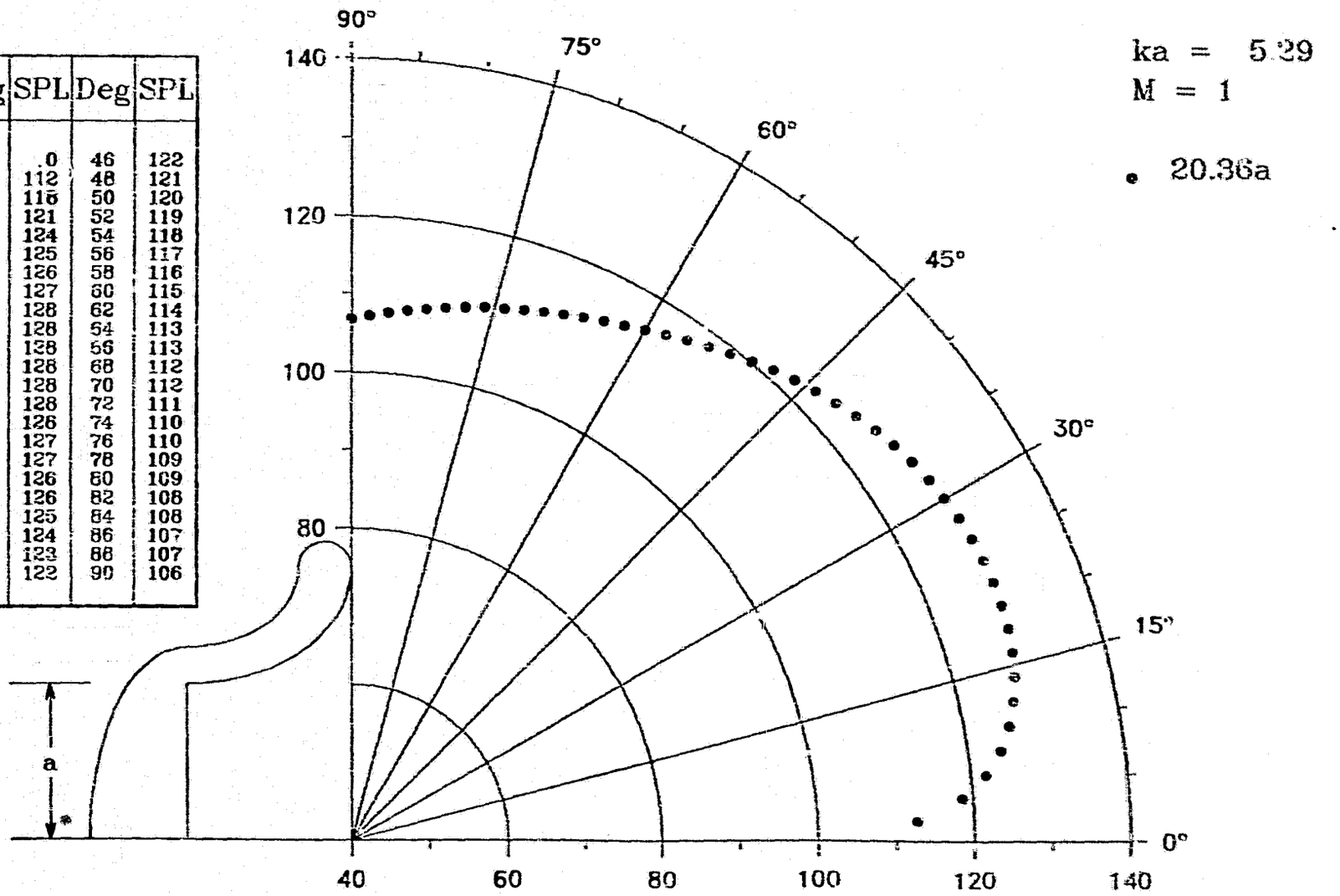

Fig. 8 SPL (dB)

LANGLEY BELLMOUTH

Deg	SPL	Deg	SPL
0	0	46	113
2	70	48	113
4	82	50	112
6	89	52	112
8	93	54	112
10	97	56	112
12	100	58	111
14	102	60	111
16	104	62	111
18	106	64	110
20	107	66	110
22	109	68	109
24	110	70	109
26	110	72	108
28	111	74	108
30	112	76	108
32	112	78	107
34	112	80	107
36	113	82	106
38	113	84	106
40	113	86	105
42	113	88	105
44	113	90	104

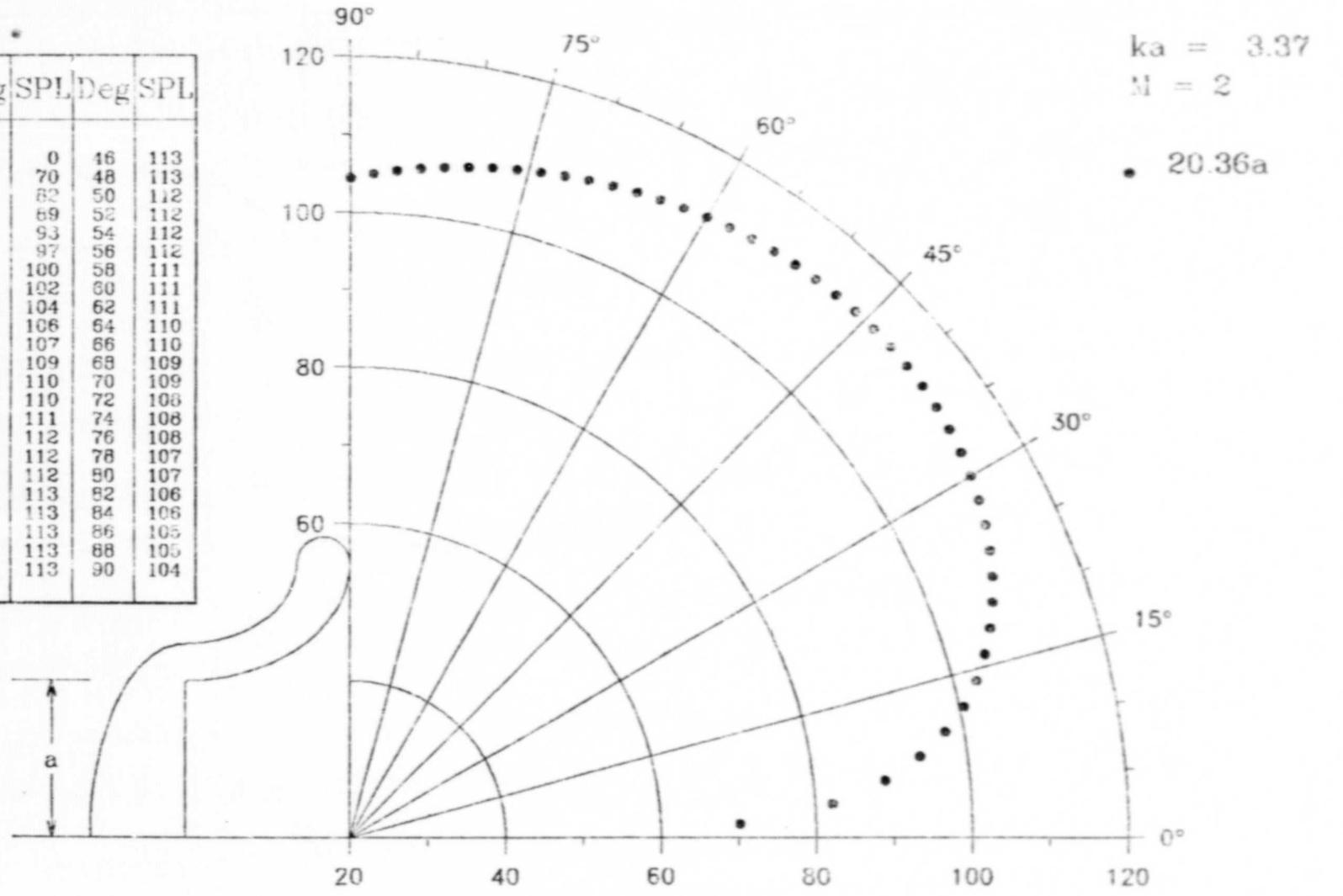

Fig. 9 SPL (dB)

LANGLEY BELLMOUTH

Deg	SPL	Deg	SPL
0	0	46	116
2	75	48	116
4	87	50	115
6	94	52	115
8	98	54	115
10	102	56	114
12	105	58	114
14	107	60	113
16	109	62	113
18	111	64	112
20	112	66	112
22	113	68	111
24	114	70	111
26	115	72	111
28	115	74	110
30	116	76	110
32	116	78	109
34	116	80	109
36	116	82	108
38	117	84	108
40	117	86	107
42	116	88	107
44	116	90	106

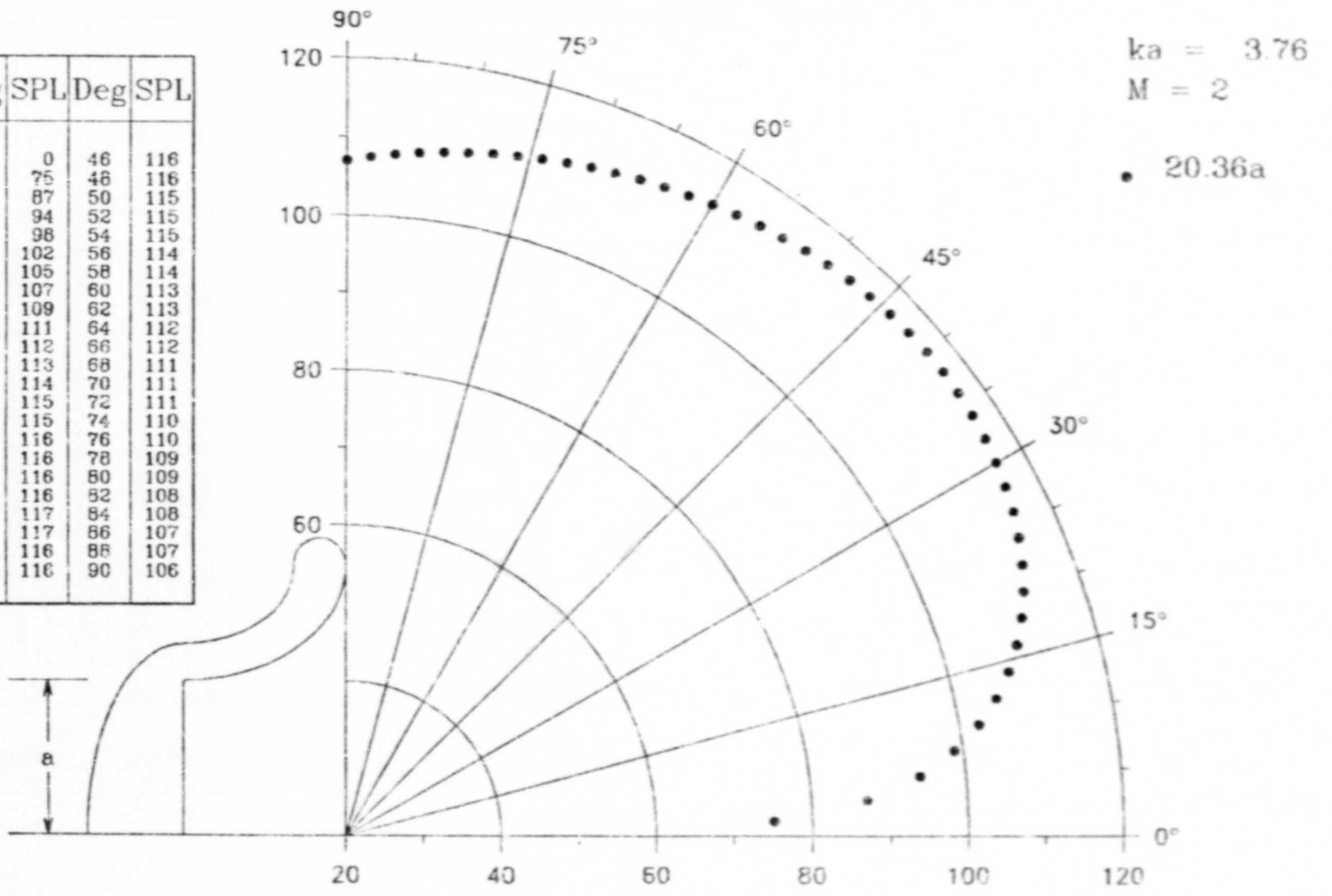

Fig. 10 SPL (dB)

LANGLEY BELLMOUTH

Deg	SPL	Deg	SPL
0	0	46	119
2	80	48	119
4	92	50	118
6	99	52	118
8	103	54	117
10	107	56	117
12	110	58	116
14	112	60	116
16	114	62	115
18	115	64	114
20	117	66	114
22	118	68	113
24	118	70	113
26	119	72	112
28	119	74	111
30	120	76	111
32	120	78	110
34	120	80	110
36	120	82	109
38	120	84	109
40	120	86	108
42	120	88	108
44	119	90	107

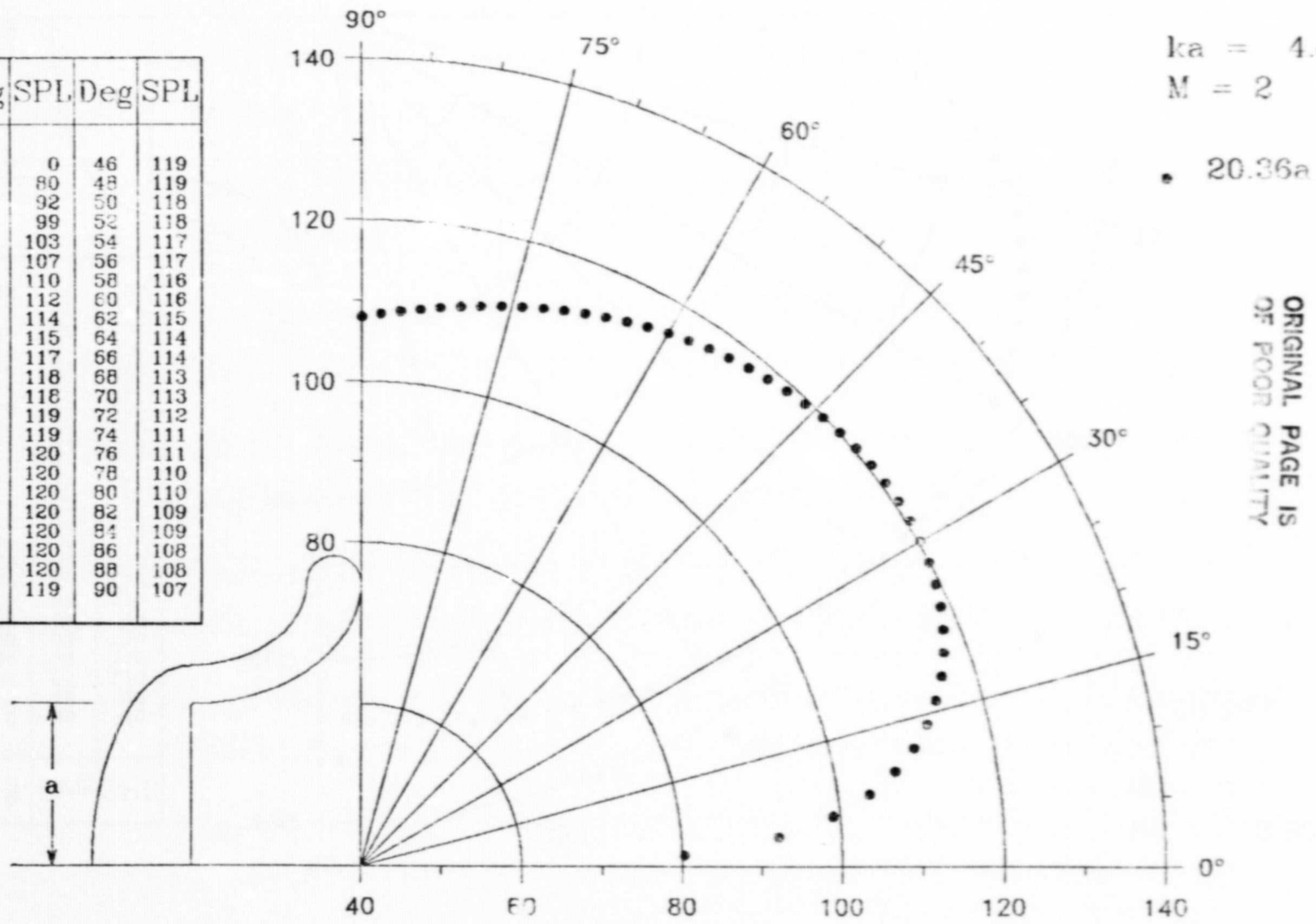

Fig. 11 SPL (dB)

LANGLEY BELLMOUTH

Deg	SPL	Deg	SPL
0	0	46	121
2	85	48	121
4	97	50	120
6	103	52	119
8	108	54	119
10	112	56	118
12	114	58	117
14	116	60	117
16	118	62	116
18	120	64	115
20	121	66	114
22	122	68	114
24	122	70	113
26	123	72	112
28	123	74	112
30	123	76	111
32	123	78	110
34	123	80	110
36	123	82	109
38	123	84	109
40	123	86	108
42	122	88	108
44	122	90	107

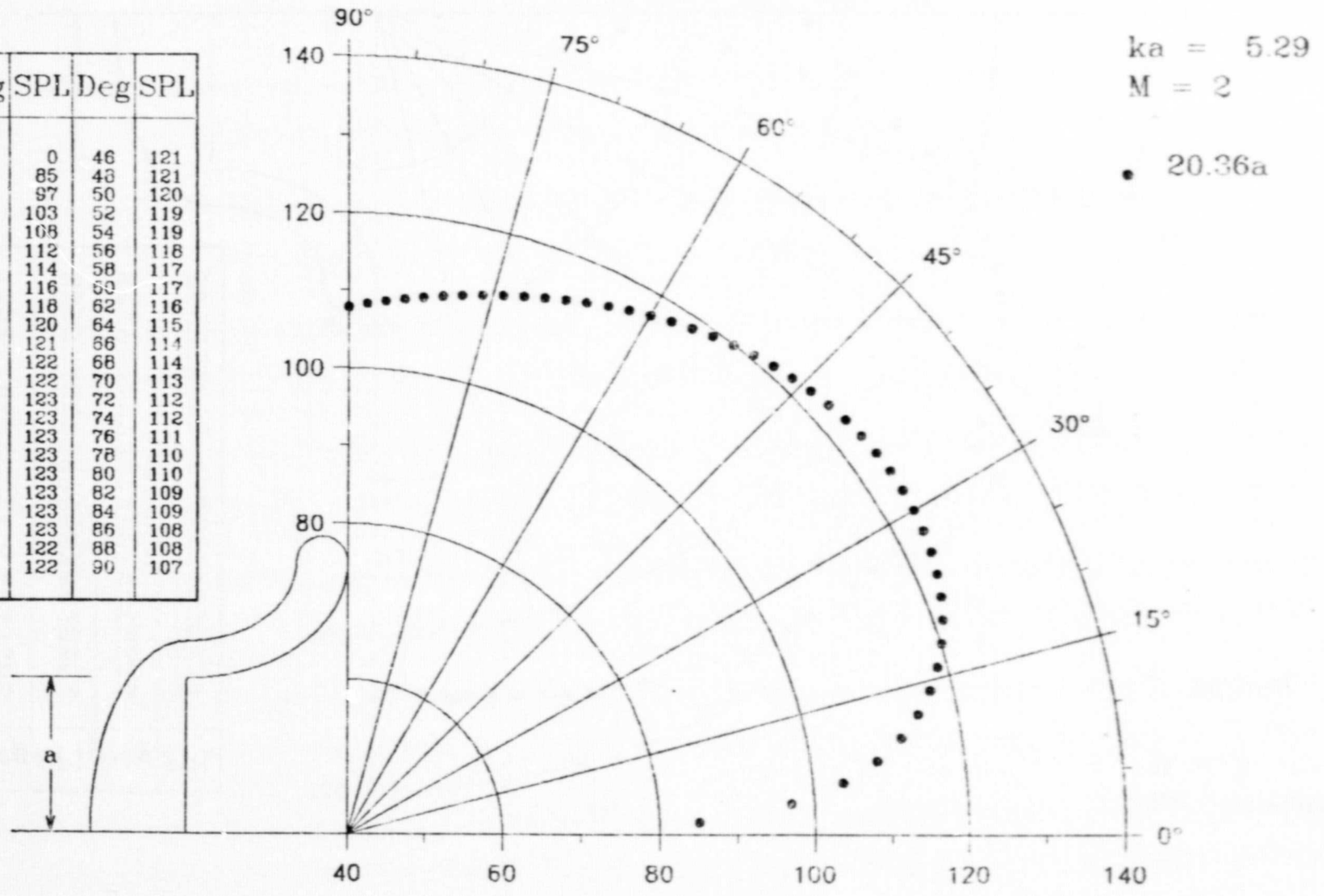

Fig. 12 SPL (dB)

LANGLEY BELLMOUTH

Deg	SPL	Deg	SPL
0	0	46	116
2	27	48	116
4	51	50	115
6	65	52	115
8	75	54	115
10	82	56	115
12	88	58	114
14	93	60	114
16	97	62	113
18	100	64	113
20	103	66	112
22	105	68	112
24	107	70	111
26	109	72	111
28	111	74	110
30	112	76	110
32	113	78	109
34	114	80	108
36	114	82	108
38	115	84	107
40	115	86	107
42	115	88	106
44	116	90	105

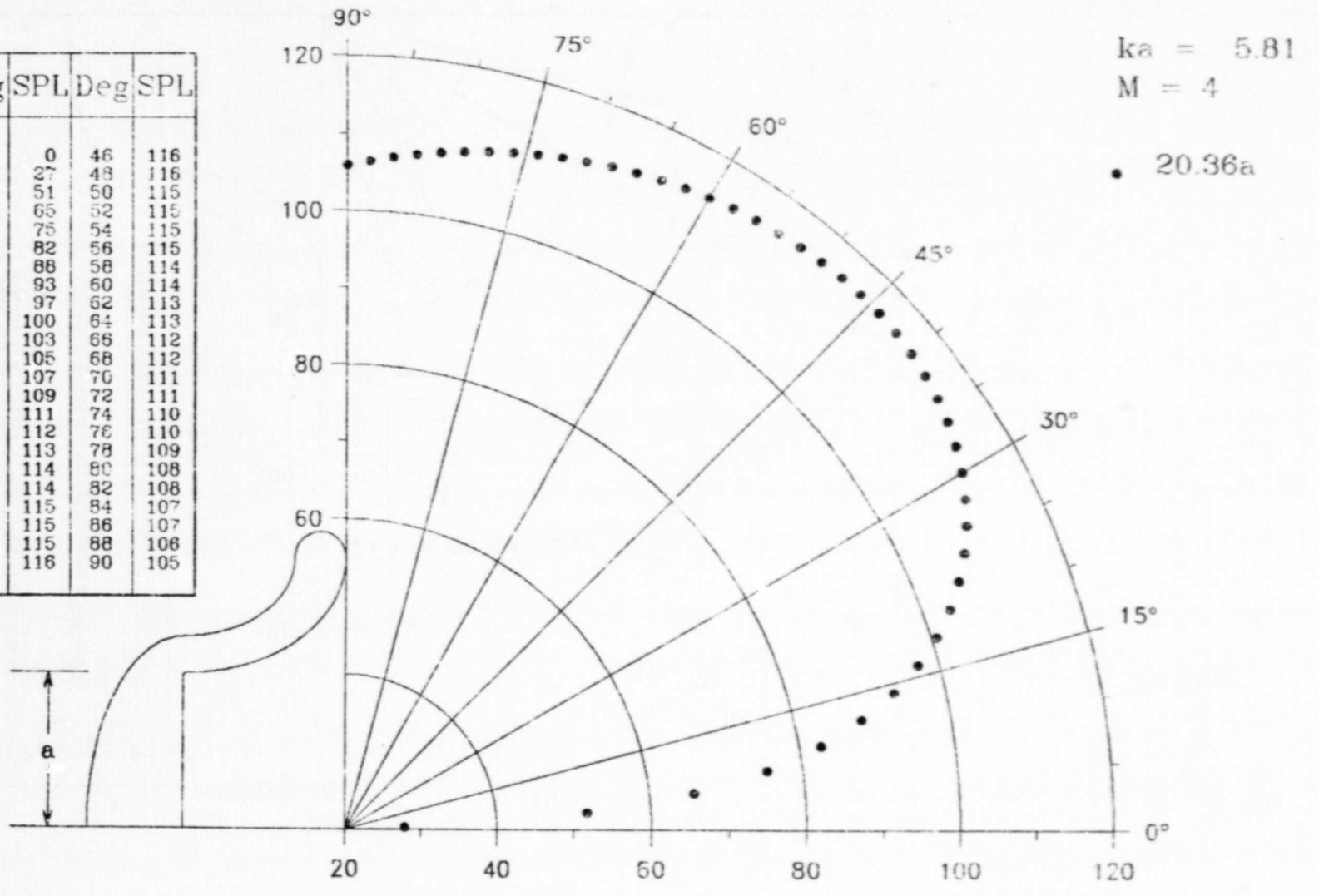

Fig. 13 SPL (dB)

LANGLEY BELLMOUTH

Deg	SPL	Deg	SPL
0	0	46	124
2	−4	48	124
4	31	50	123
6	52	52	122
8	67	54	122
10	78	56	121
12	85	58	120
14	94	60	119
16	100	62	118
18	105	64	117
20	110	66	116
22	113	68	115
24	116	70	114
26	119	72	113
28	121	74	113
30	122	76	112
32	124	78	111
34	124	80	111
36	125	82	110
38	125	84	109
40	125	86	109
42	125	88	108
44	125	90	108

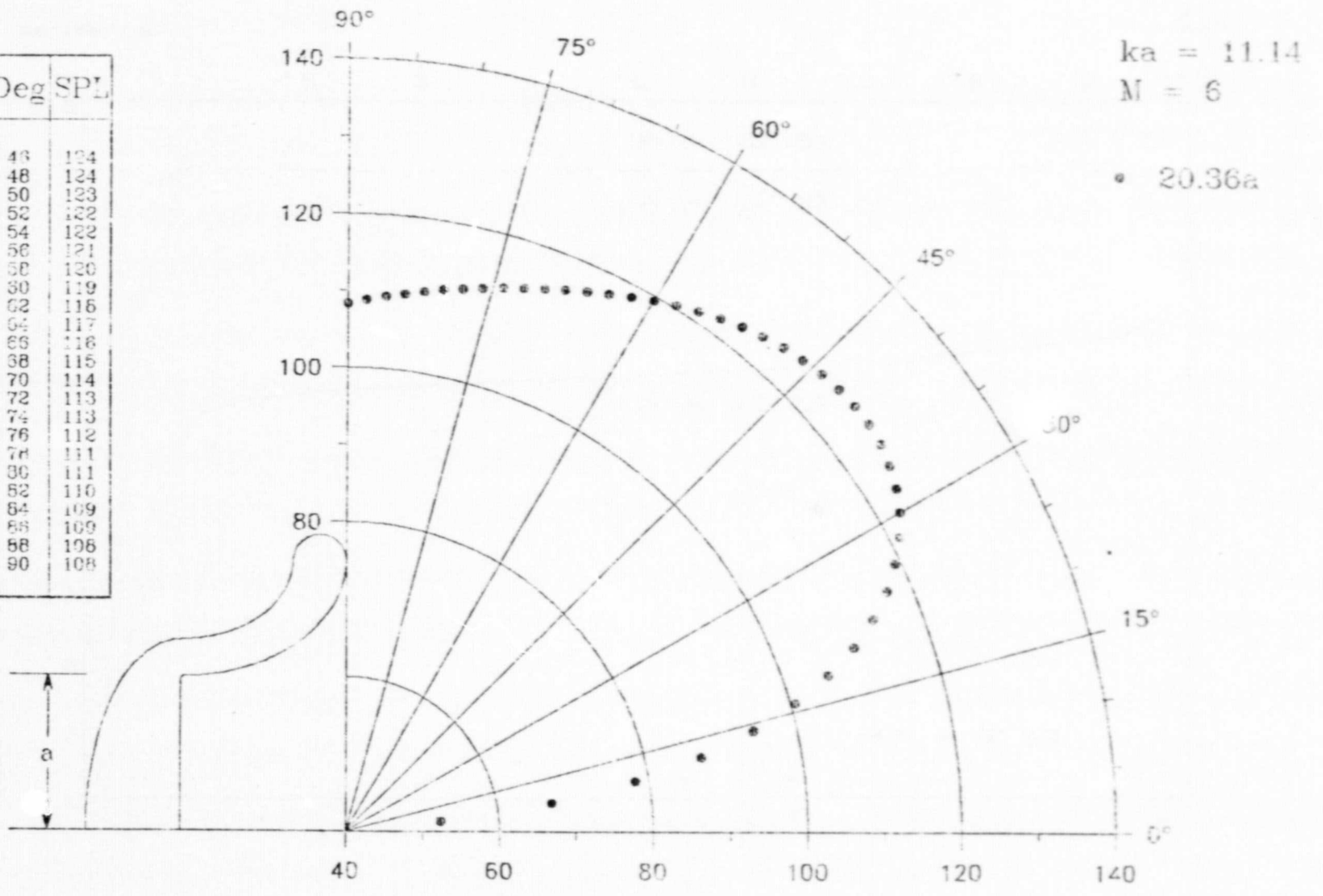

Fig. 14 SPL (dB)

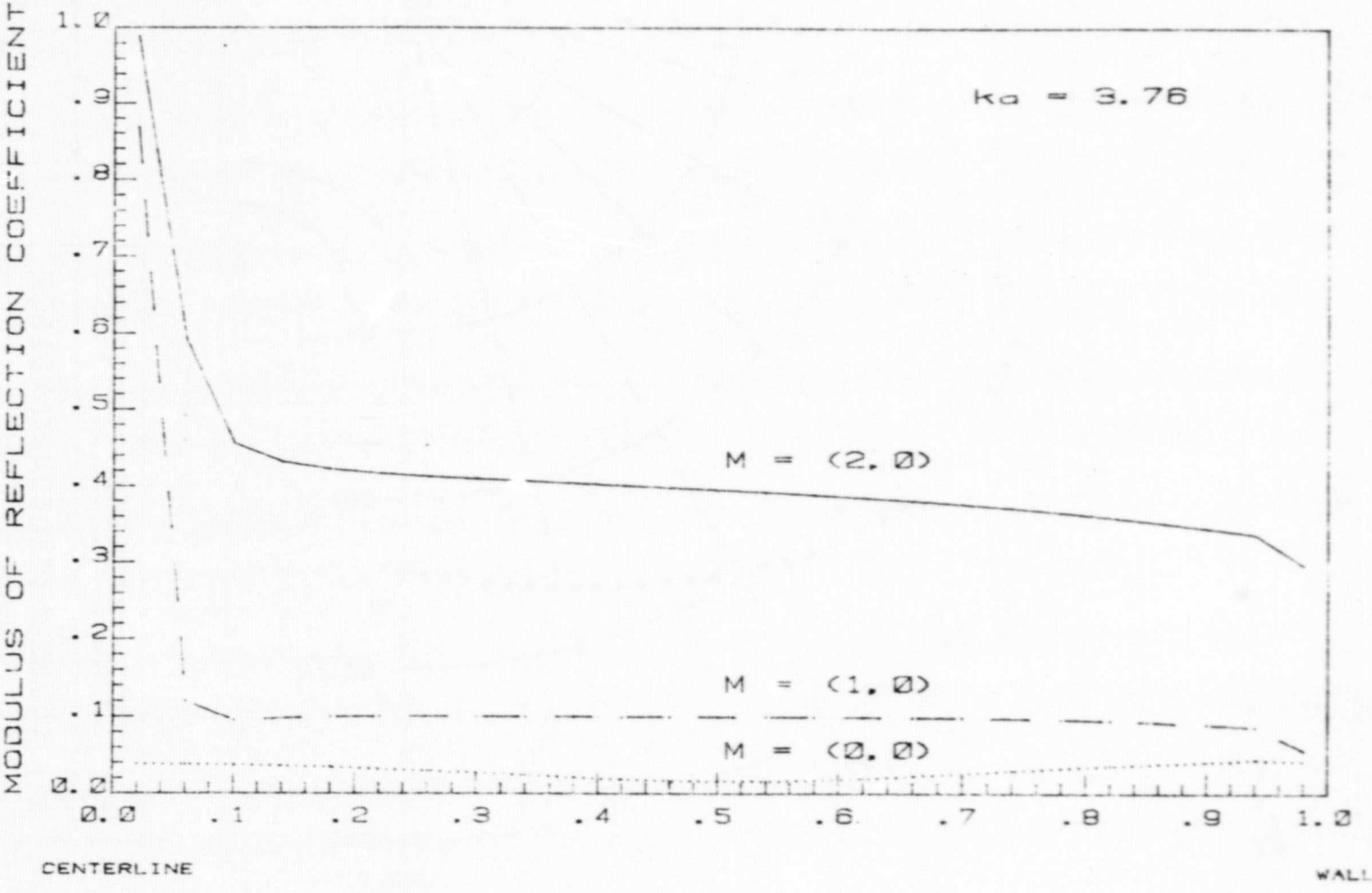

LANGLEY BELLMOUTH (Exit Plane)

Fig. 15

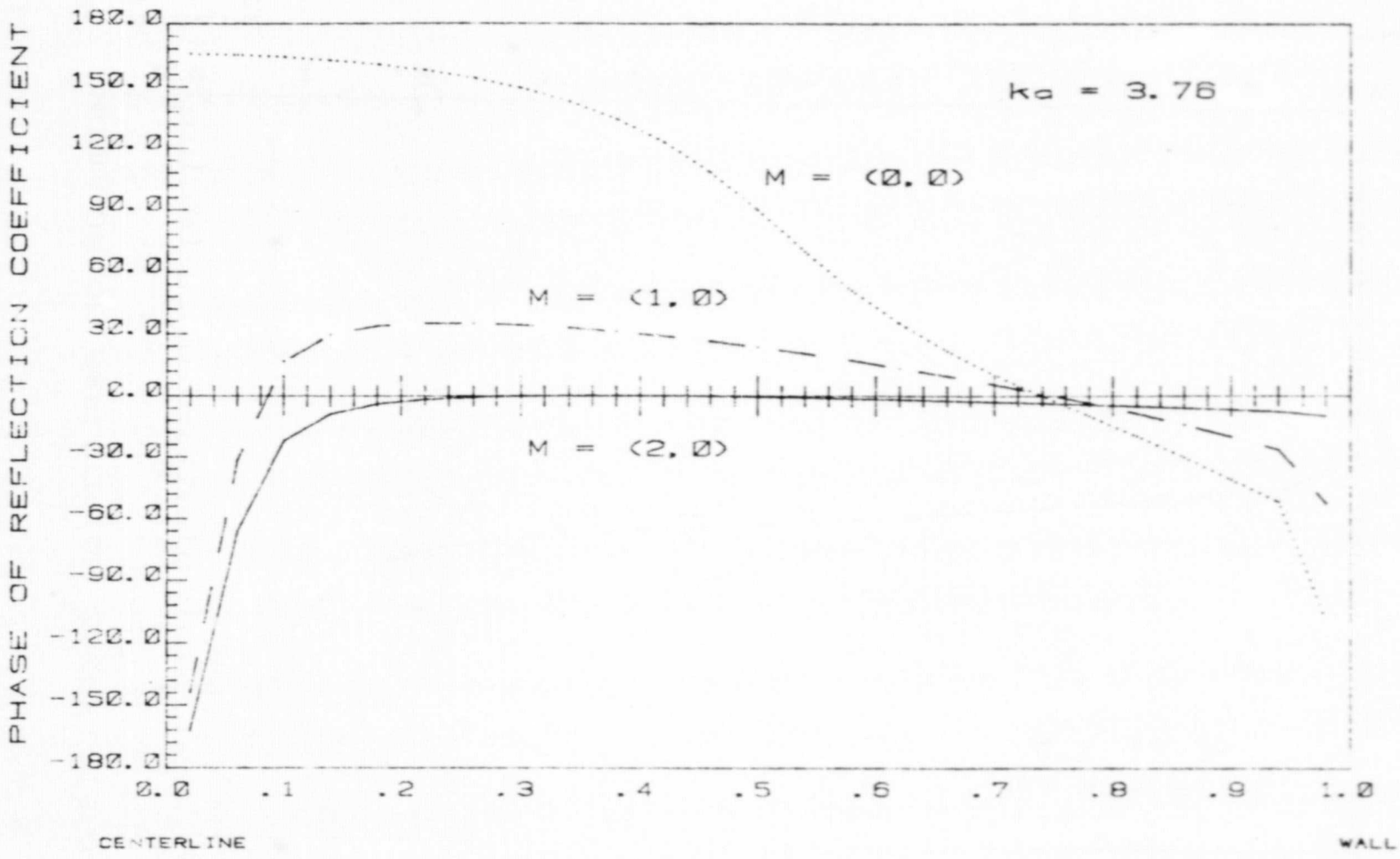

LANGLEY BELLMOUTH (Exit Plane)

Fig. 16

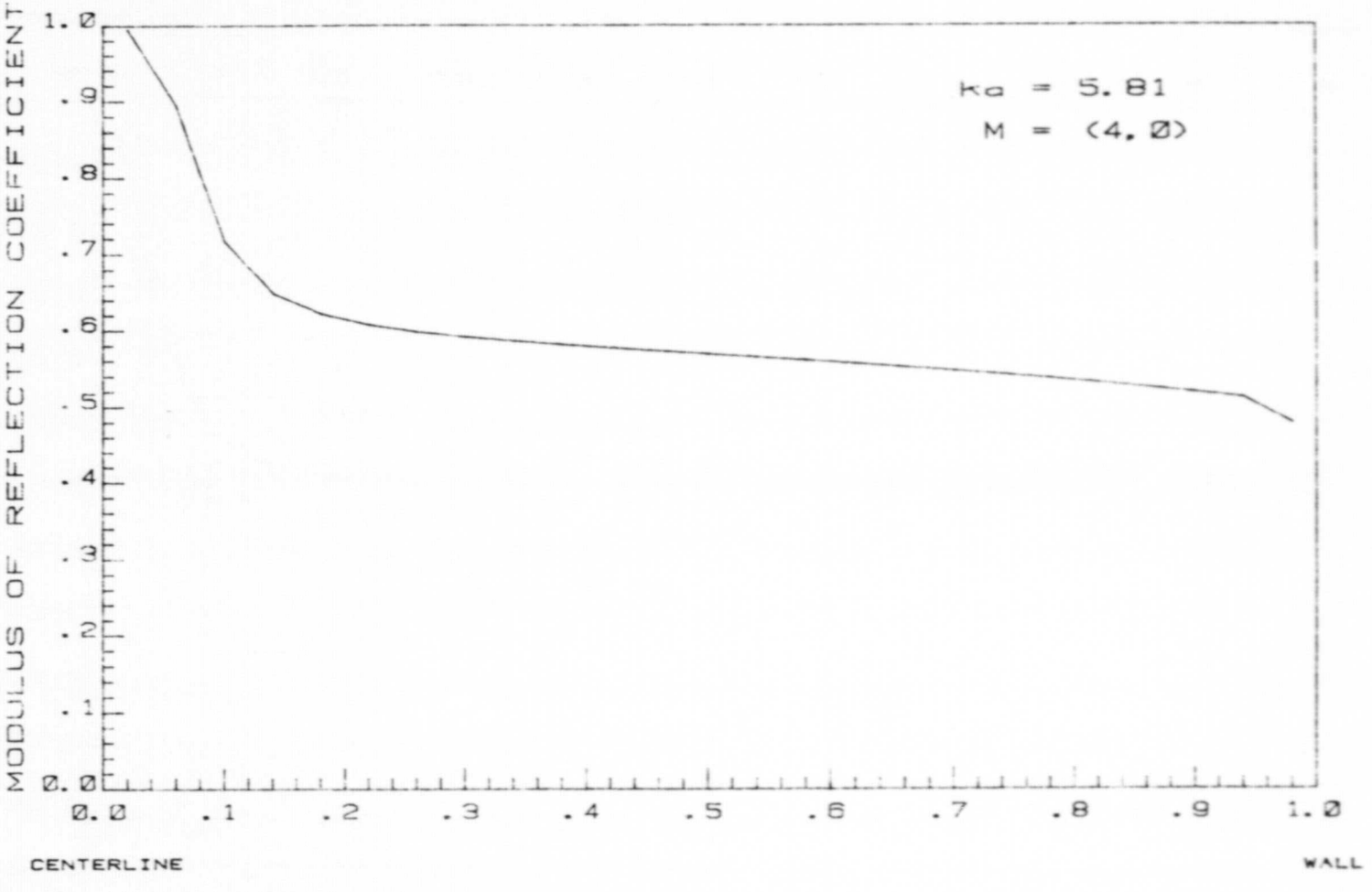

LANGLEY BELLMOUTH (Exit Plane)

Fig. 17

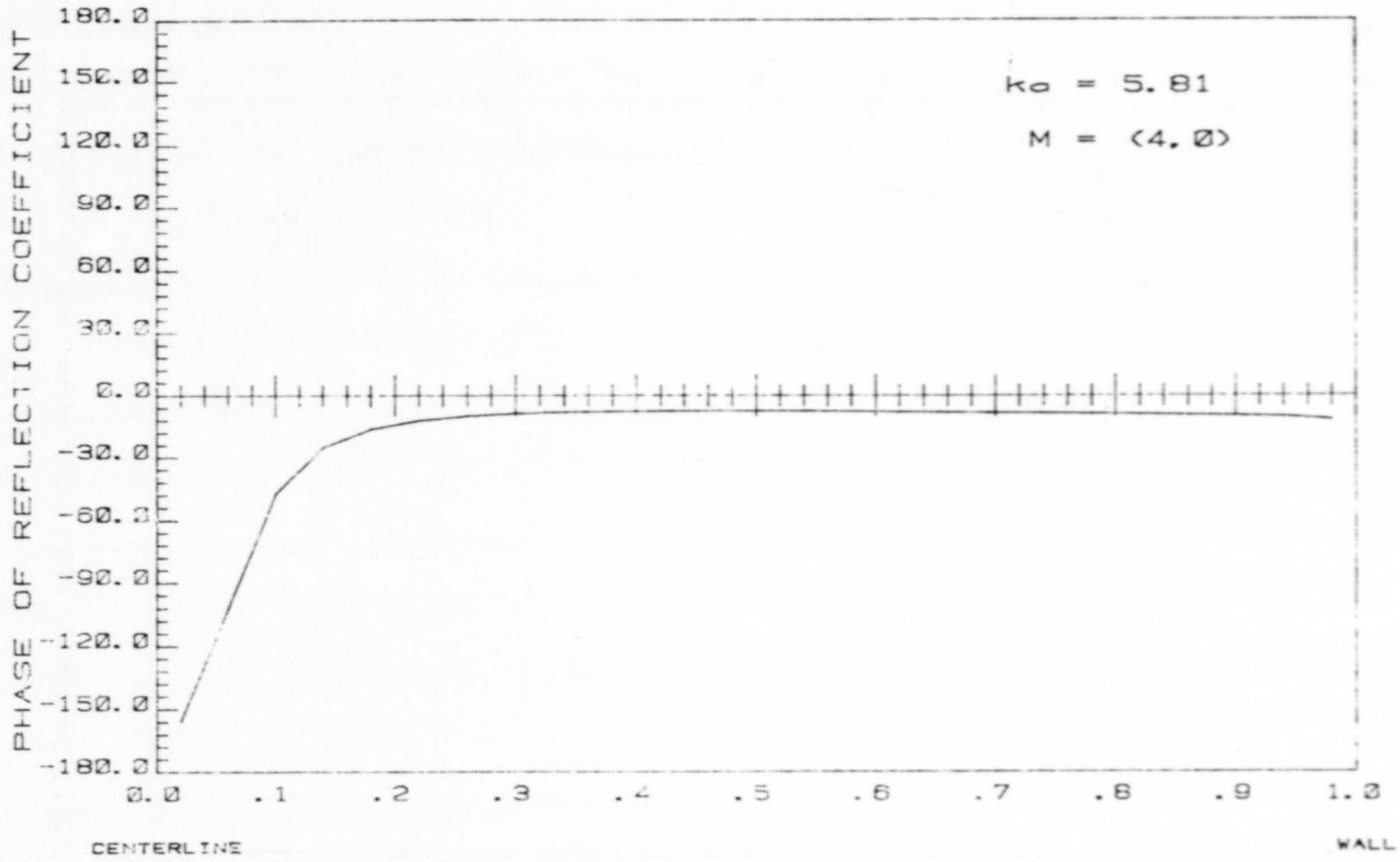

LANGLEY BELLMOUTH (Exit Plane)

Fig. 18

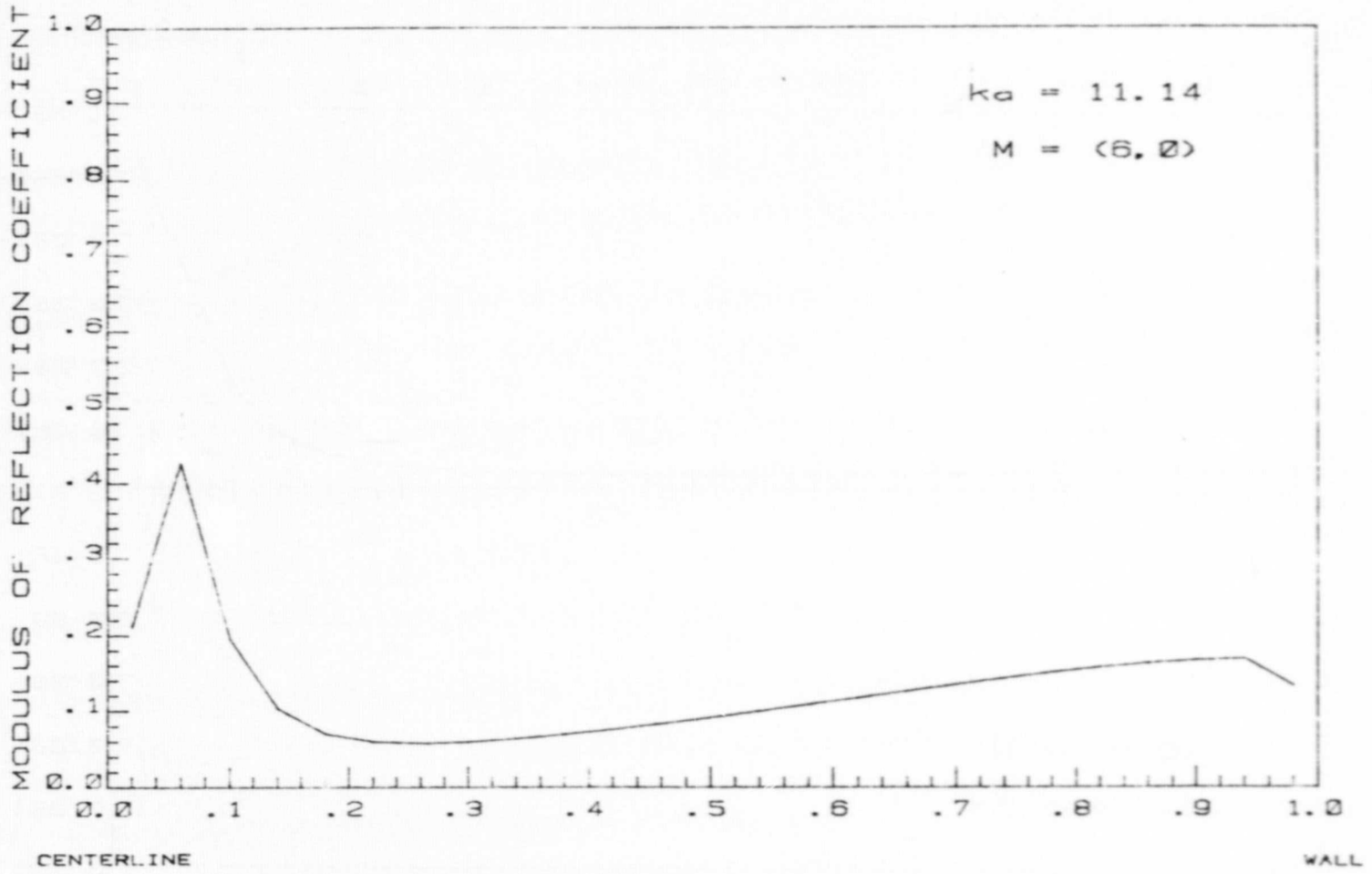

LANGLEY BELLMOUTH (Exit Plane)

Fig. 19

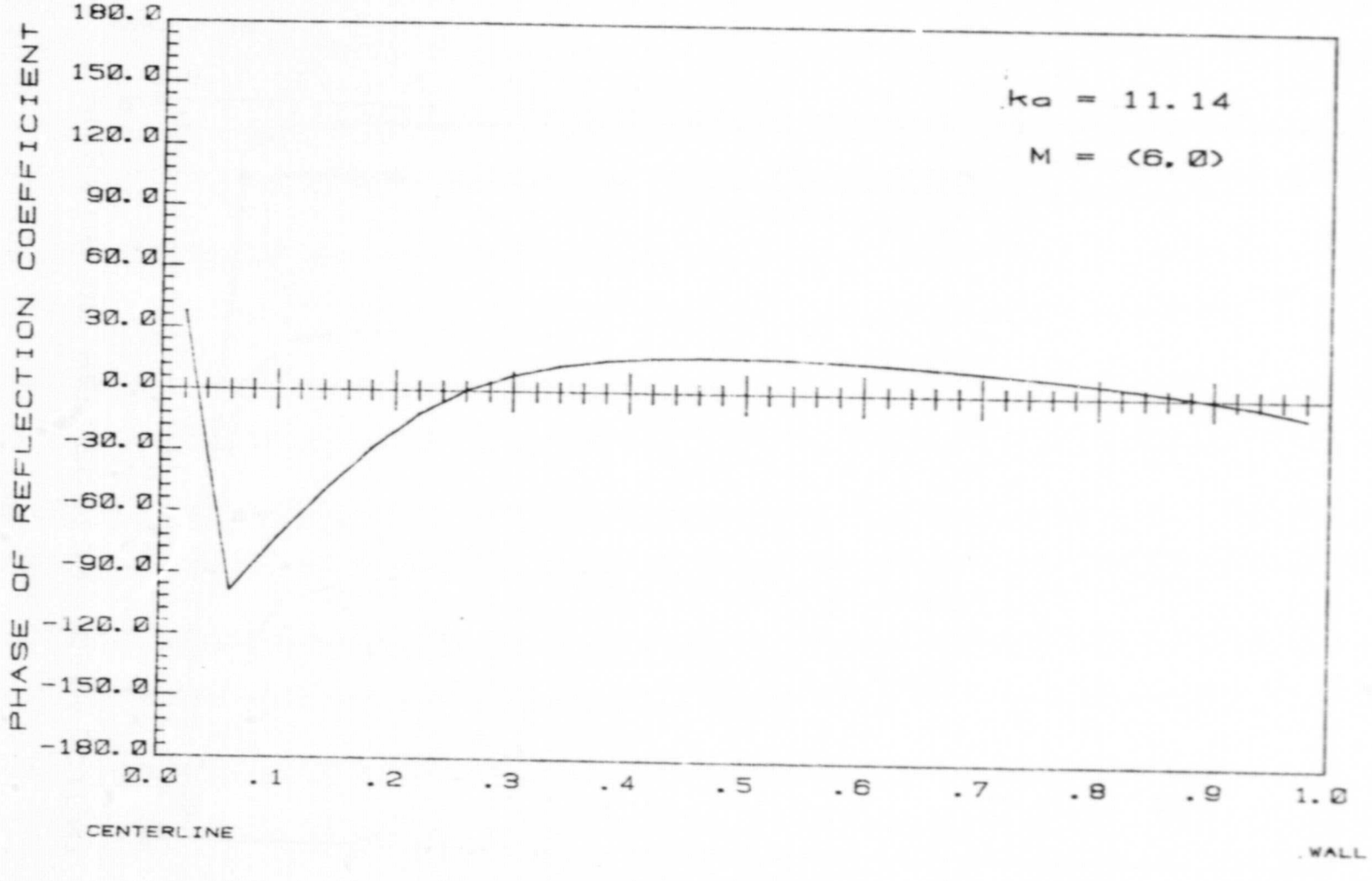

LANGLEY BELLMOUTH (Exit Plane)

Fig. 20

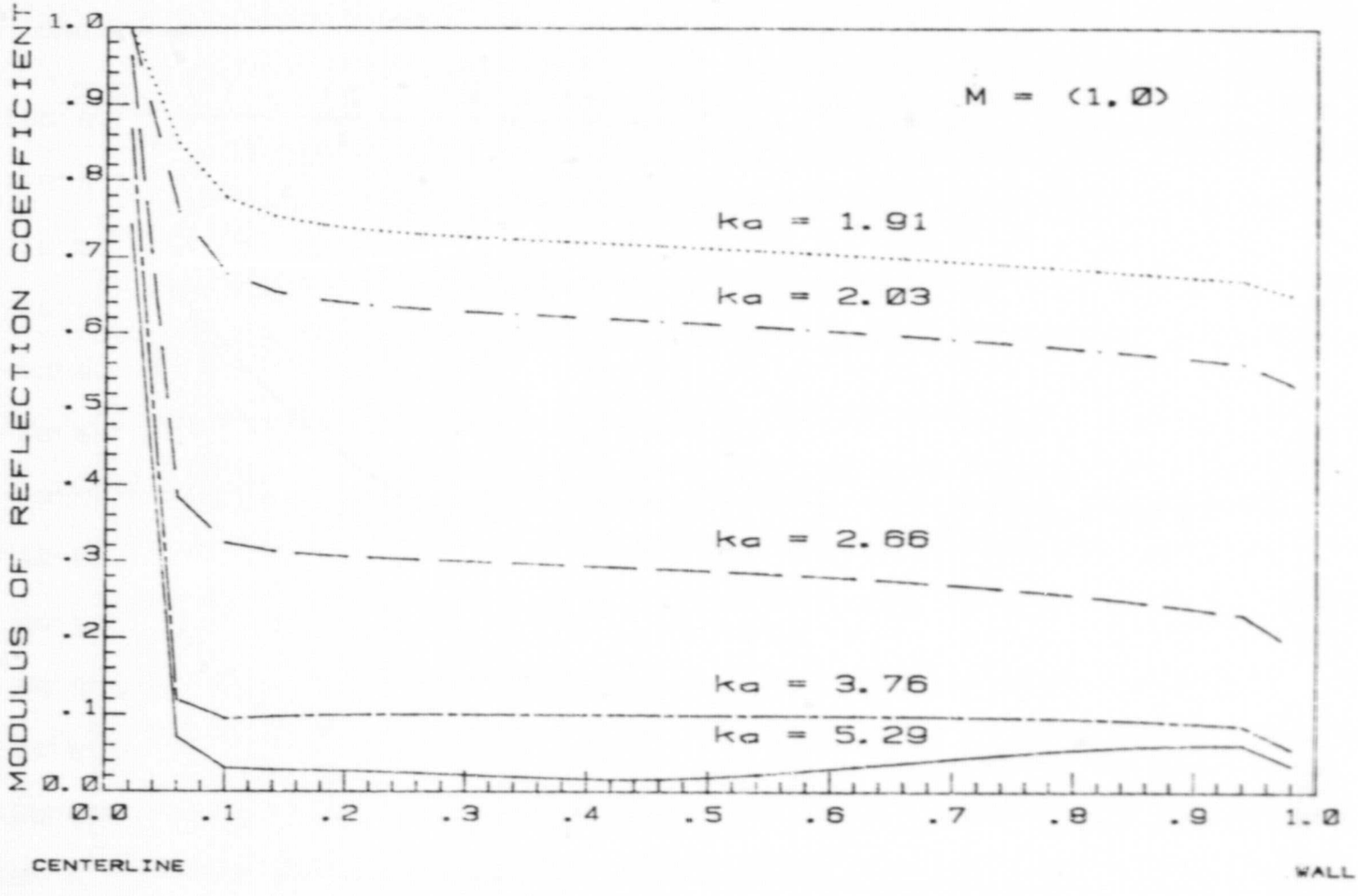

LANGLEY BELLMOUTH (Exit Plane)

Fig. 21

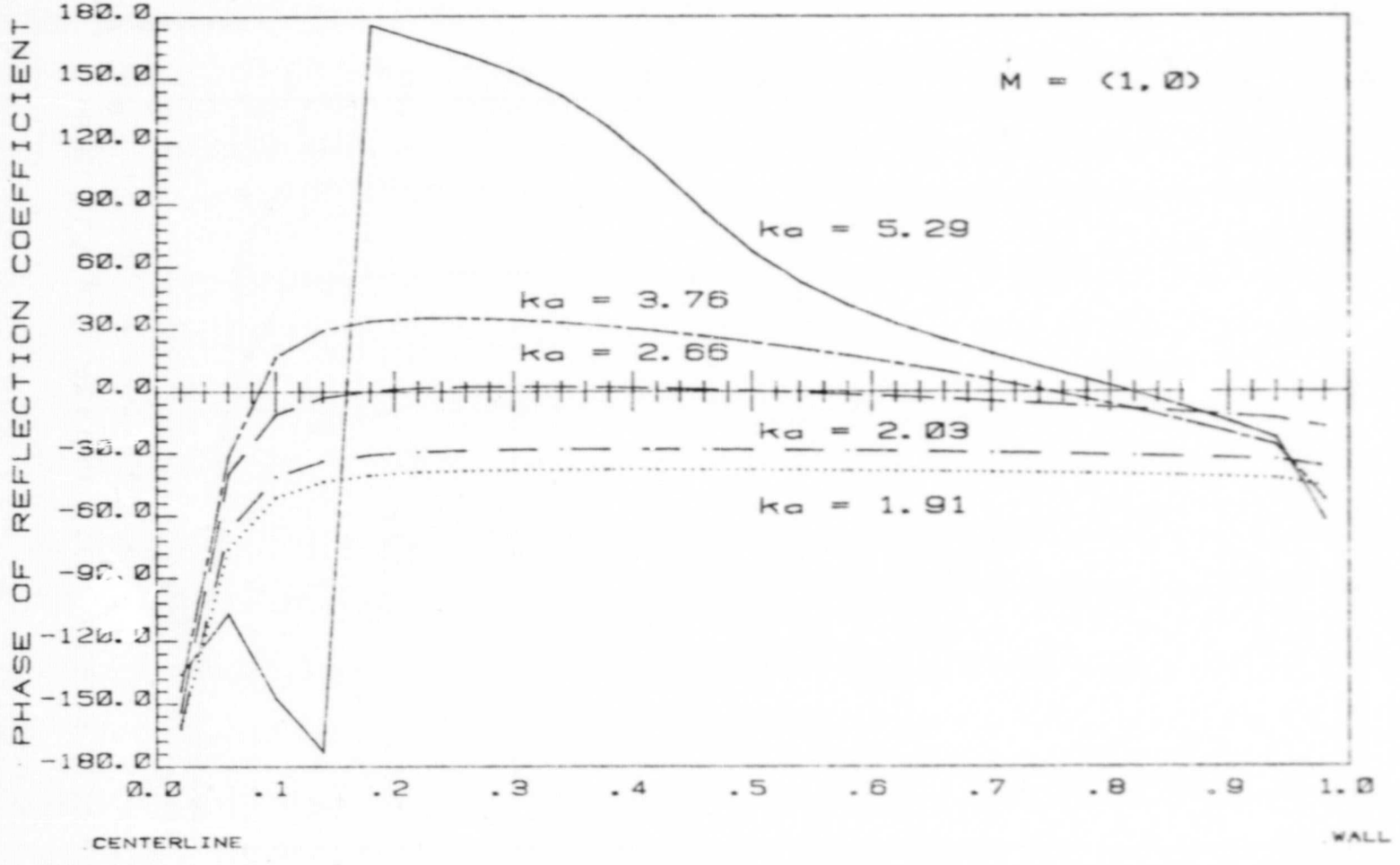

LANGLEY BELLMOUTH (Exit Plane)

Fig. 22

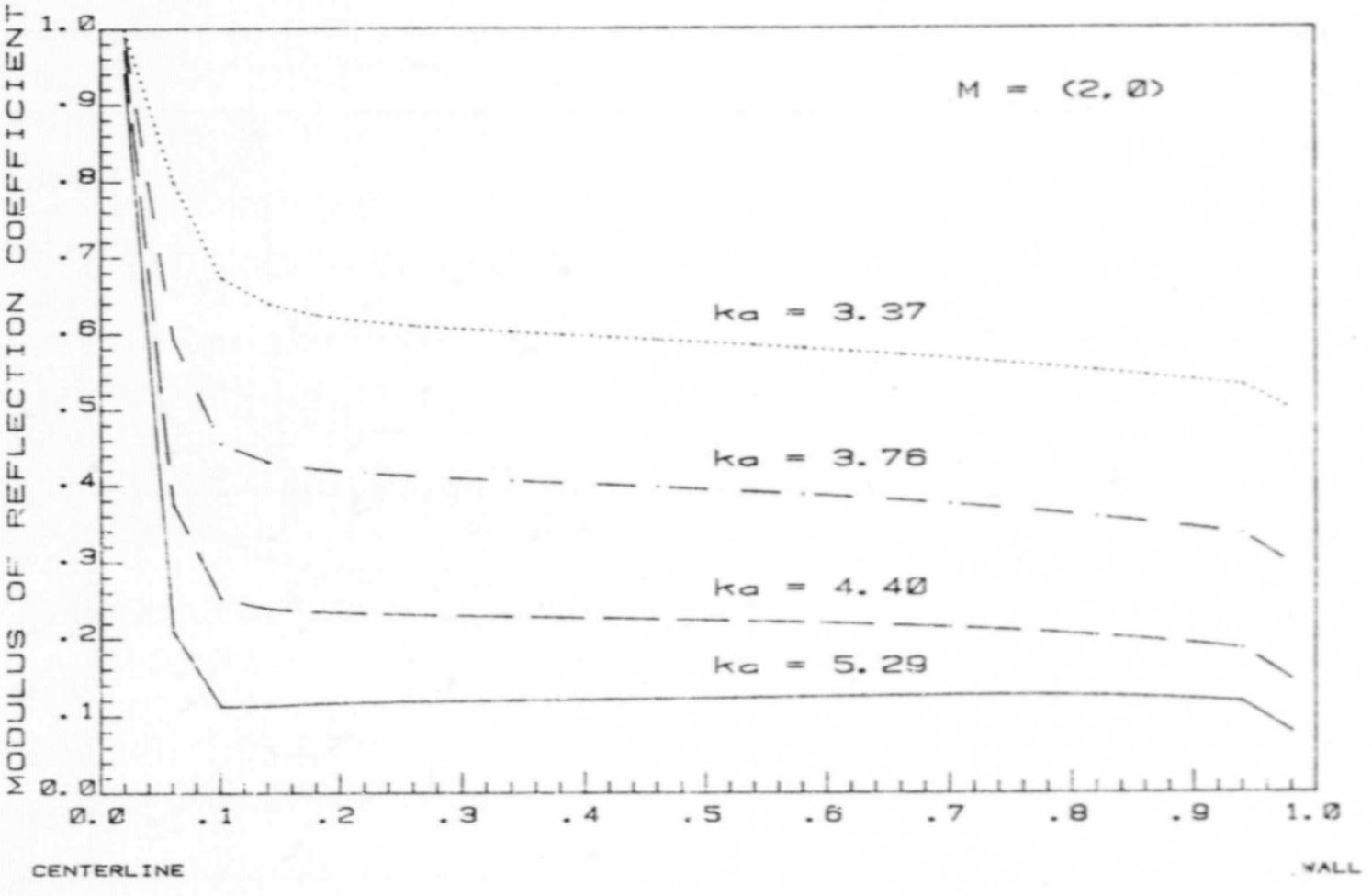

LANGLEY BELLMOUTH (Exit Plane)

Fig. 23

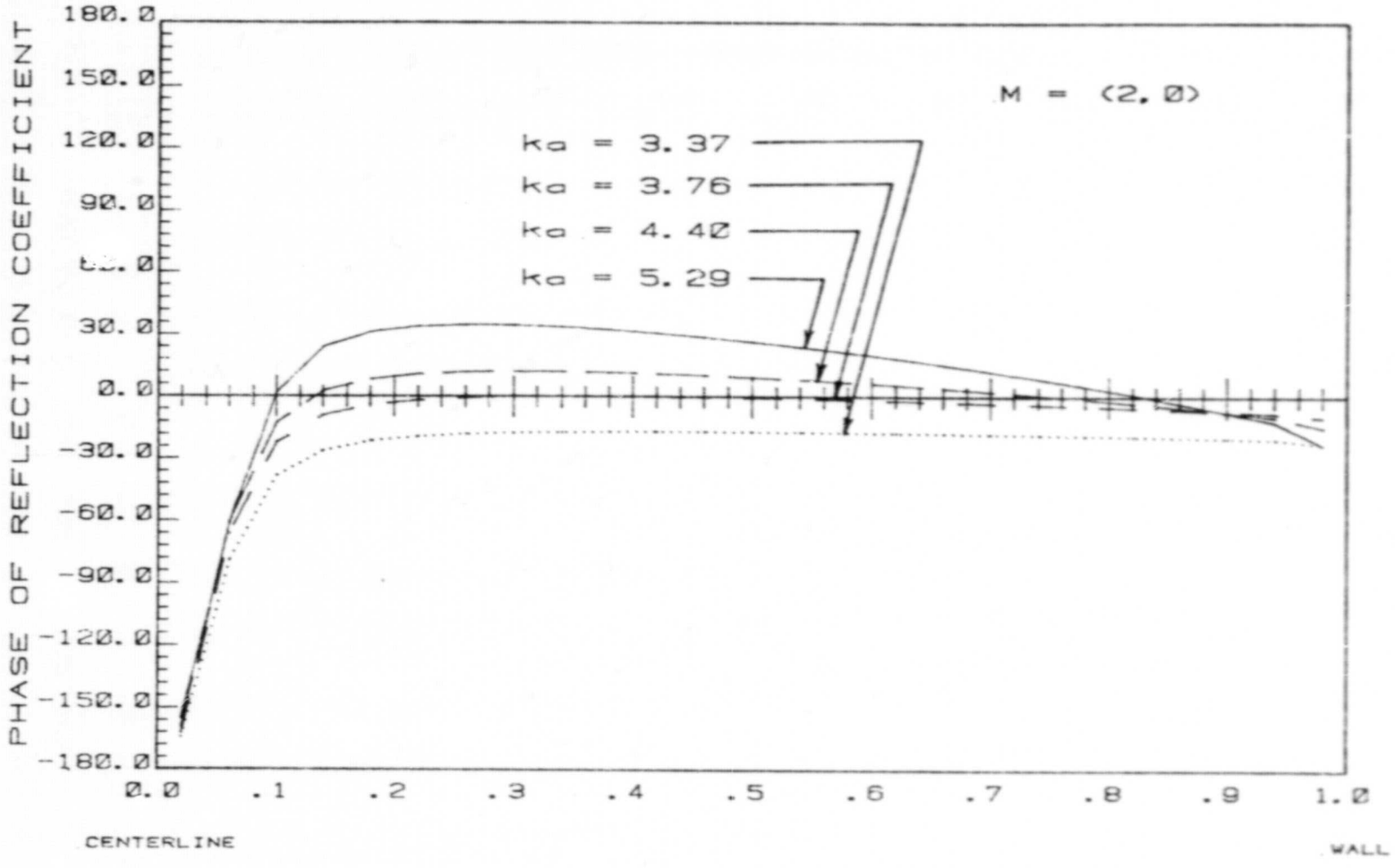

LANGLEY BELLMOUTH (Exit Plane)

Fig. 24

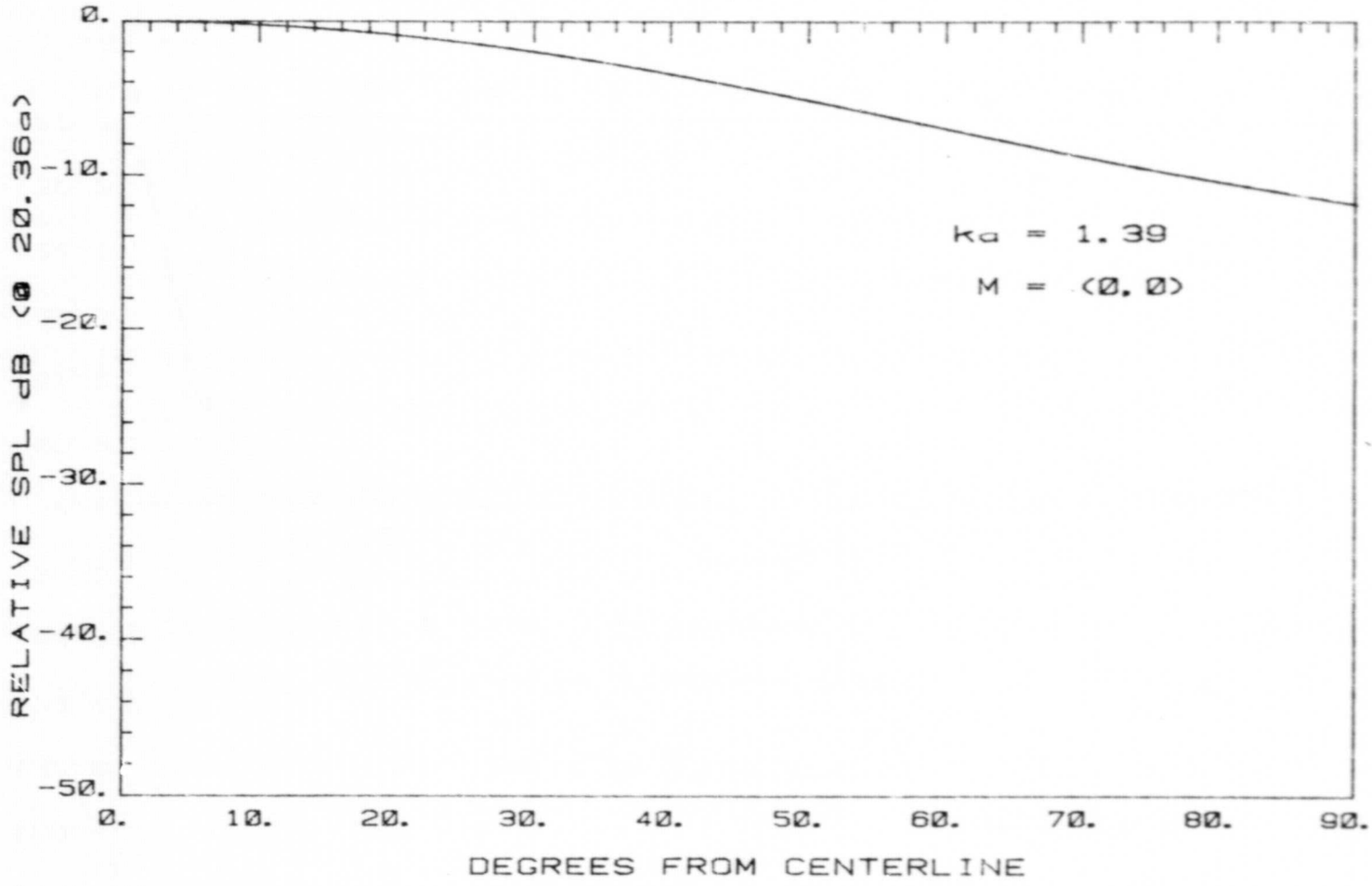

LANGLEY BELLMOUTH

Fig. 25

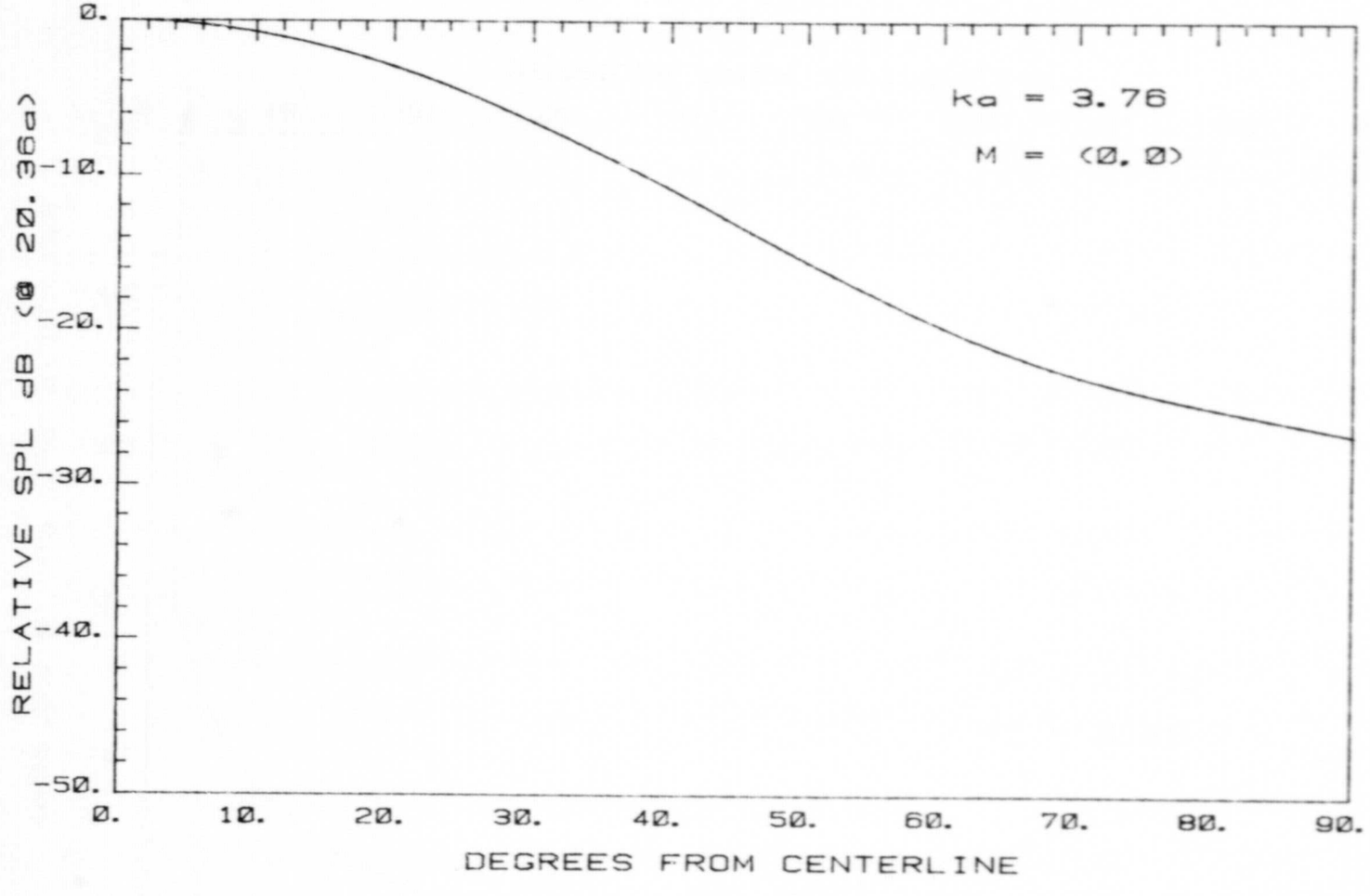

LANGLEY BELLMOUTH

Fig. 26

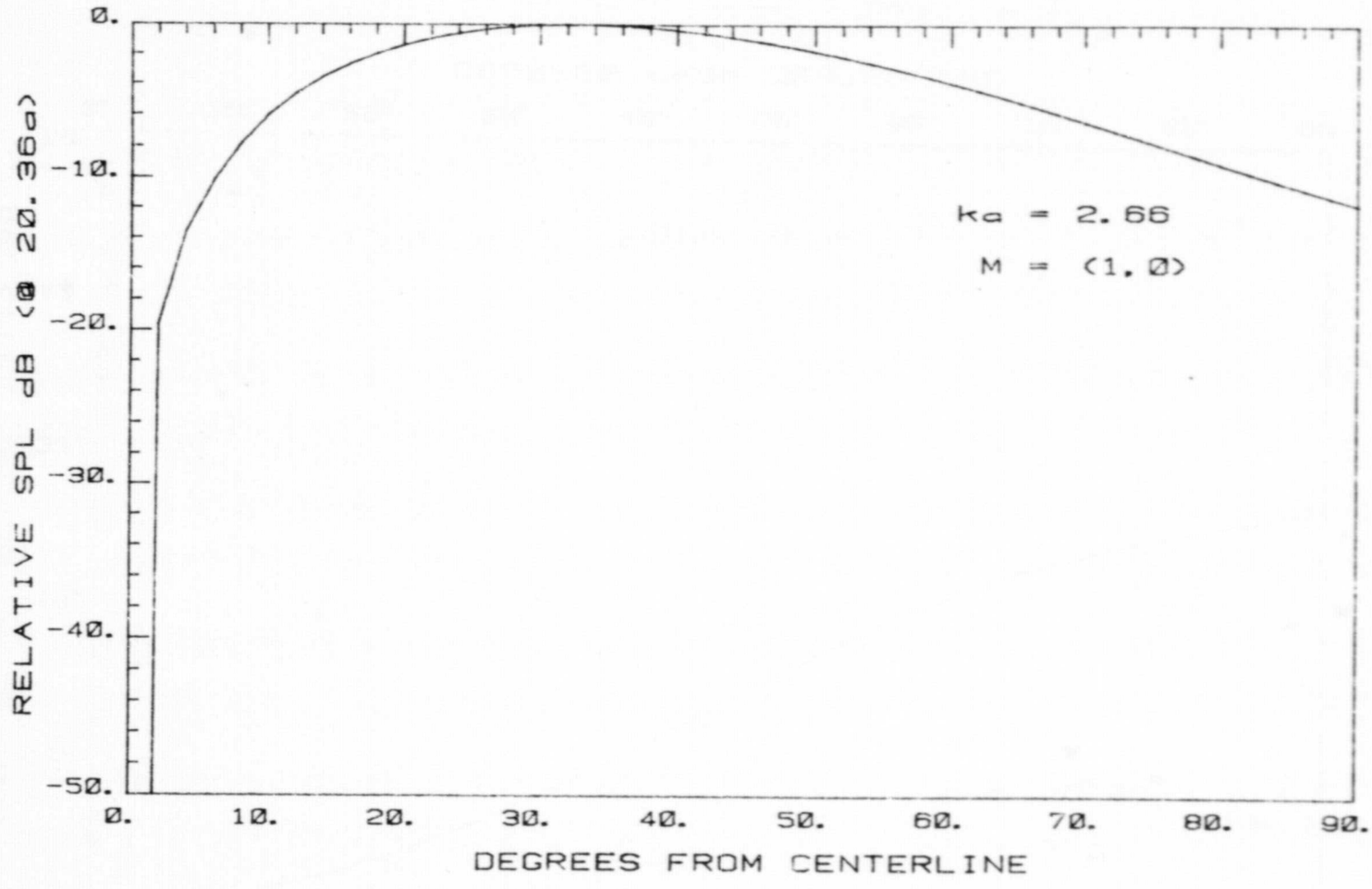

LANGLEY BELLMOUTH

Fig. 27

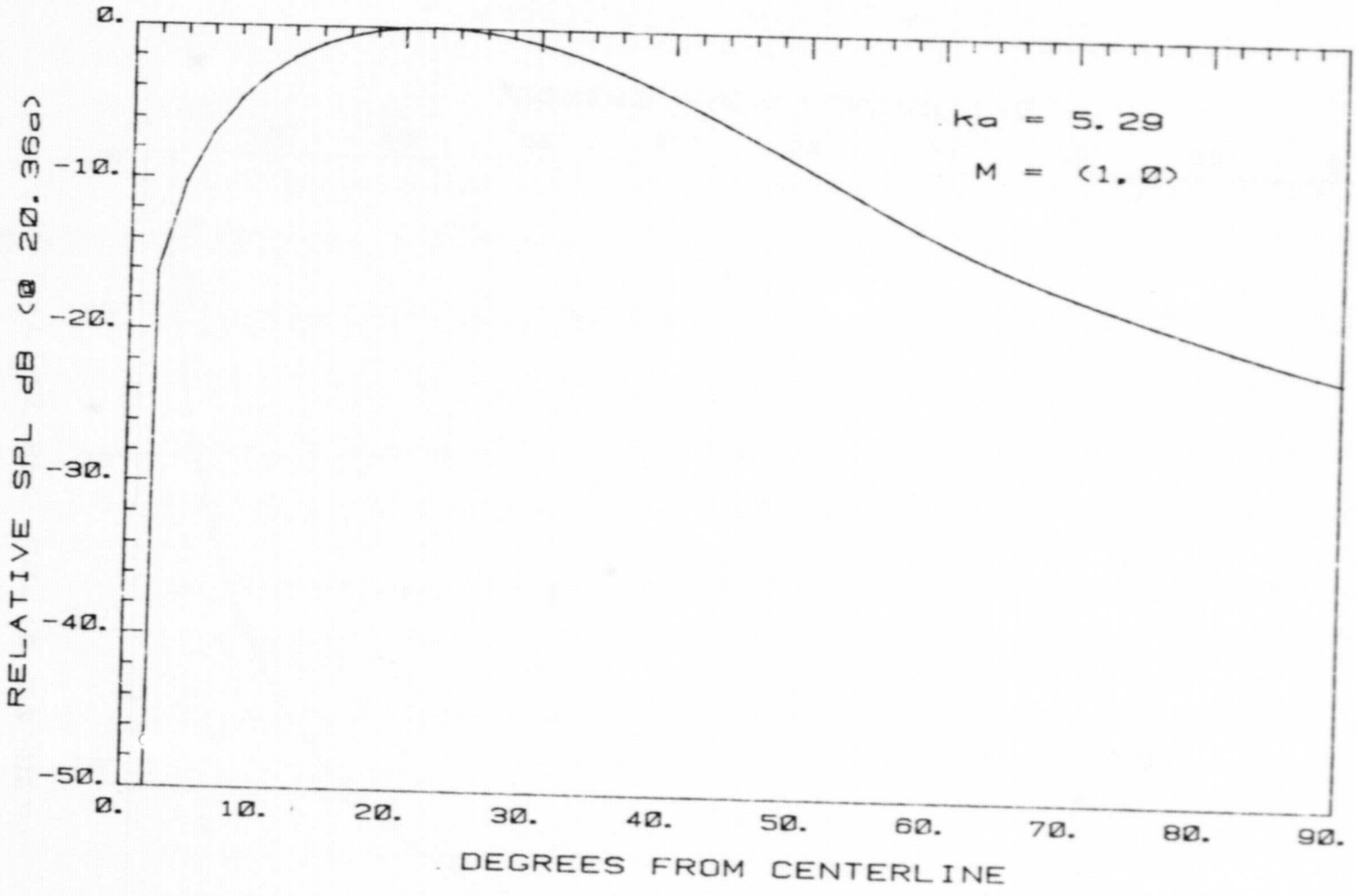

LANGLEY BELLMOUTH

Fig. 28

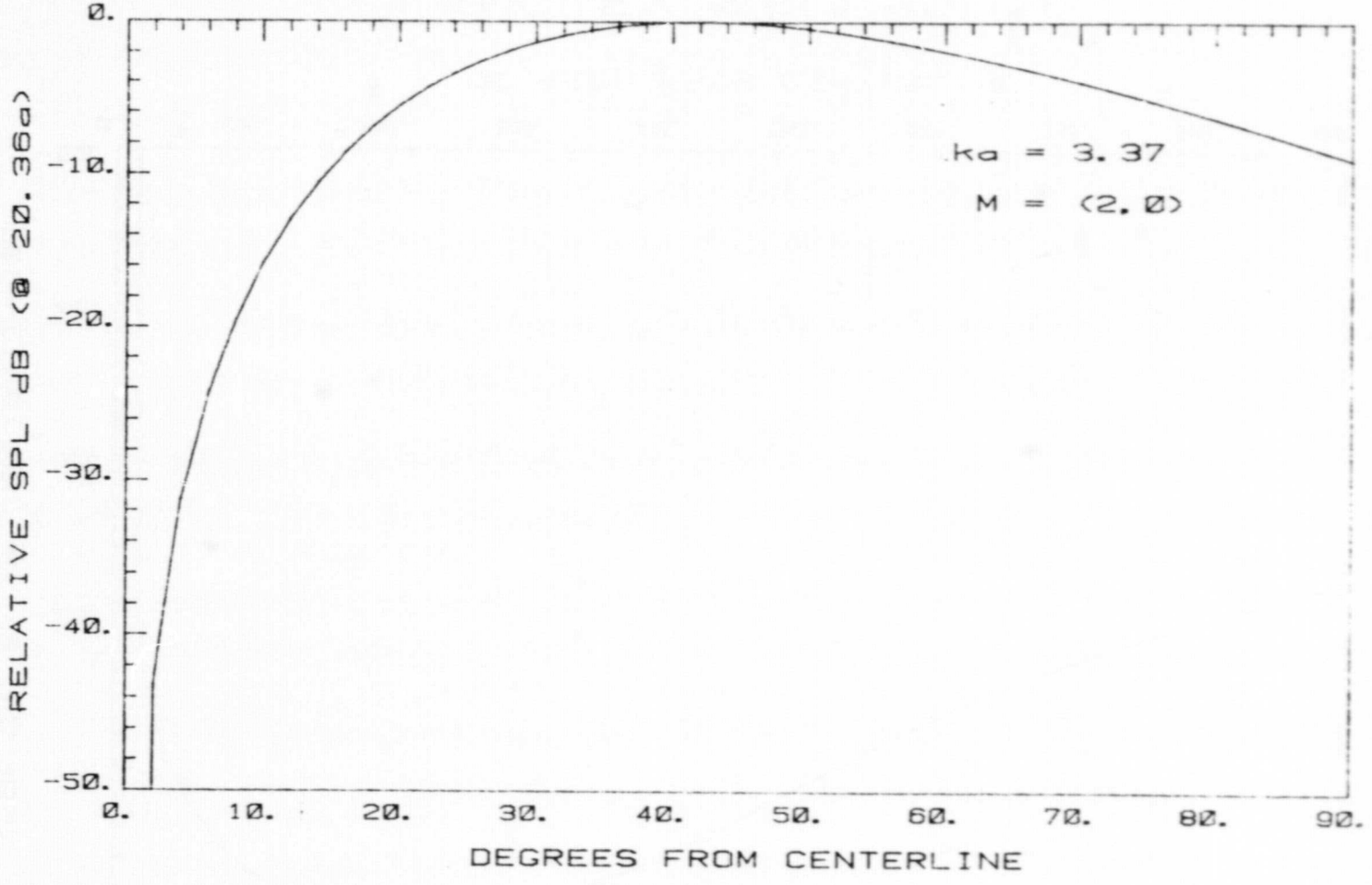

LANGLEY BELLMOUTH

Fig. 29

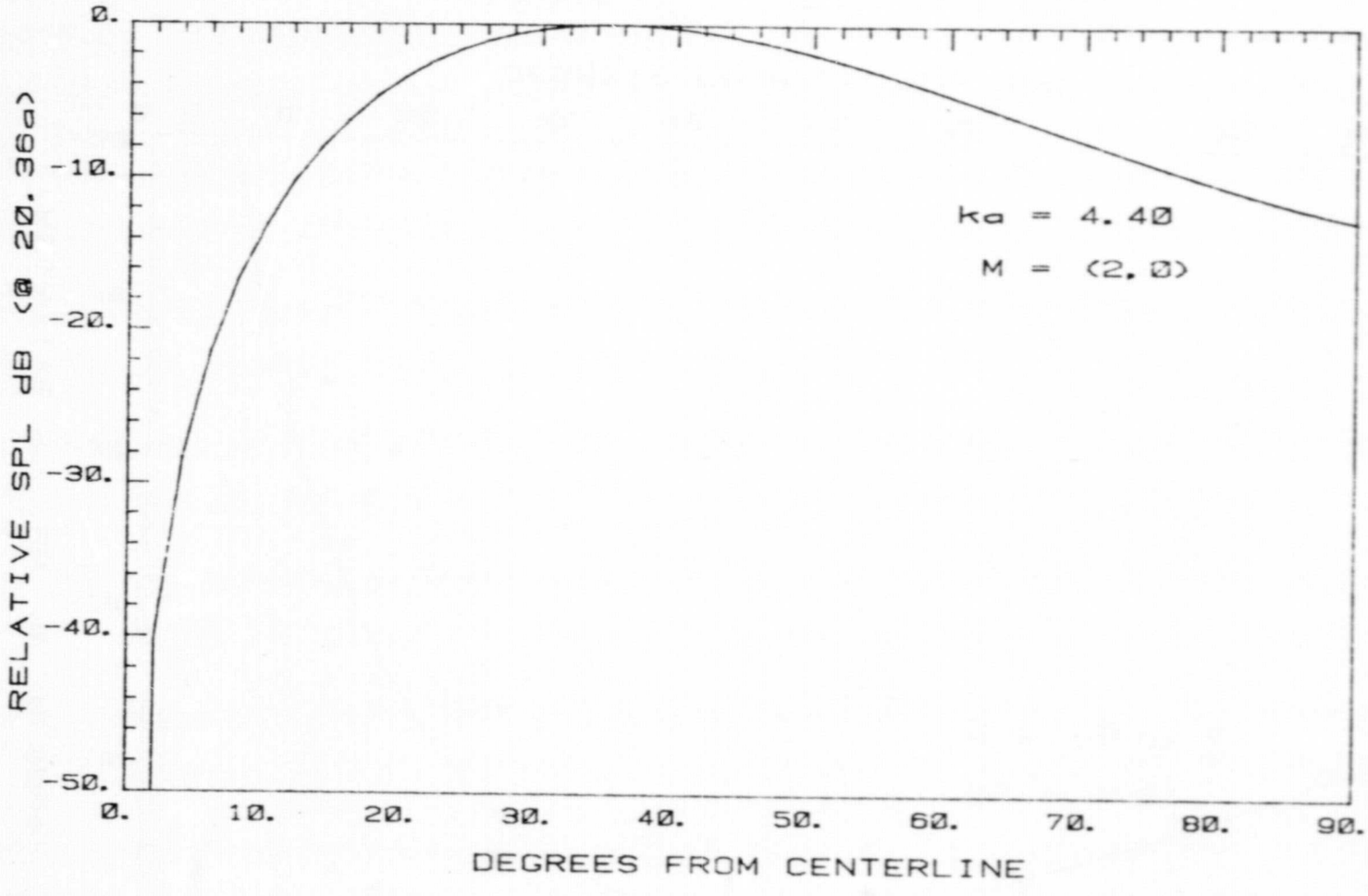

LANGLEY BELLMOUTH

Fig. 30

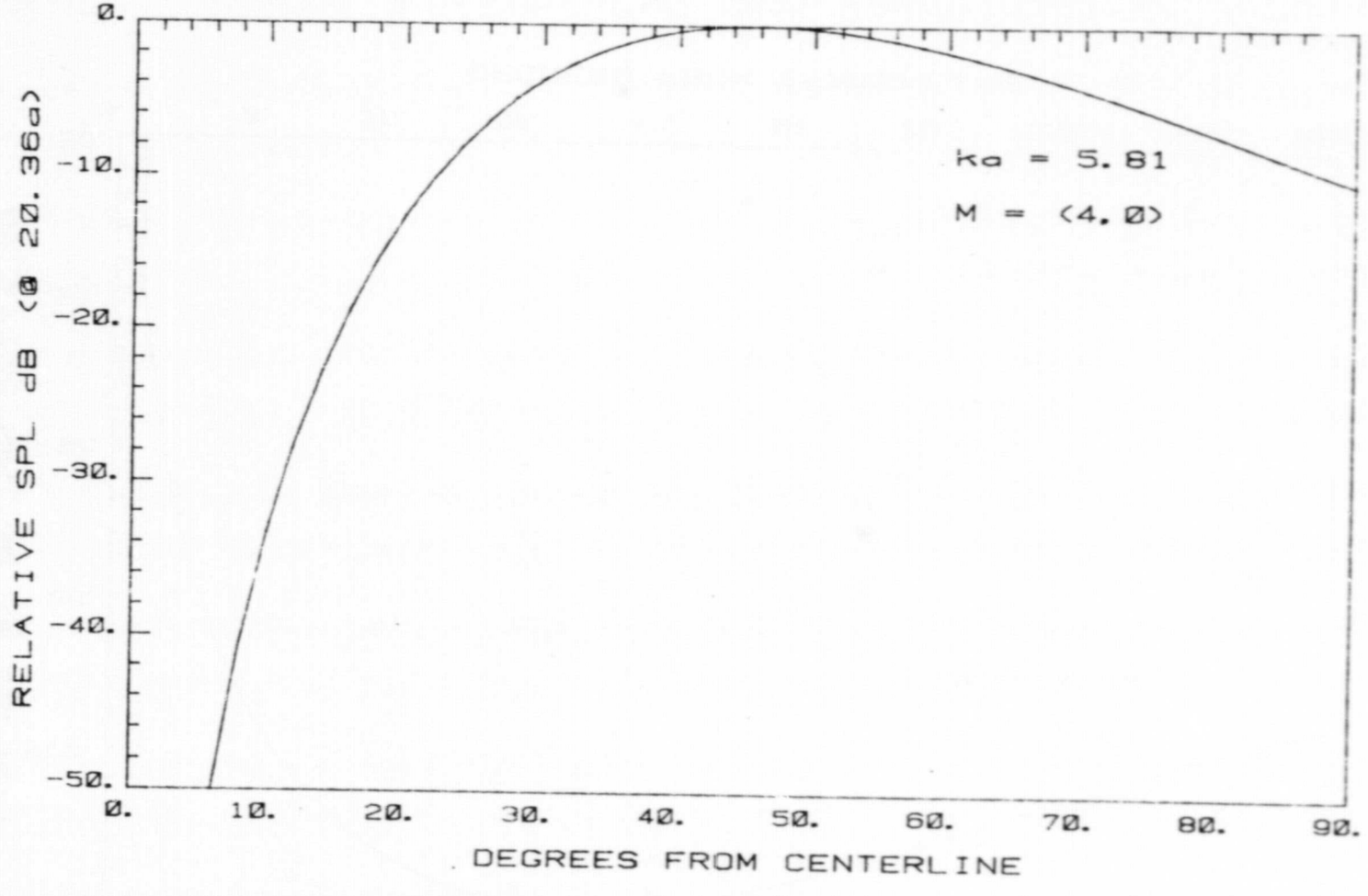

LANGLEY BELLMOUTH

Fig. 31

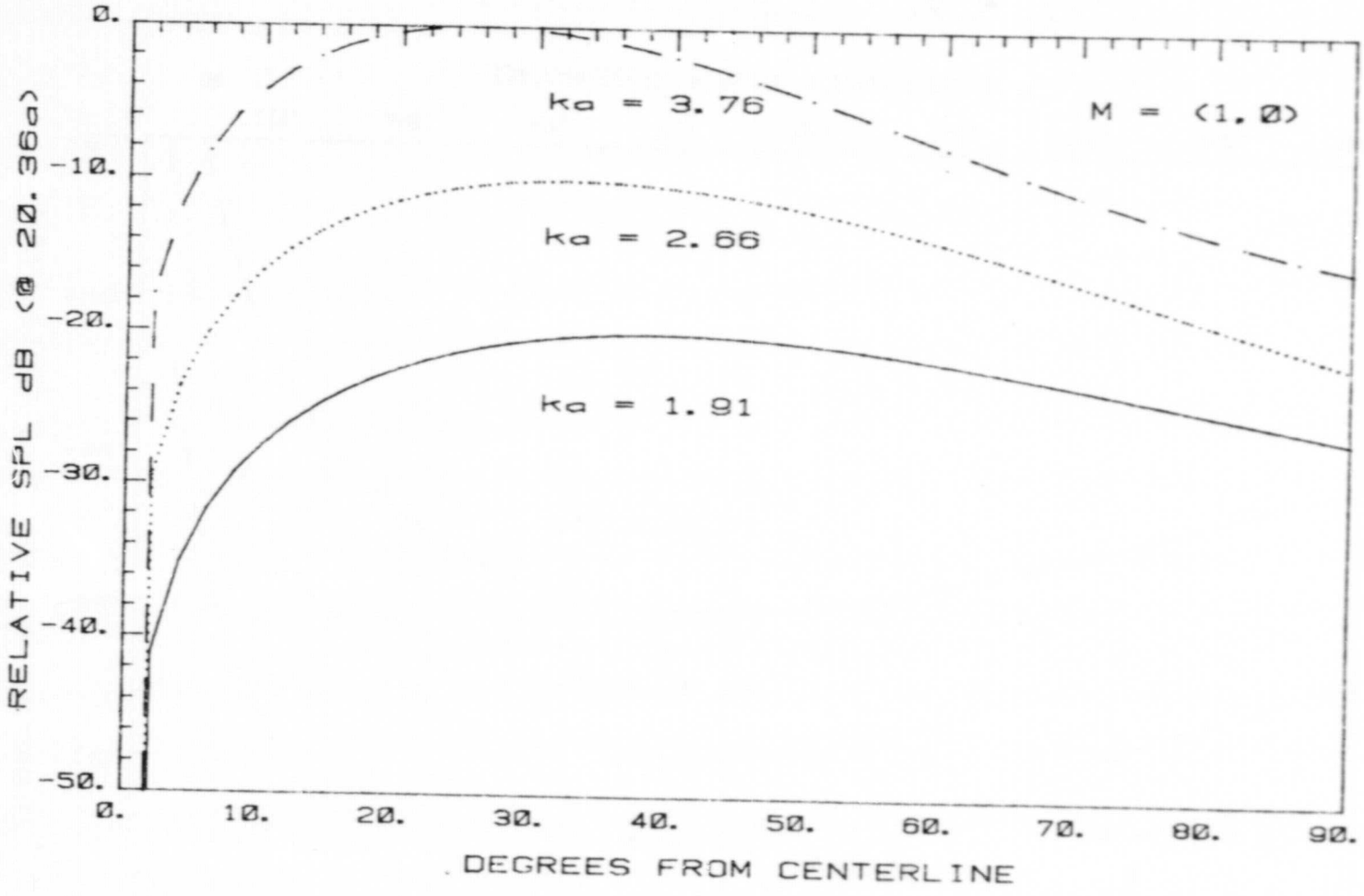

LANGLEY BELLMOUTH

Fig. 32

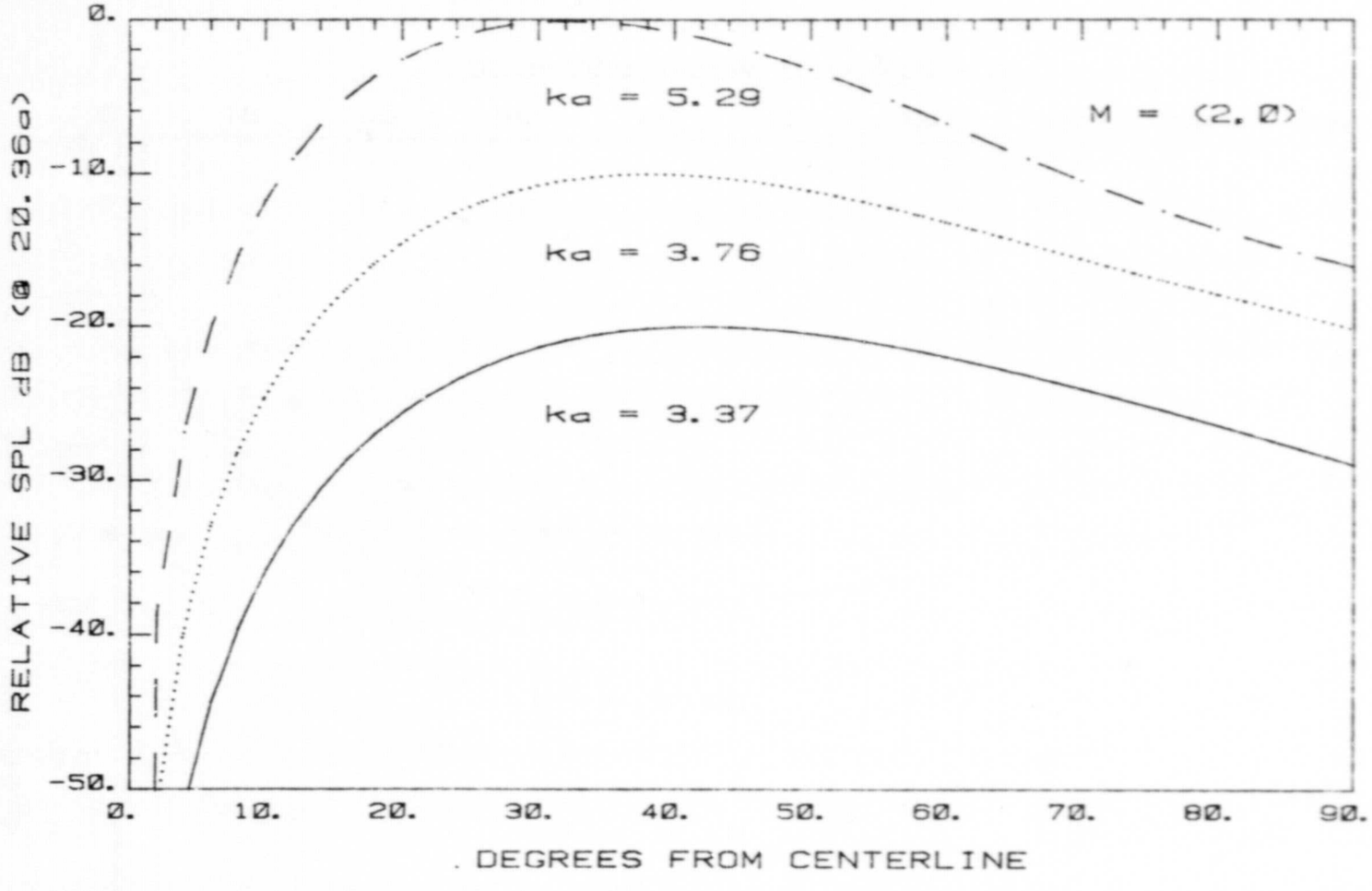

LANGLEY BELLMOUTH

Fig. 33

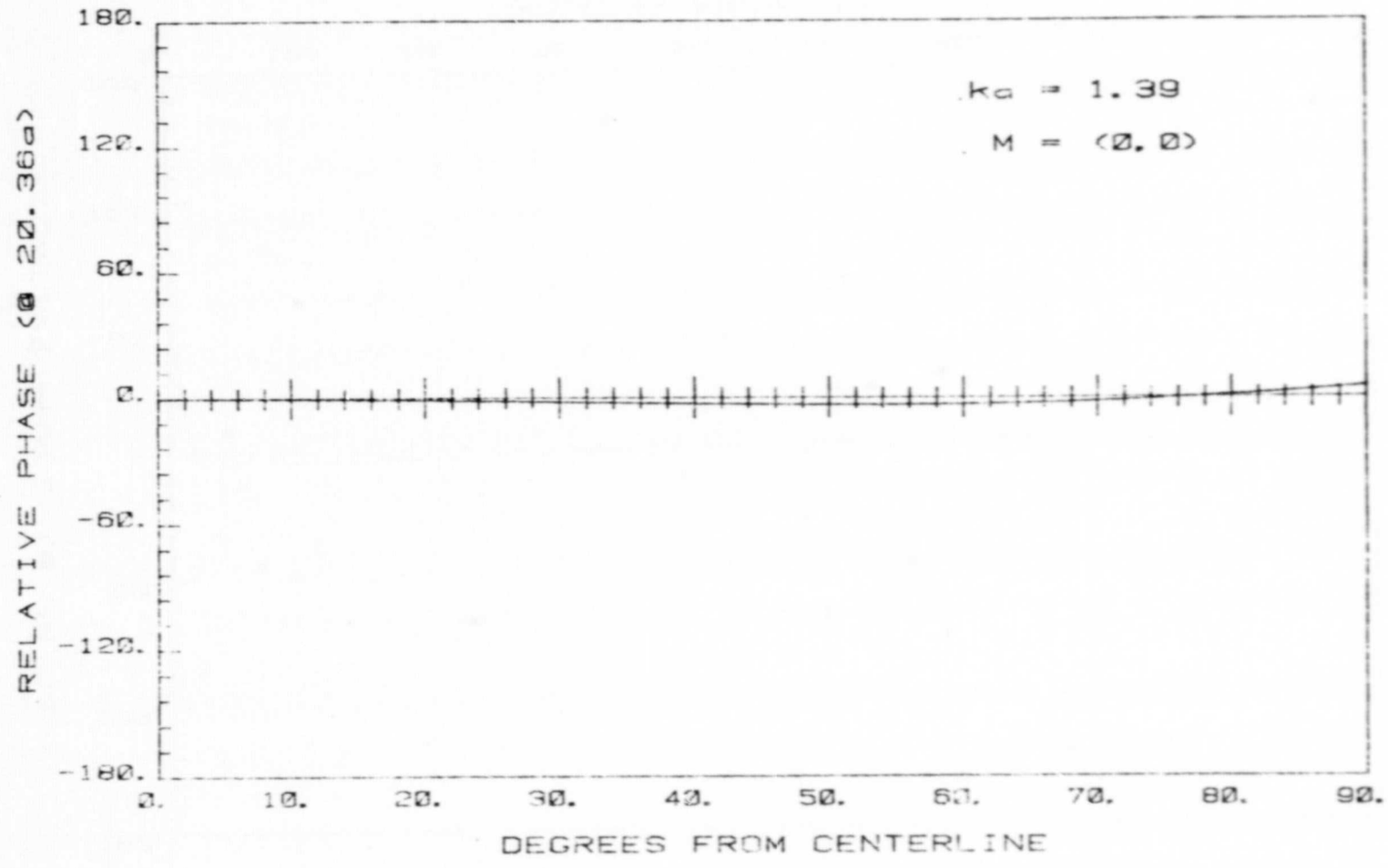

LANGLEY BELLMOUTH

Fig. 34

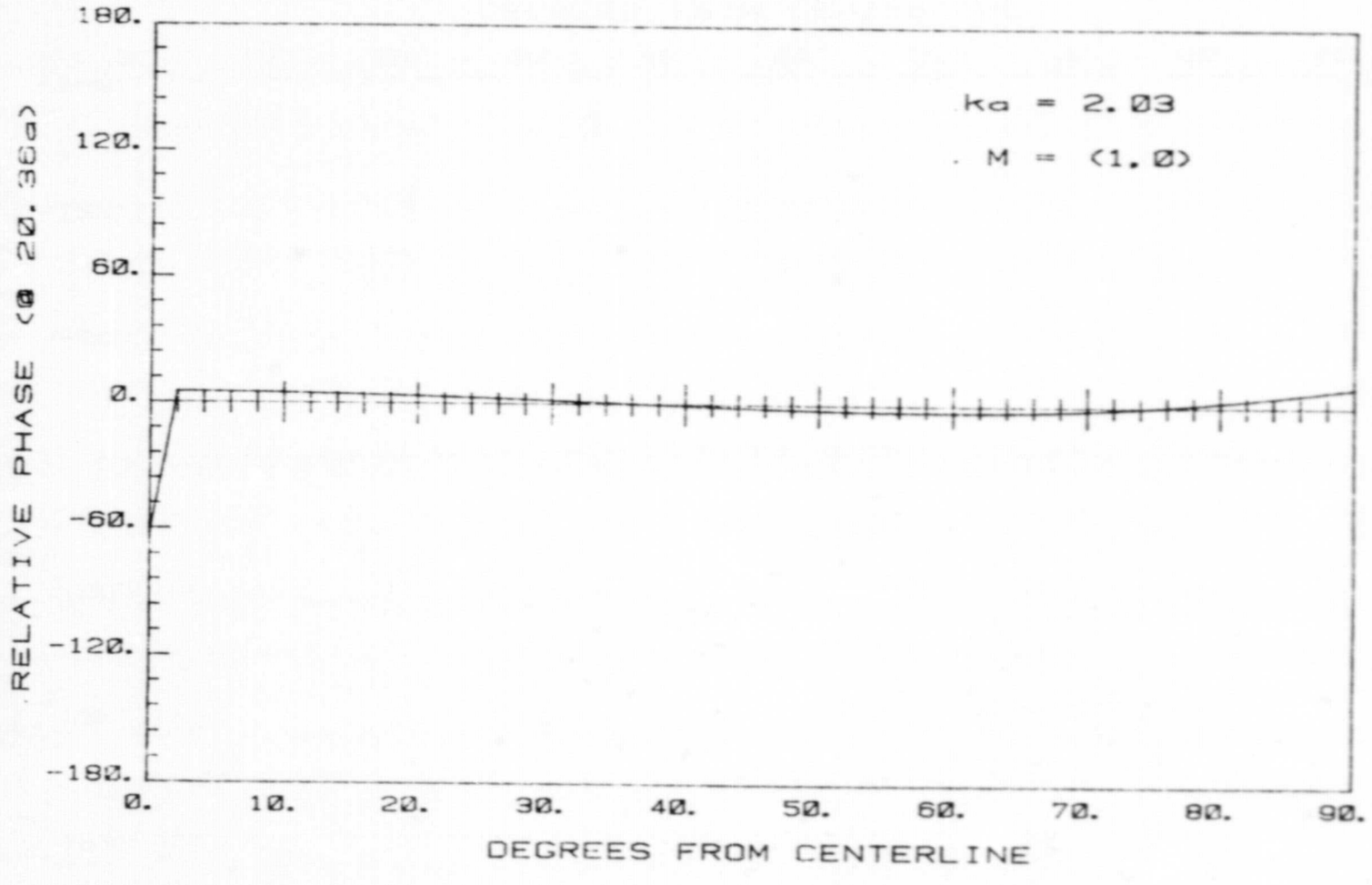

LANGLEY BELLMOUTH

Fig. 35

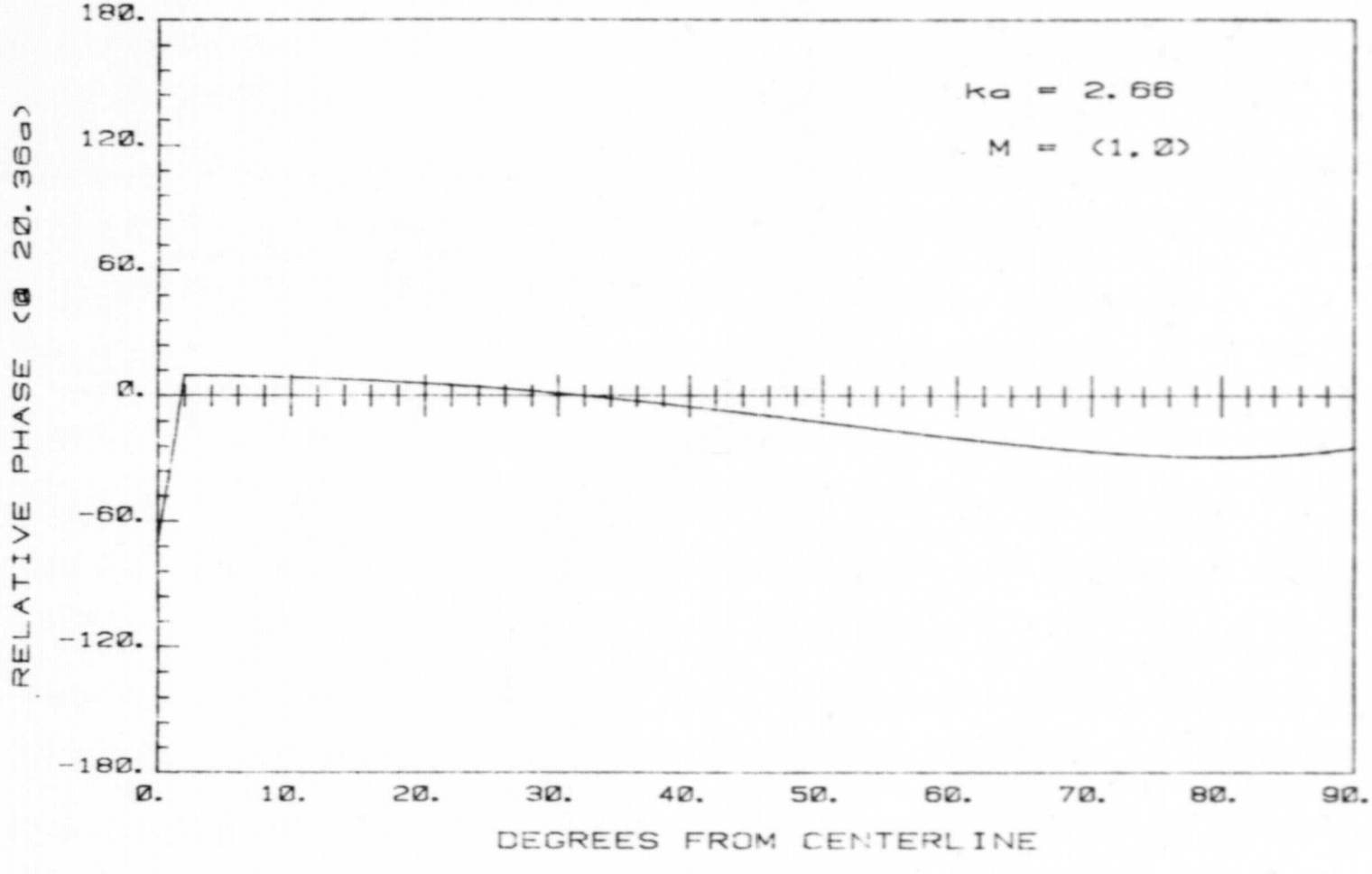

LANGLEY BELLMOUTH

Fig. 36

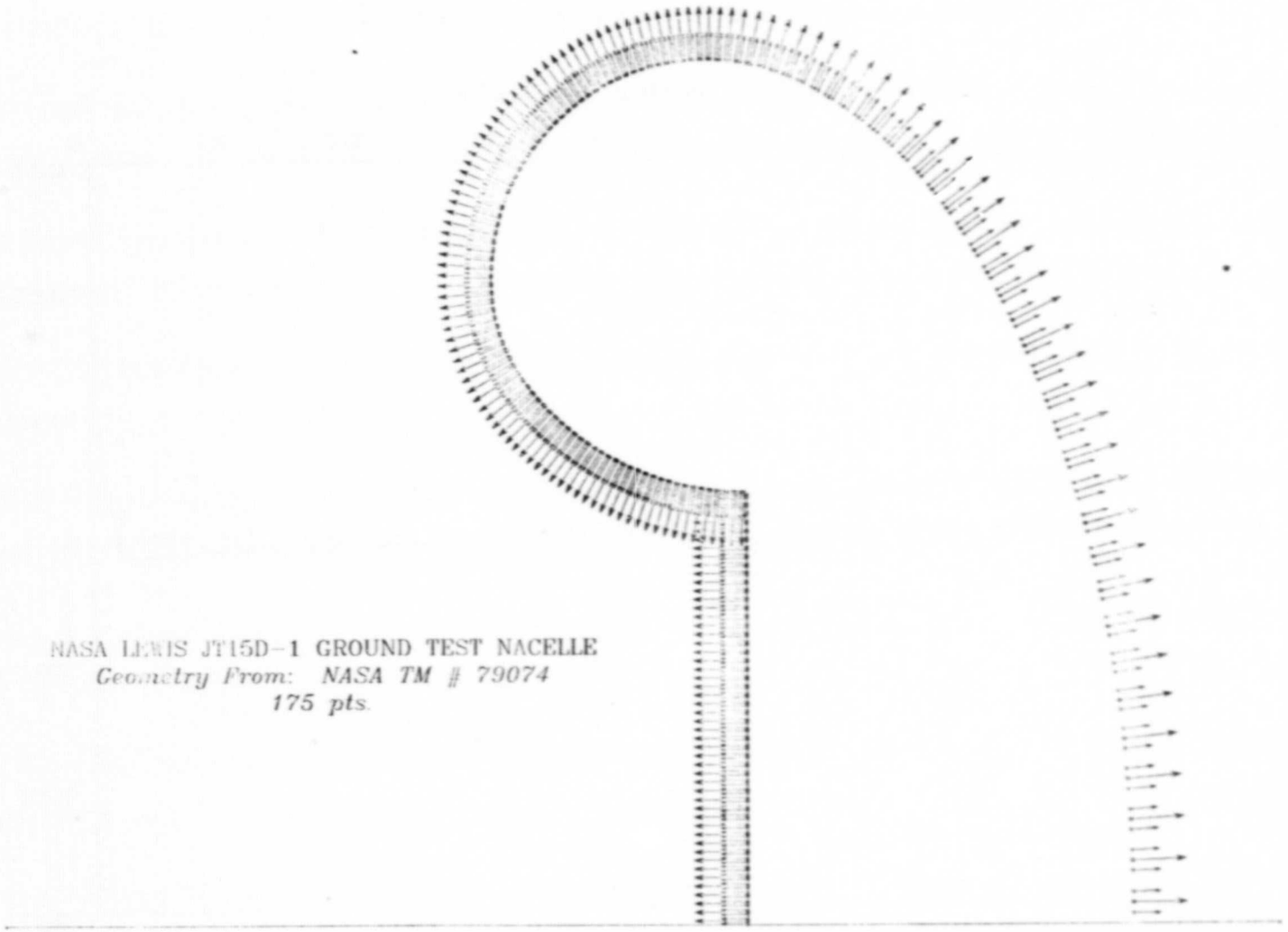

Fig. 37 Lewis JT15D-1 Geometry used for Computer Calculations.

LEWIS JT15D-1

Deg	SPL	Deg	SPL
0	0	46	114
2	0	48	115
4	0	50	116
6	-71	52	117
8	-39	54	117
10	-14	56	117
12	4	58	117
14	20	60	117
16	31	62	117
18	46	64	116
20	56	66	116
22	65	68	116
24	73	70	115
26	79	72	114
28	85	74	114
30	91	76	113
32	95	78	112
34	99	80	112
36	103	82	111
38	106	84	110
40	108	86	109
42	111	88	109
44	112	90	108

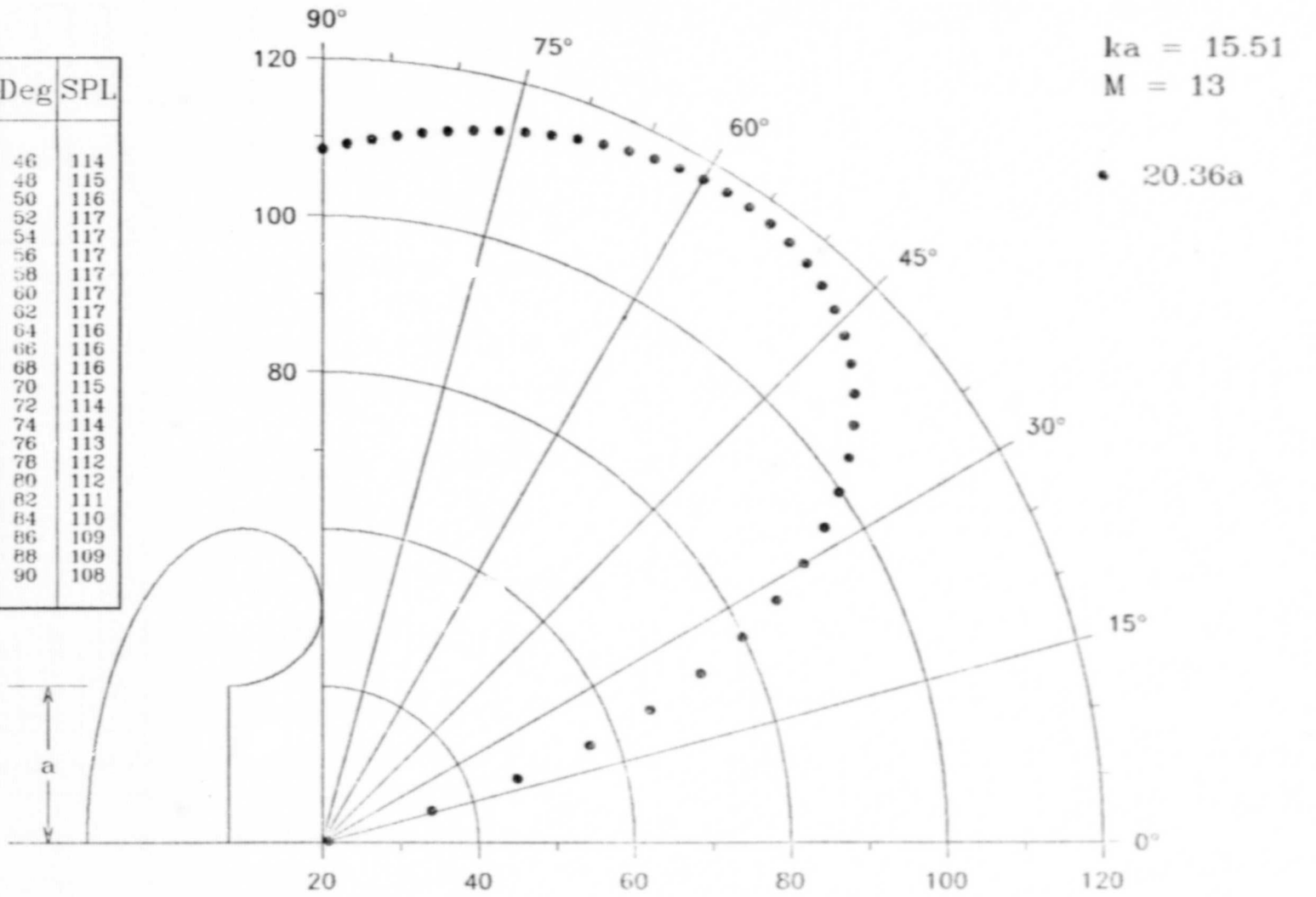

Fig. 38 SPL (dB)

LEWIS JT15D-1

Deg	SPL	Deg	SPL
0	0	46	125
2	0	48	125
4	-89	50	125
6	-44	52	125
8	-13	54	125
10	10	56	124
12	30	58	124
14	45	60	123
16	58	62	122
18	69	64	121
20	79	66	120
22	87	68	119
24	94	70	118
26	100	72	117
28	105	74	116
30	109	76	115
32	113	78	114
34	116	80	113
36	119	82	112
38	121	84	112
40	122	86	111
42	124	88	110
44	124	90	110

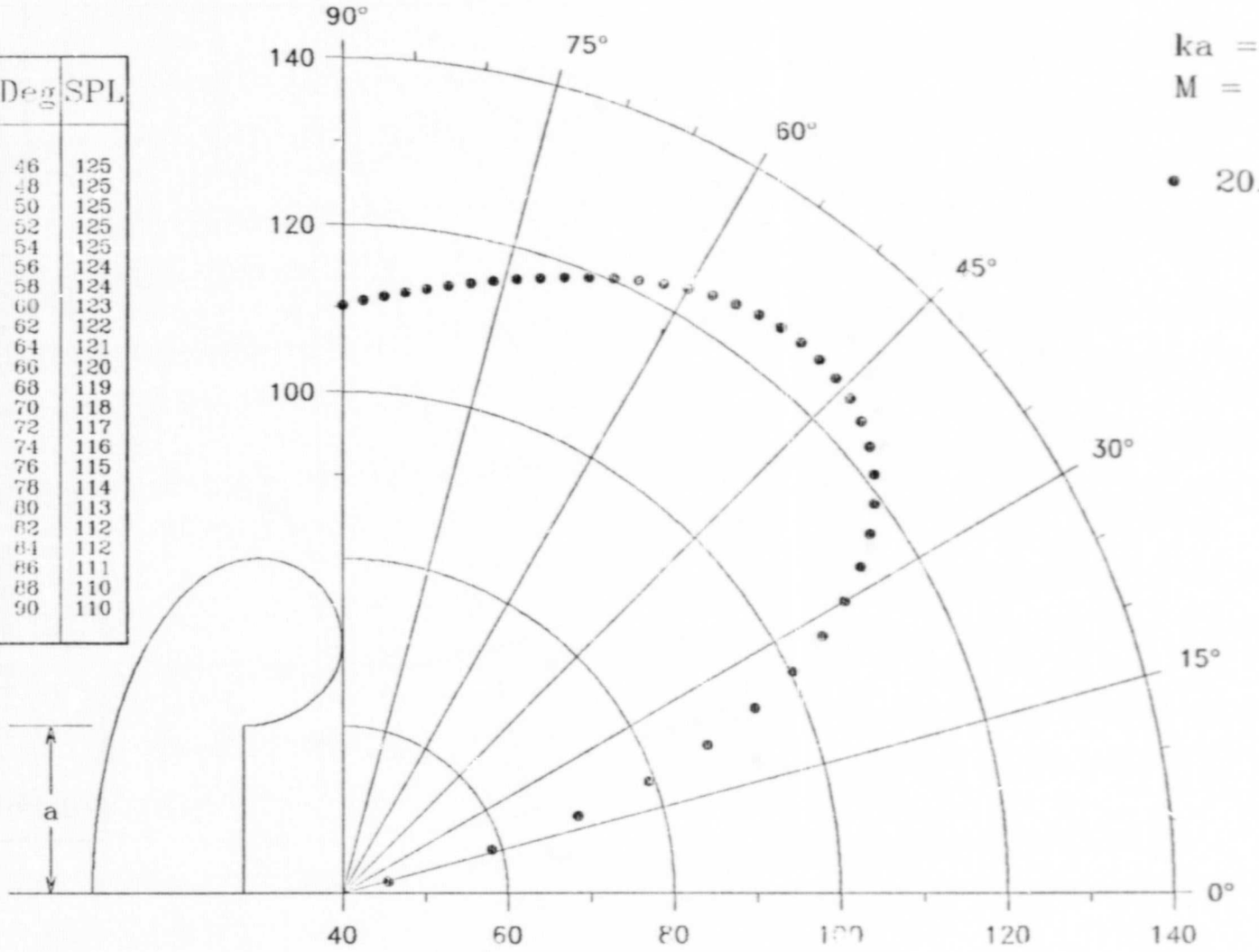

Fig. 39 SPL (dB)

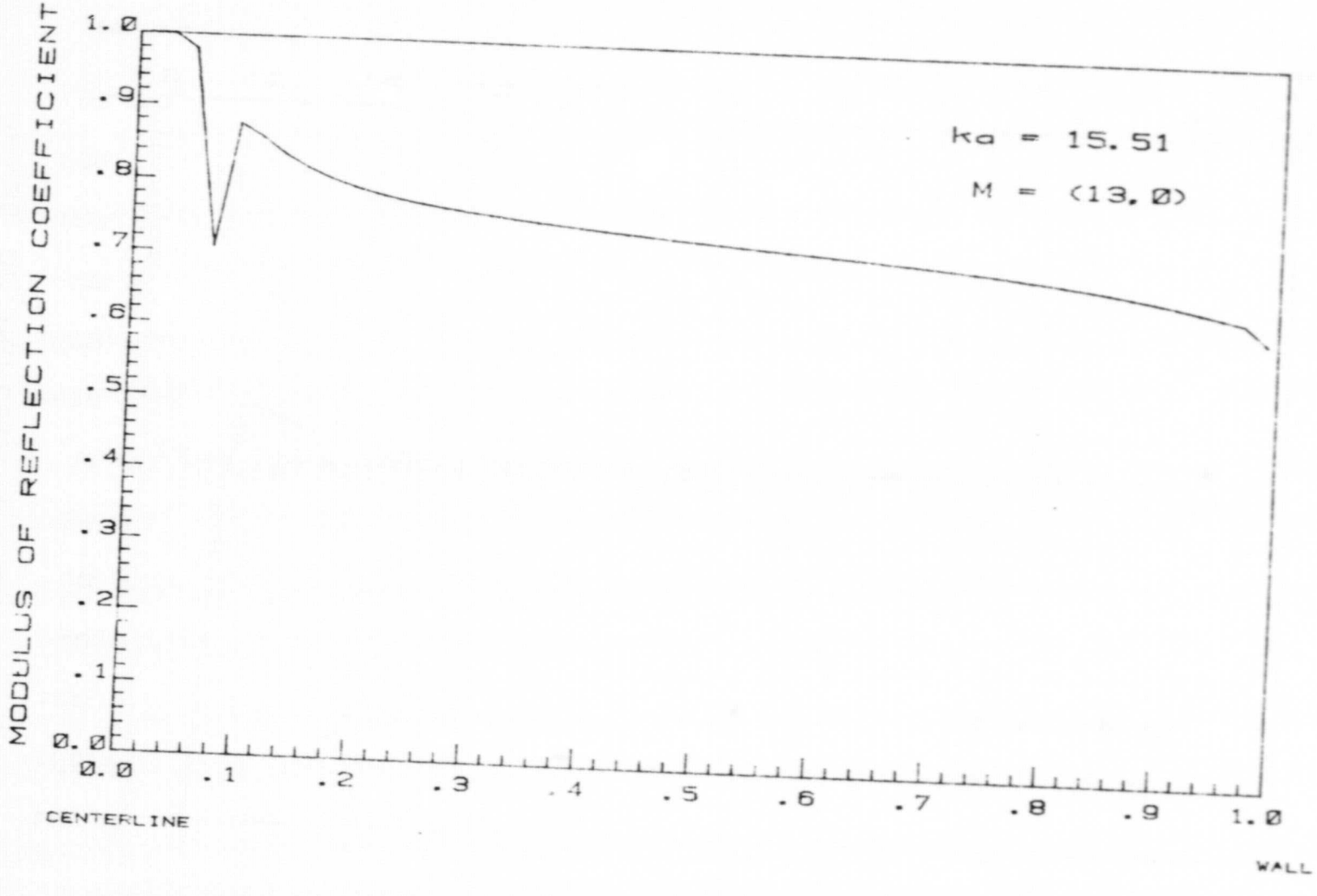

LEWIS JT15D-1 (Exit Plane)

Fig. 40

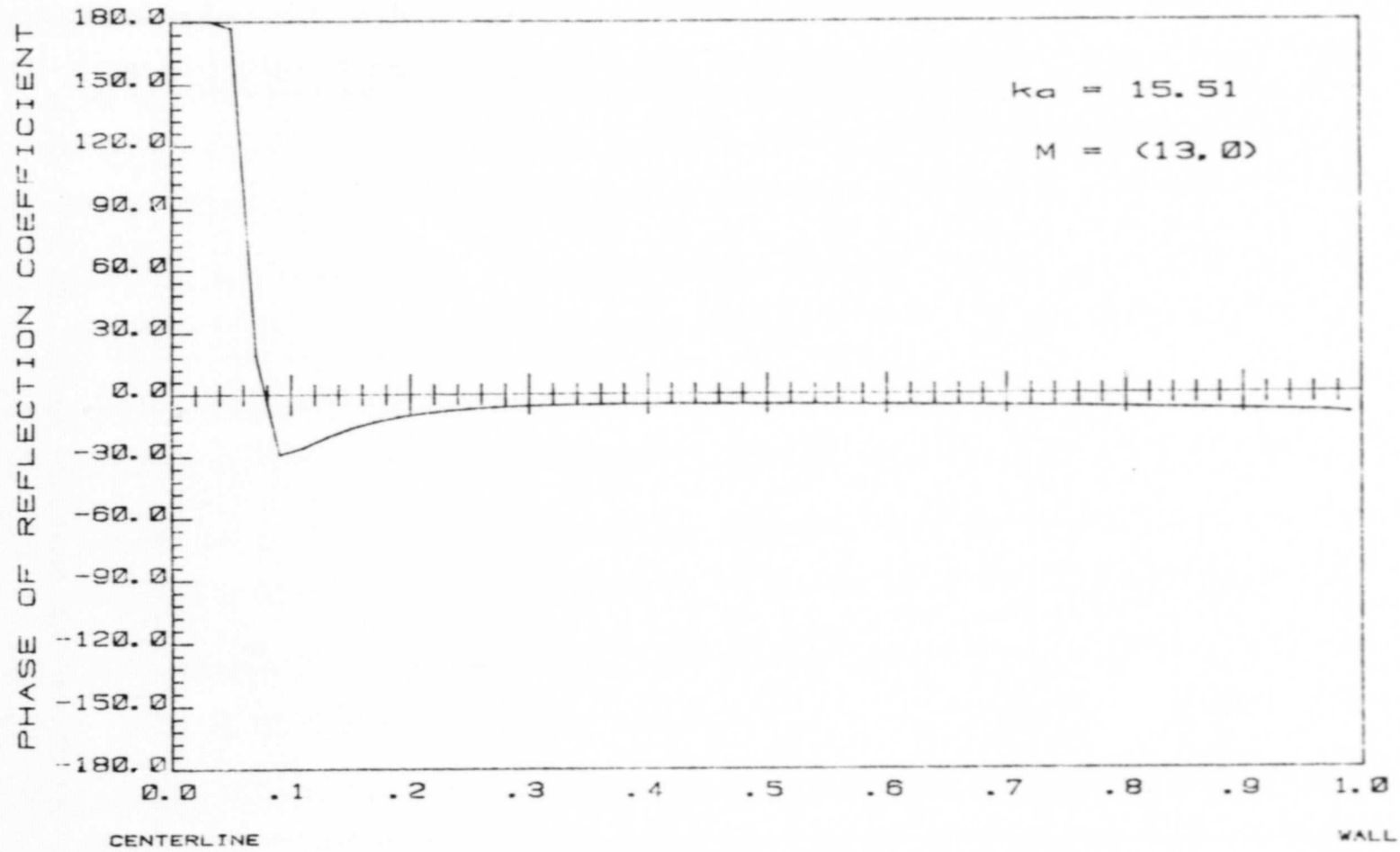

LEWIS JT15D-1 (Exit Plane)

Fig. 41

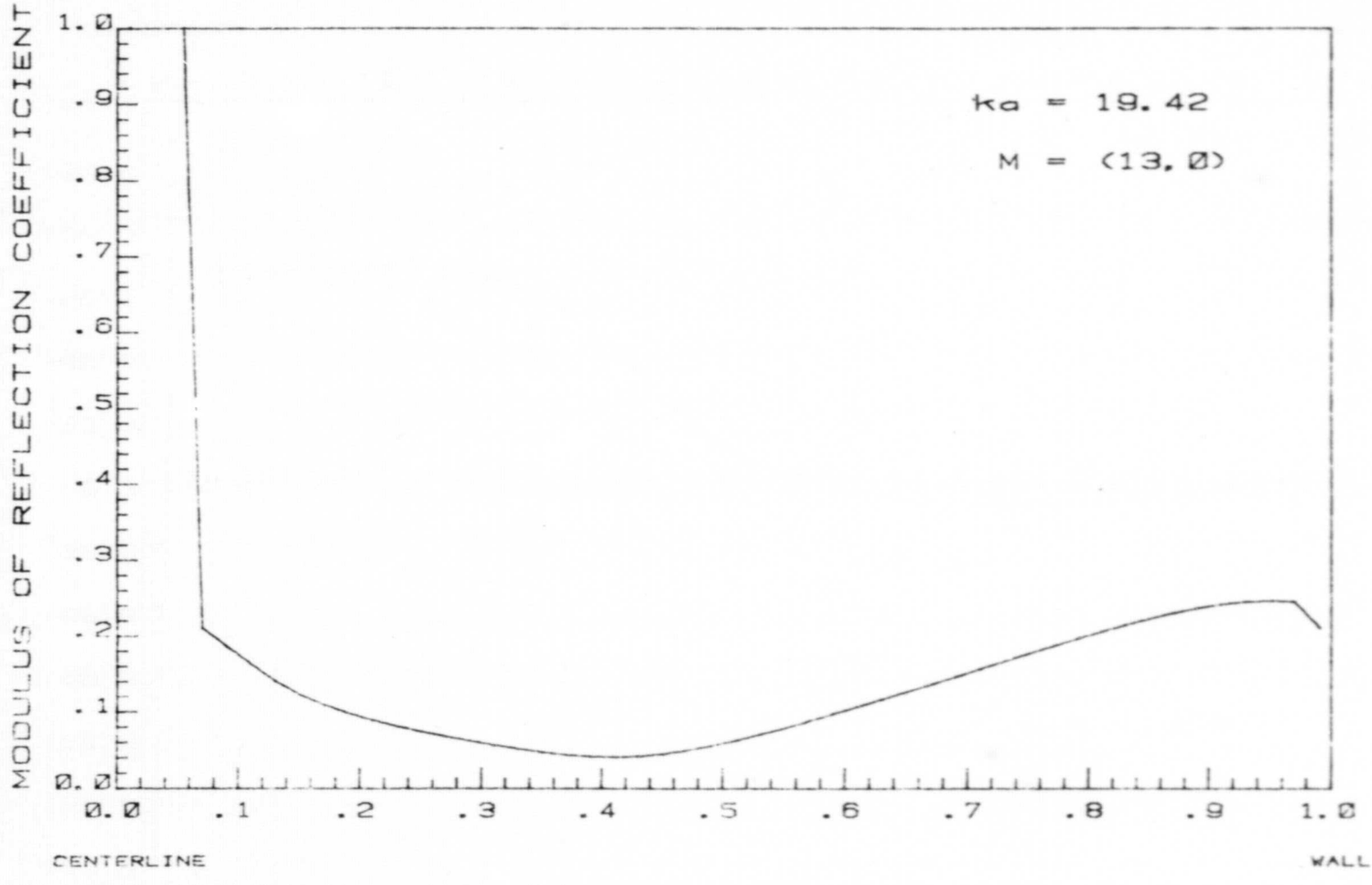

LEWIS JT15D-1 (Exit Plane)

Fig. 42

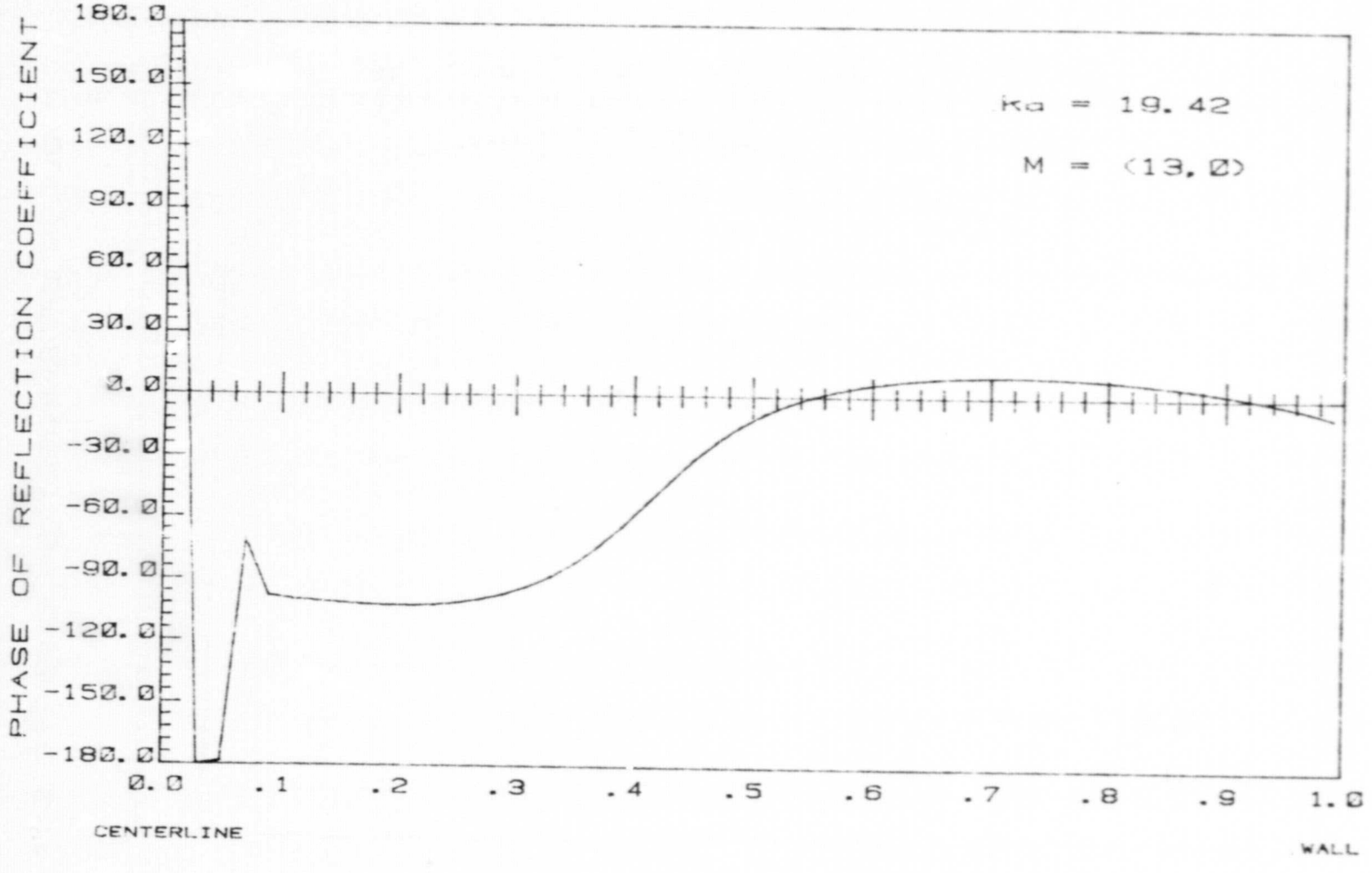

LEWIS JT15D-1 (Exit Plane)

Fig. 43

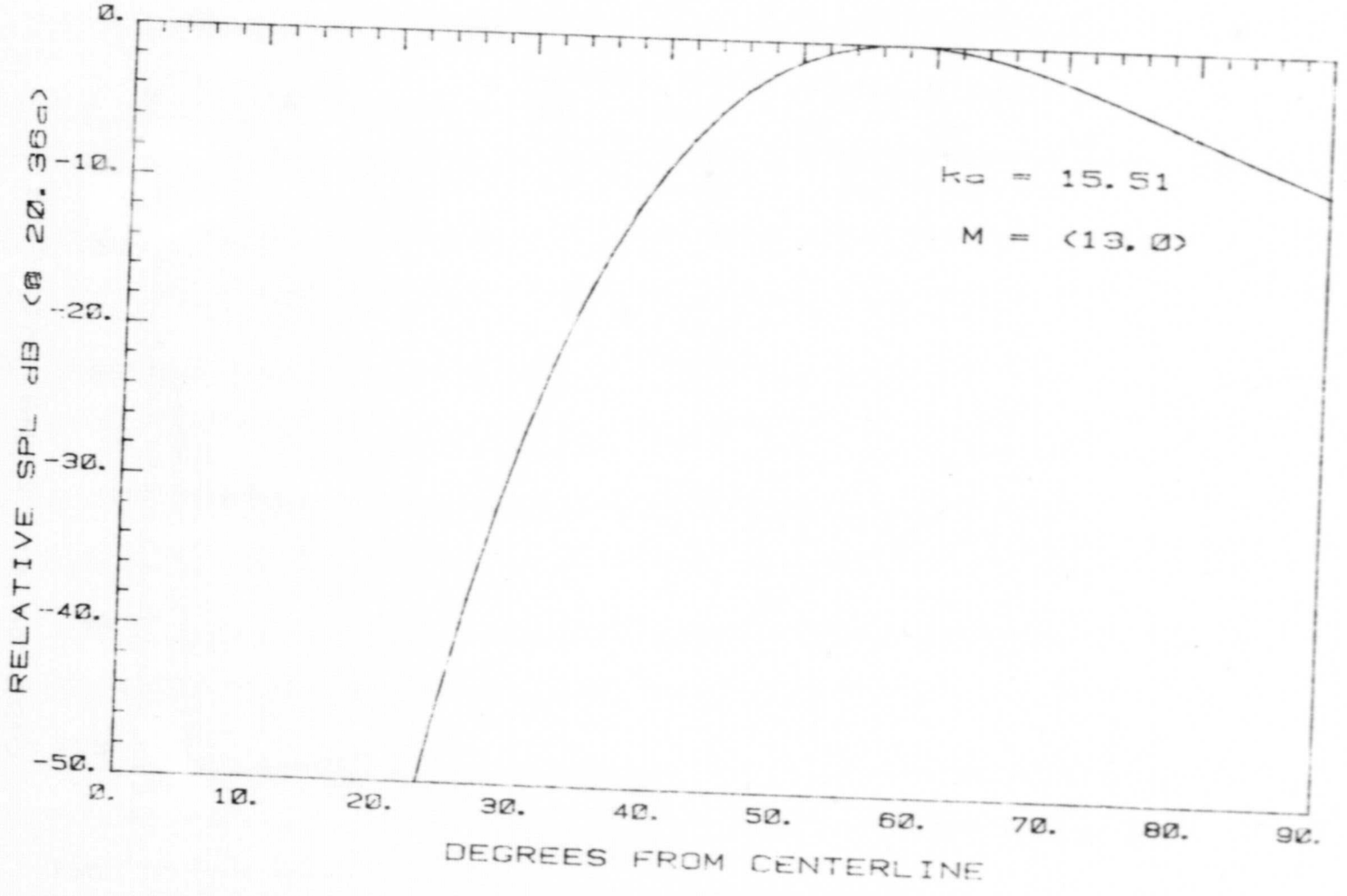

LEWIS JT15D-1

Fig. 44

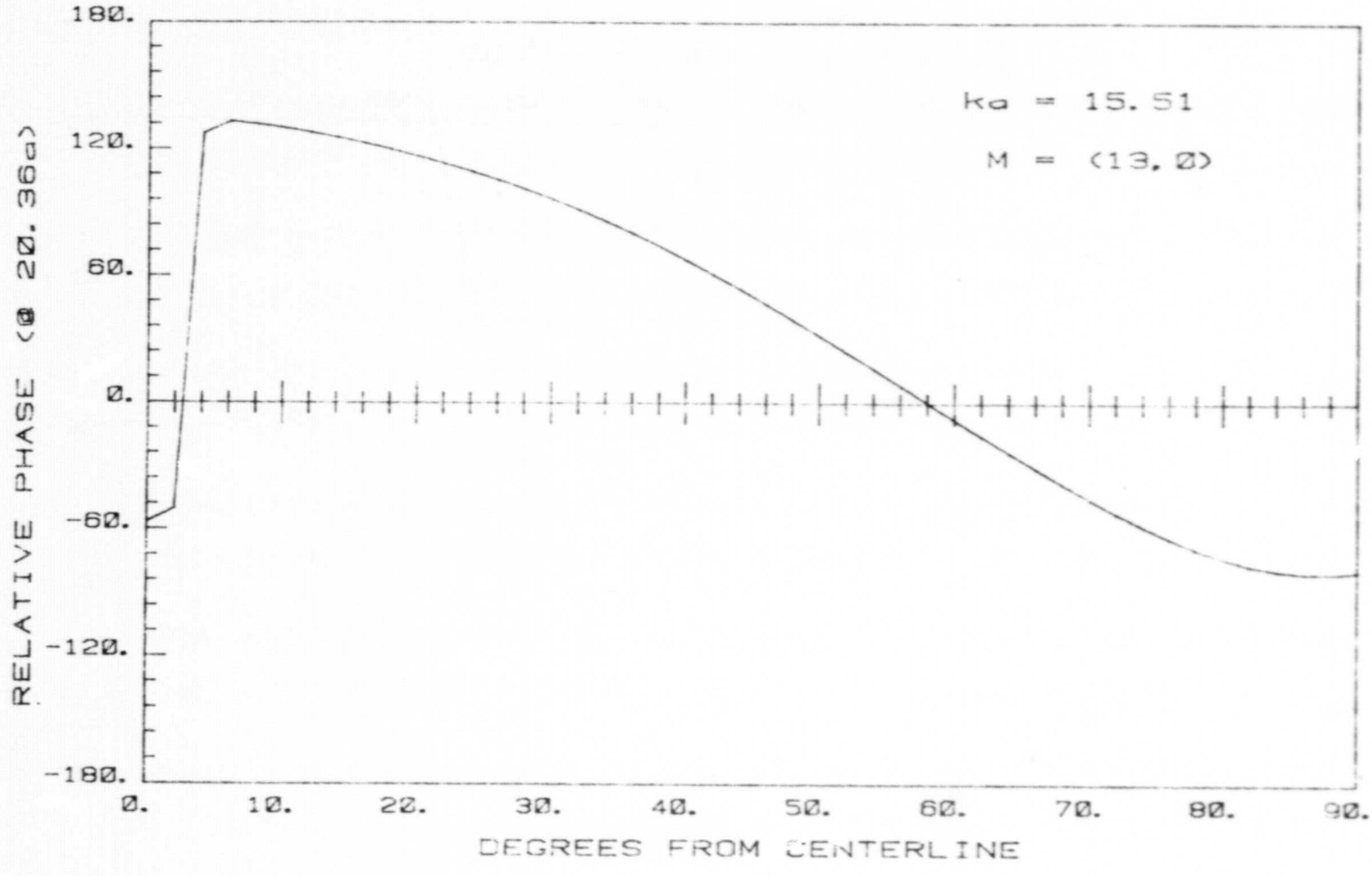

LEWIS JT15D-1

Fig. 45

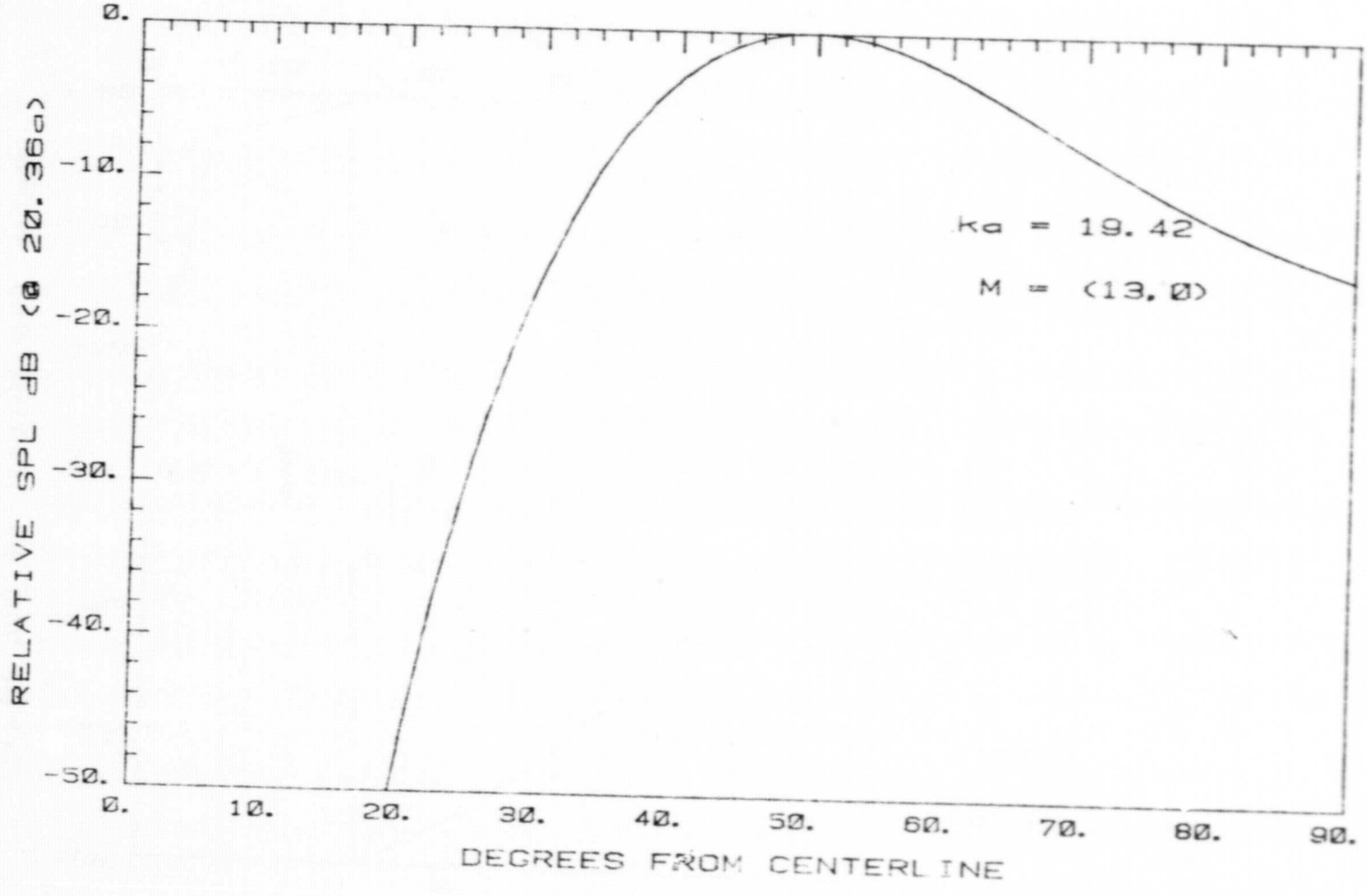

LEWIS JT15D-1

Fig. 46

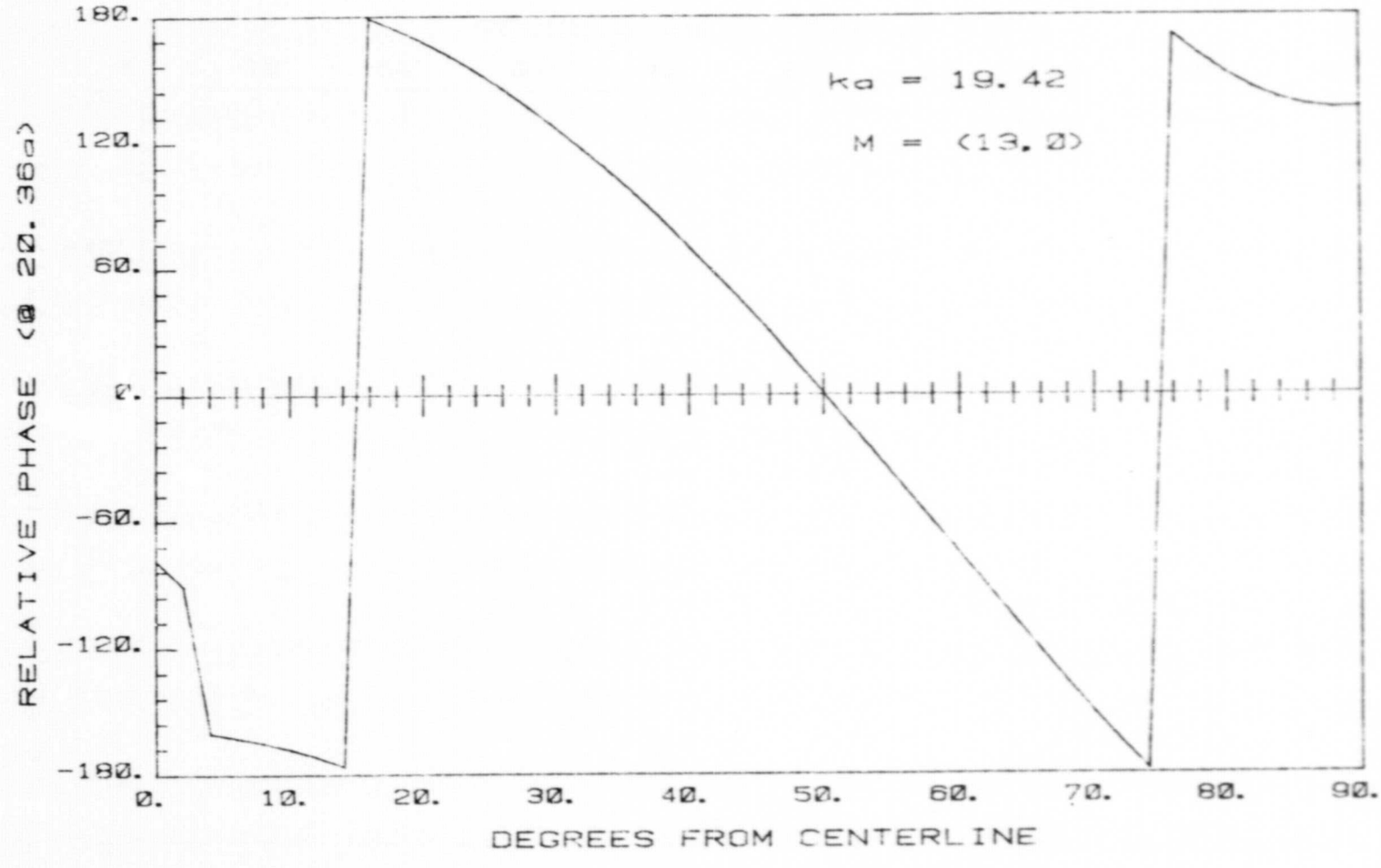

LEWIS JT15D-1

Fig. 47

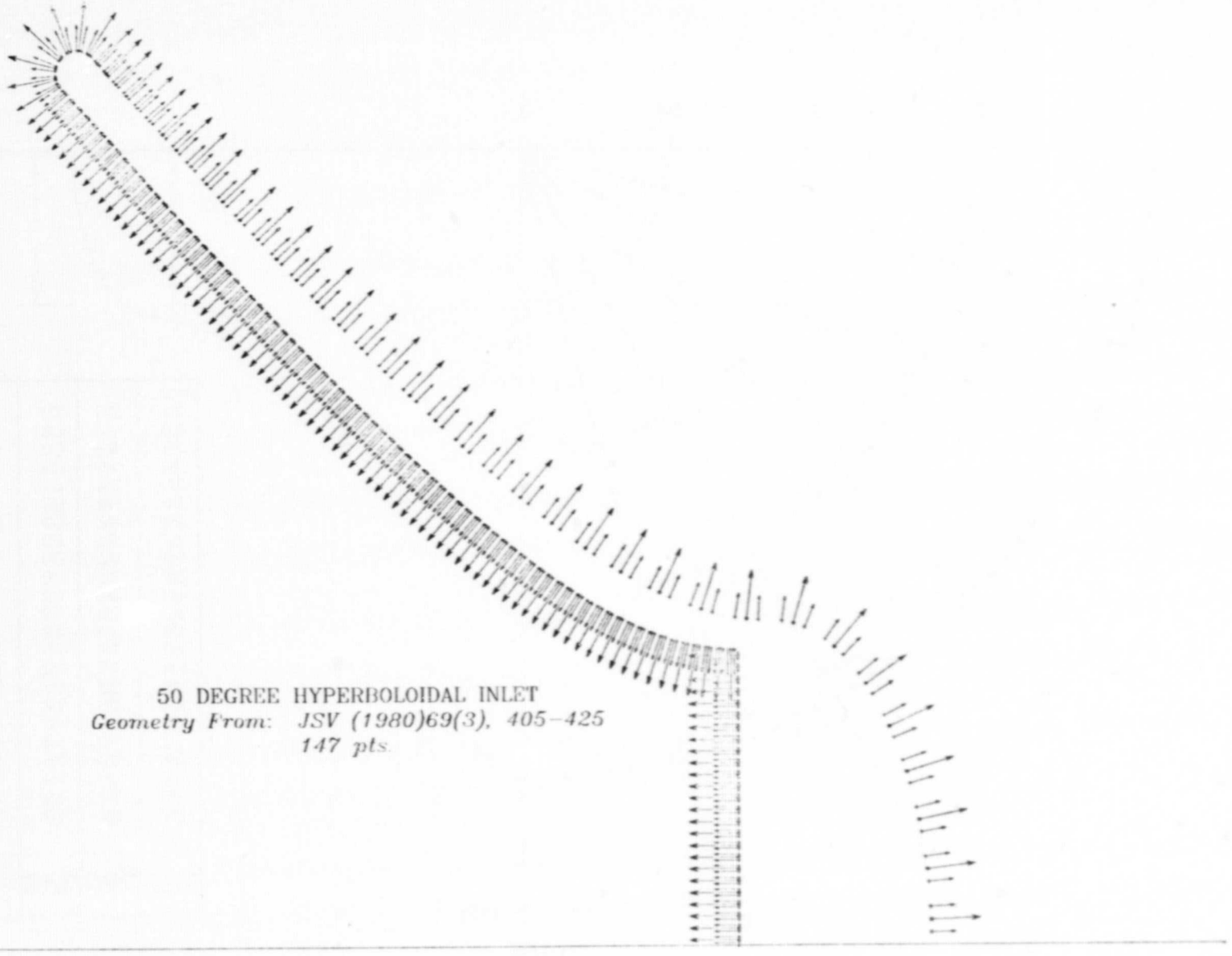

Fig. 48 50 Degree Hyperbolodial Inlet Geometry used
for Computer Calculations.

50 DEGREE HYPERBOLOIDAL INLET

Deg	SPL	Deg	SPL
0	84	46	83
2	84	48	83
4	84	50	83
6	84	52	83
8	84	54	83
10	84	56	83
12	84	58	83
14	84	60	83
16	84	62	83
18	84	64	82
20	84	66	82
22	84	68	82
24	84	70	82
26	83	72	82
28	83	74	82
30	83	76	82
32	83	78	82
34	83	80	82
36	83	82	82
38	83	84	82
40	83	86	82
42	83	88	82
44	83	90	82

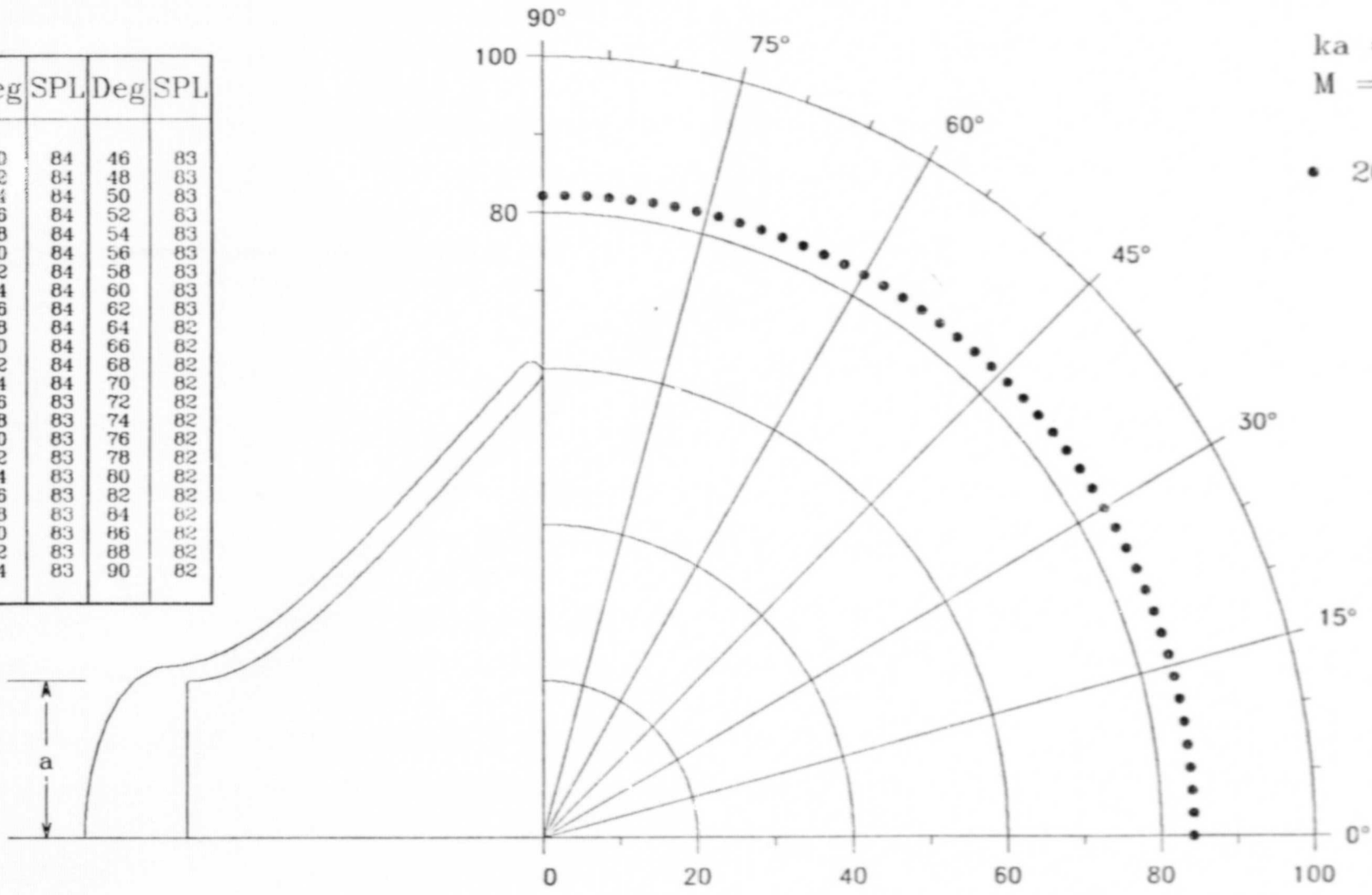

Fig. 49 SPL (dB)

50 DEGREE HYPERBOLOIDAL INLET

Deg	SPL	Deg	SPL
0	108	46	104
2	108	48	104
4	108	50	104
6	107	52	104
8	107	54	103
10	107	56	103
12	107	58	103
14	107	60	103
16	107	62	102
18	107	64	102
20	107	66	102
22	107	68	101
24	107	70	101
26	106	72	101
28	106	74	101
30	106	76	100
32	106	78	100
34	106	80	100
36	105	82	100
38	105	84	99
40	105	86	99
42	105	88	99
44	105	90	99

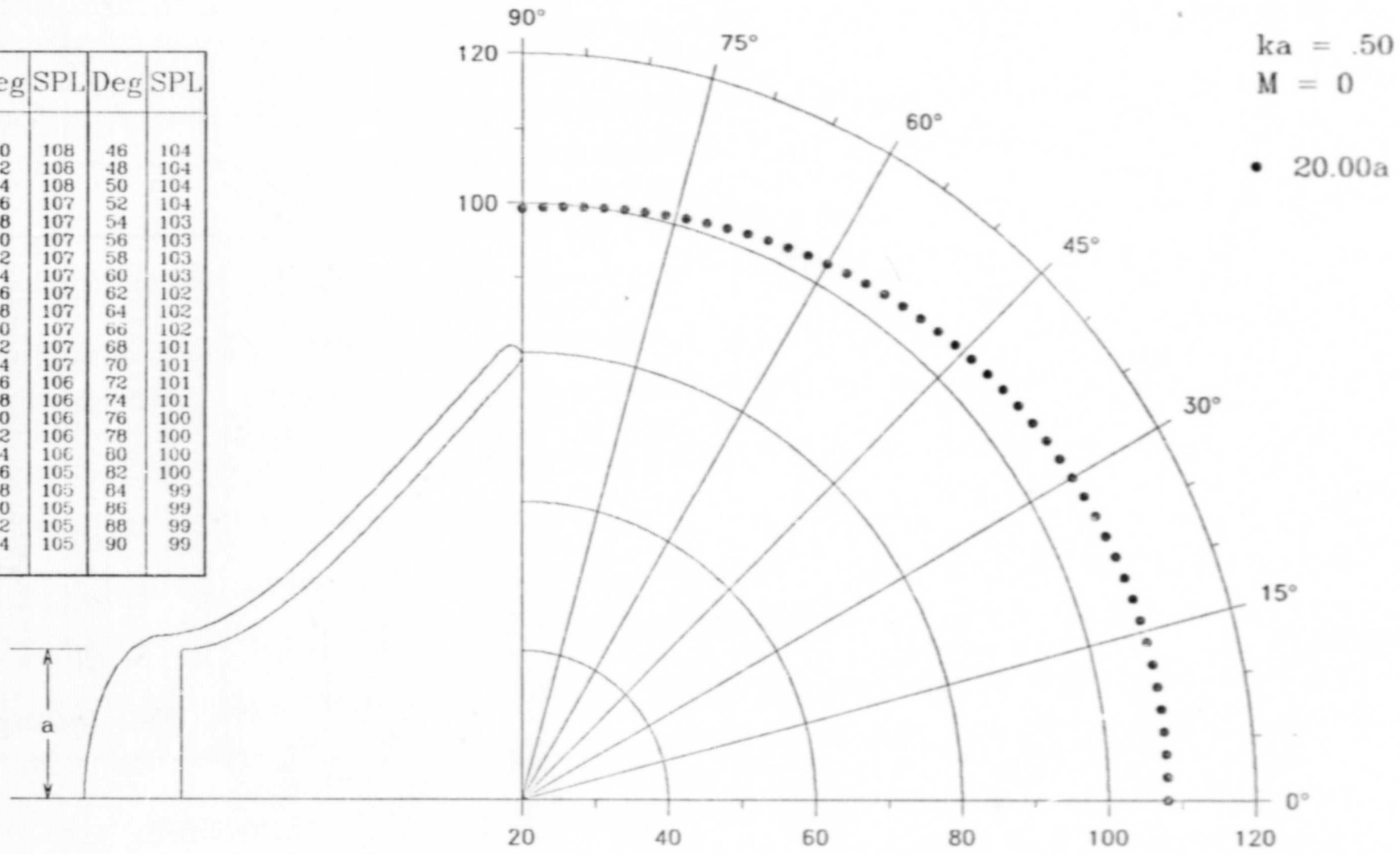

Fig. 50 SPL (dB)

50 DEGREE HYPERBOLOIDAL INLET

Deg	SPL	Deg	SPL
0	119	46	112
2	119	48	111
4	119	50	111
6	119	52	110
8	119	54	110
10	119	56	109
12	119	58	109
14	118	60	108
16	118	62	108
18	118	64	107
20	118	66	107
22	117	68	106
24	117	70	106
26	117	72	105
28	116	74	105
30	116	76	104
32	115	78	104
34	115	80	104
36	114	82	103
38	114	84	103
40	113	86	102
42	113	88	102
44	112	90	102

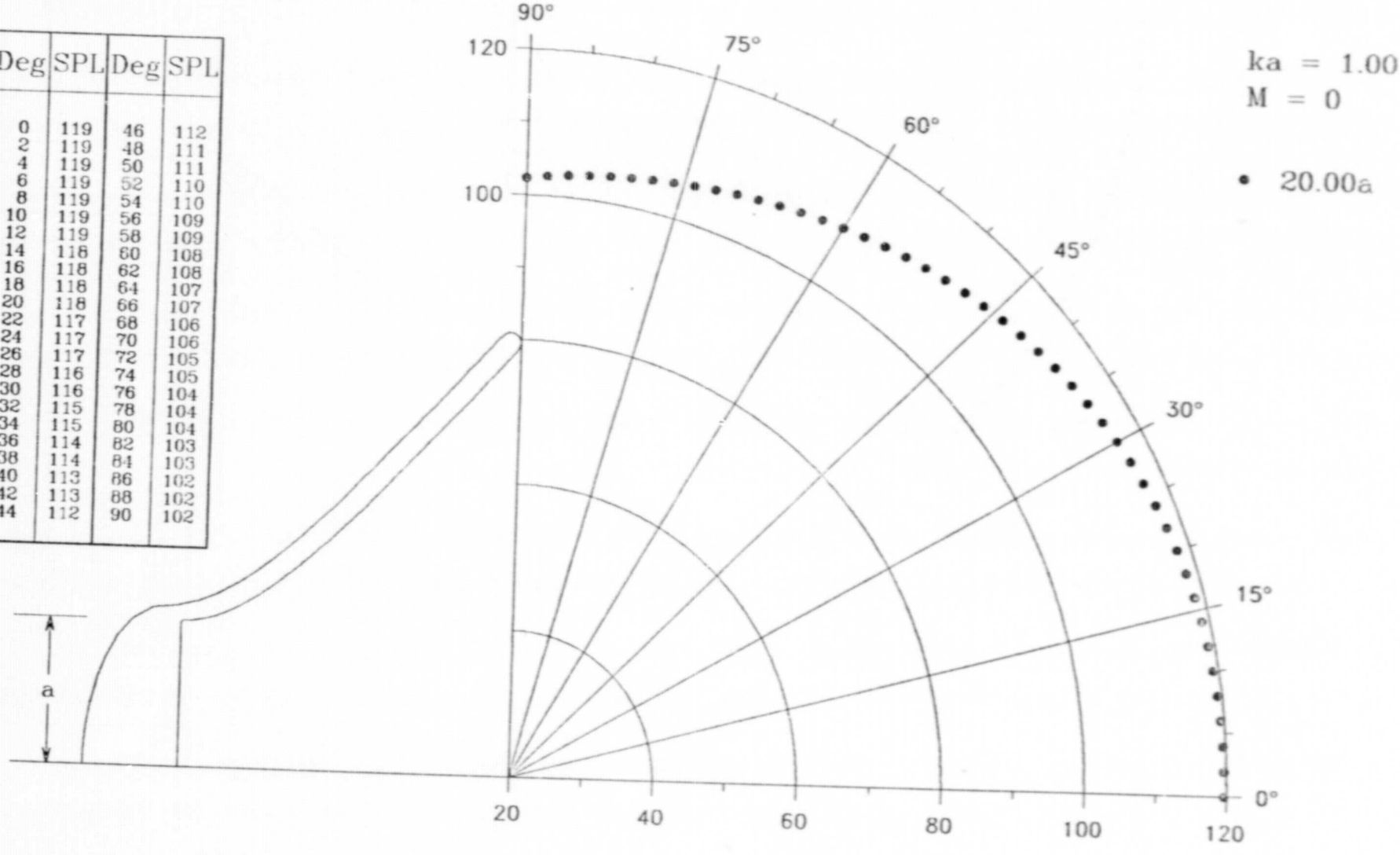

Fig. 51 SPL (dB)

50 DEGREE HYPERBOLOIDAL INLET

Deg	SPL	Deg	SPL
0	132	46	121
2	132	48	119
4	132	50	118
6	131	52	117
8	131	54	116
10	130	56	115
12	130	58	114
14	129	60	114
16	129	62	113
18	128	64	112
20	128	66	112
22	127	68	111
24	127	70	111
26	127	72	111
28	127	74	110
30	126	76	110
32	126	78	110
34	125	80	109
36	125	82	109
38	124	84	109
40	123	86	108
42	122	88	108
44	122	90	108

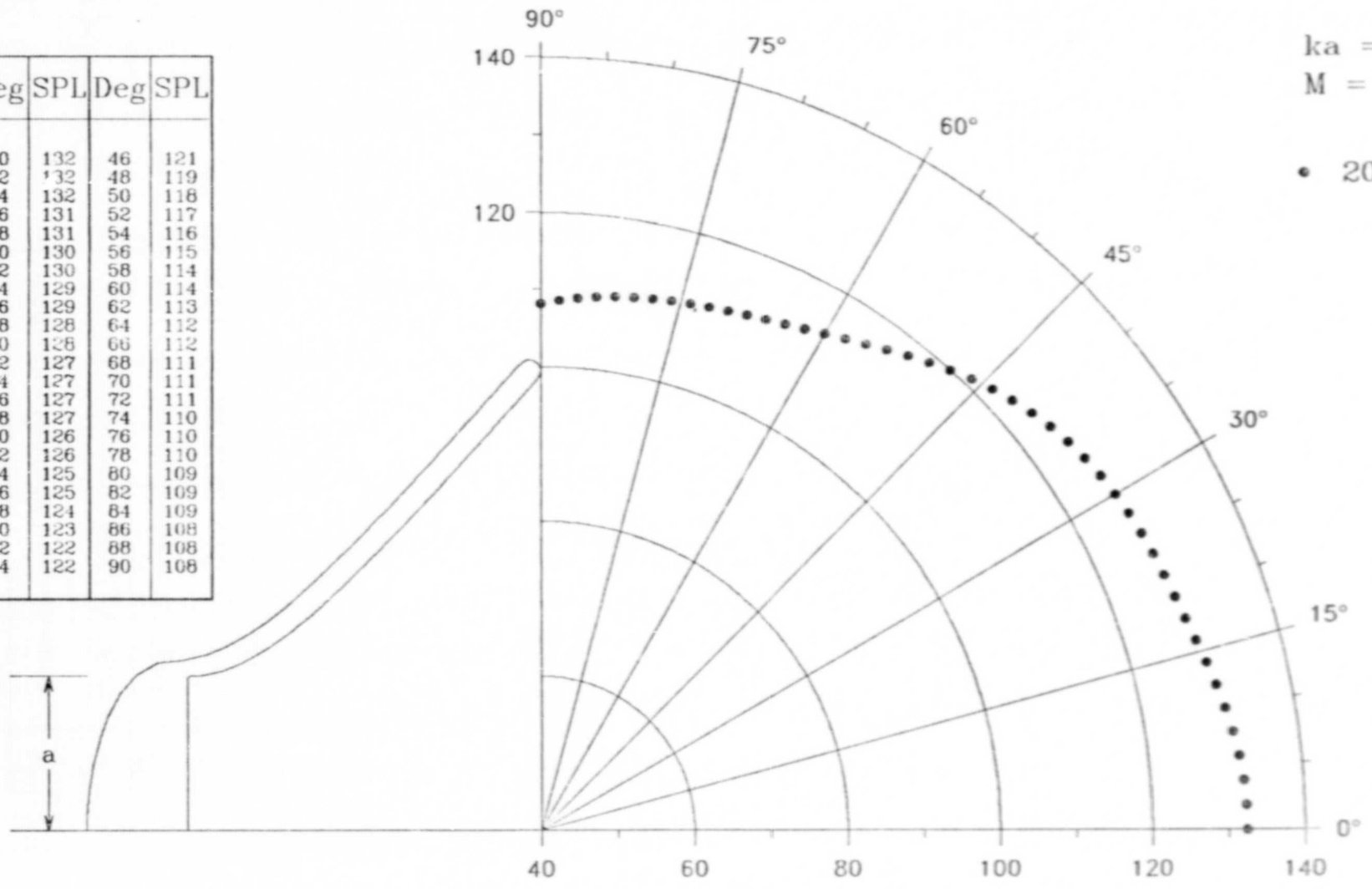

Fig. 52 SPL (dB)

50 DEGREE HYPERBOLOIDAL INLET

Deg	SPL	Deg	SPL
0	132	46	122
2	132	48	120
4	133	50	119
6	133	52	117
8	134	54	116
10	134	56	115
12	134	58	114
14	134	60	113
16	134	62	113
18	134	64	112
20	134	66	112
22	133	68	112
24	132	70	111
26	131	72	111
28	130	74	111
30	130	76	110
32	129	78	110
34	128	80	109
36	127	82	109
38	126	84	108
40	125	86	108
42	124	88	107
44	123	90	107

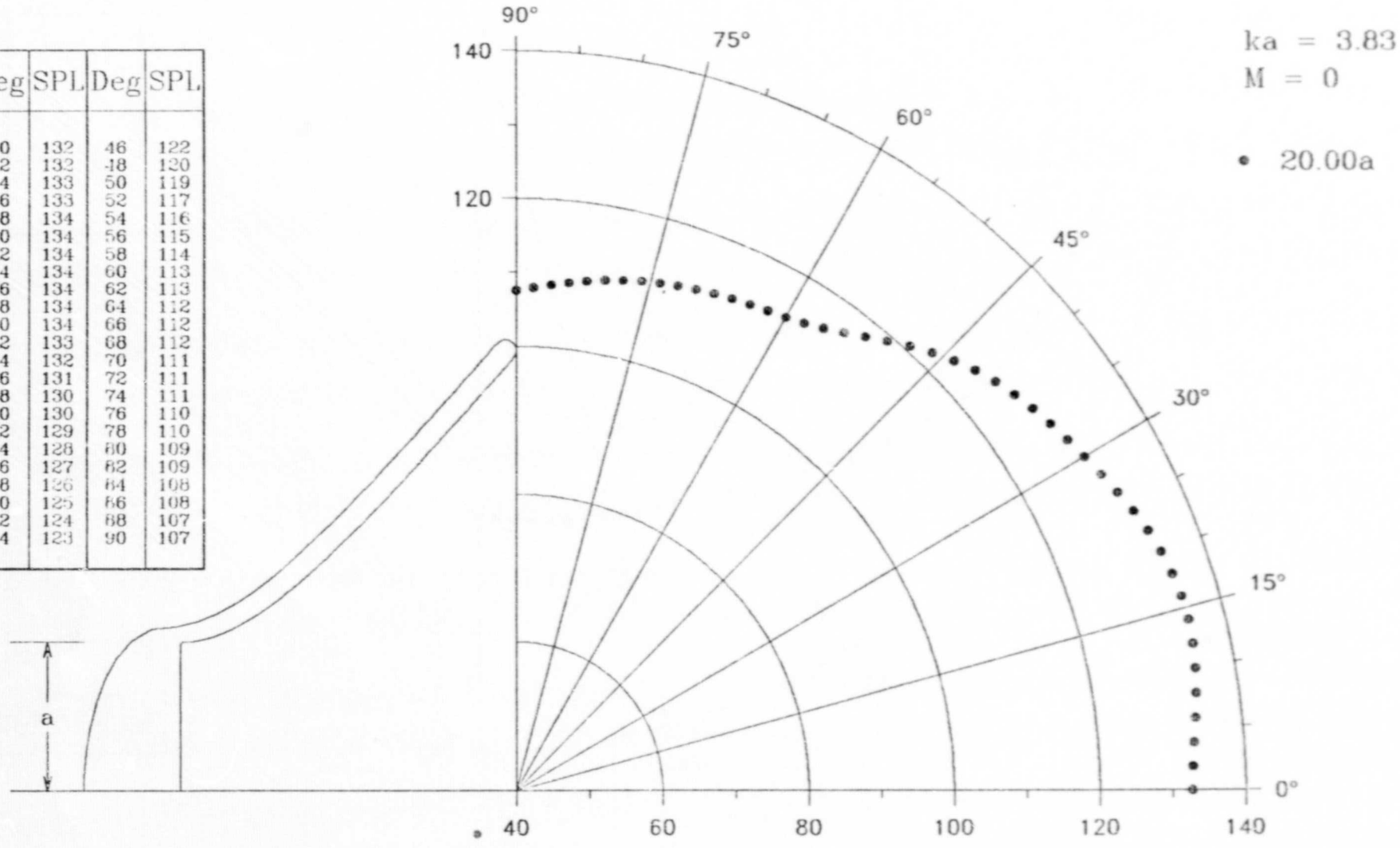

Fig. 53 SPL (dB)

50 DEGREE HYPERBOLOIDAL INLET

Deg	SPL	Deg	SPL
0	137	46	119
2	137	48	118
4	137	50	117
6	137	52	116
8	137	54	116
10	137	56	115
12	137	58	114
14	137	60	113
16	136	62	111
18	136	64	110
20	135	66	109
22	134	68	108
24	134	70	107
26	133	72	107
28	132	74	106
30	131	76	105
32	130	78	105
34	128	80	104
36	127	82	104
38	125	84	104
40	124	86	103
42	122	88	103
44	120	90	103

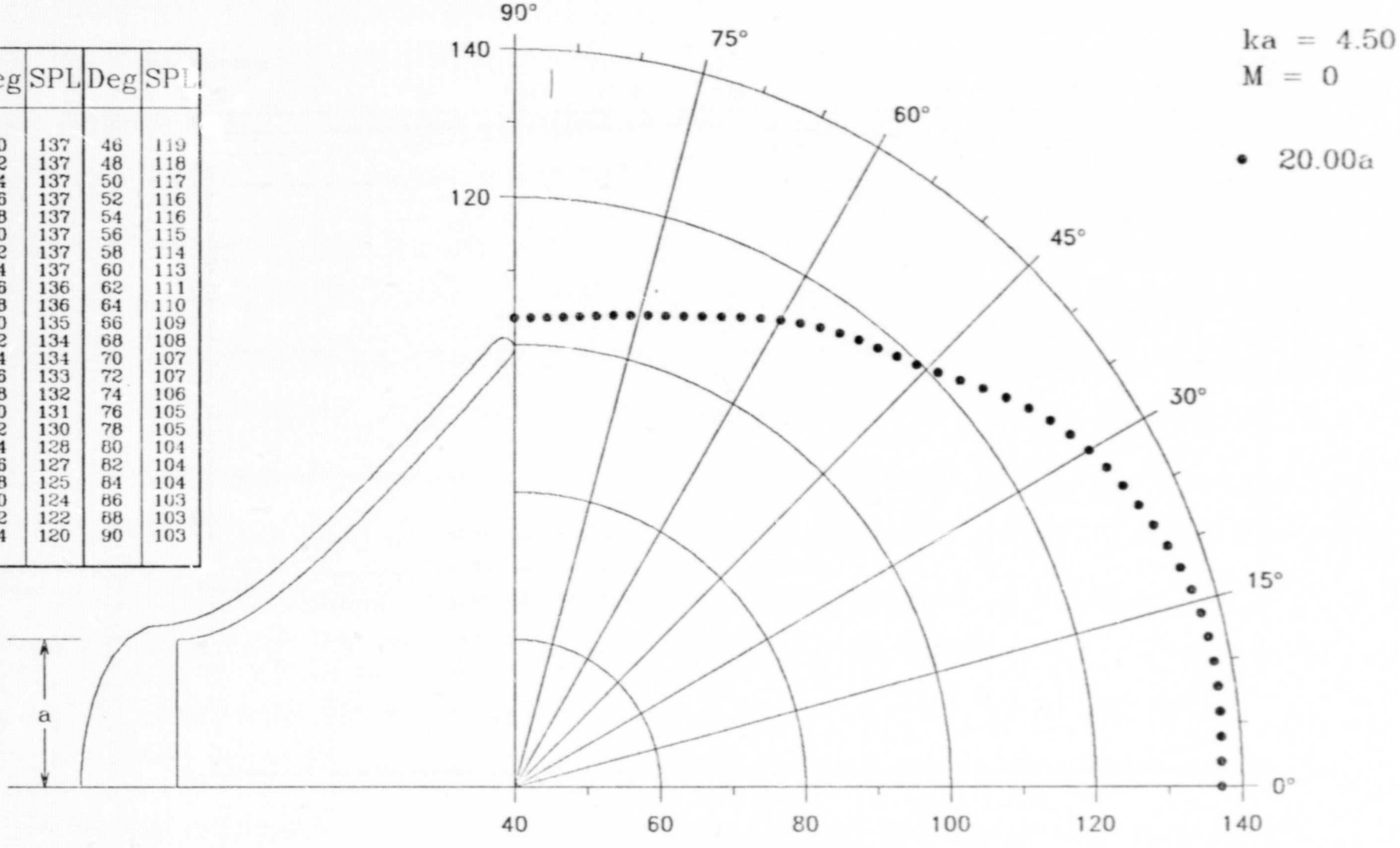

Fig. 54 SPL (dB)

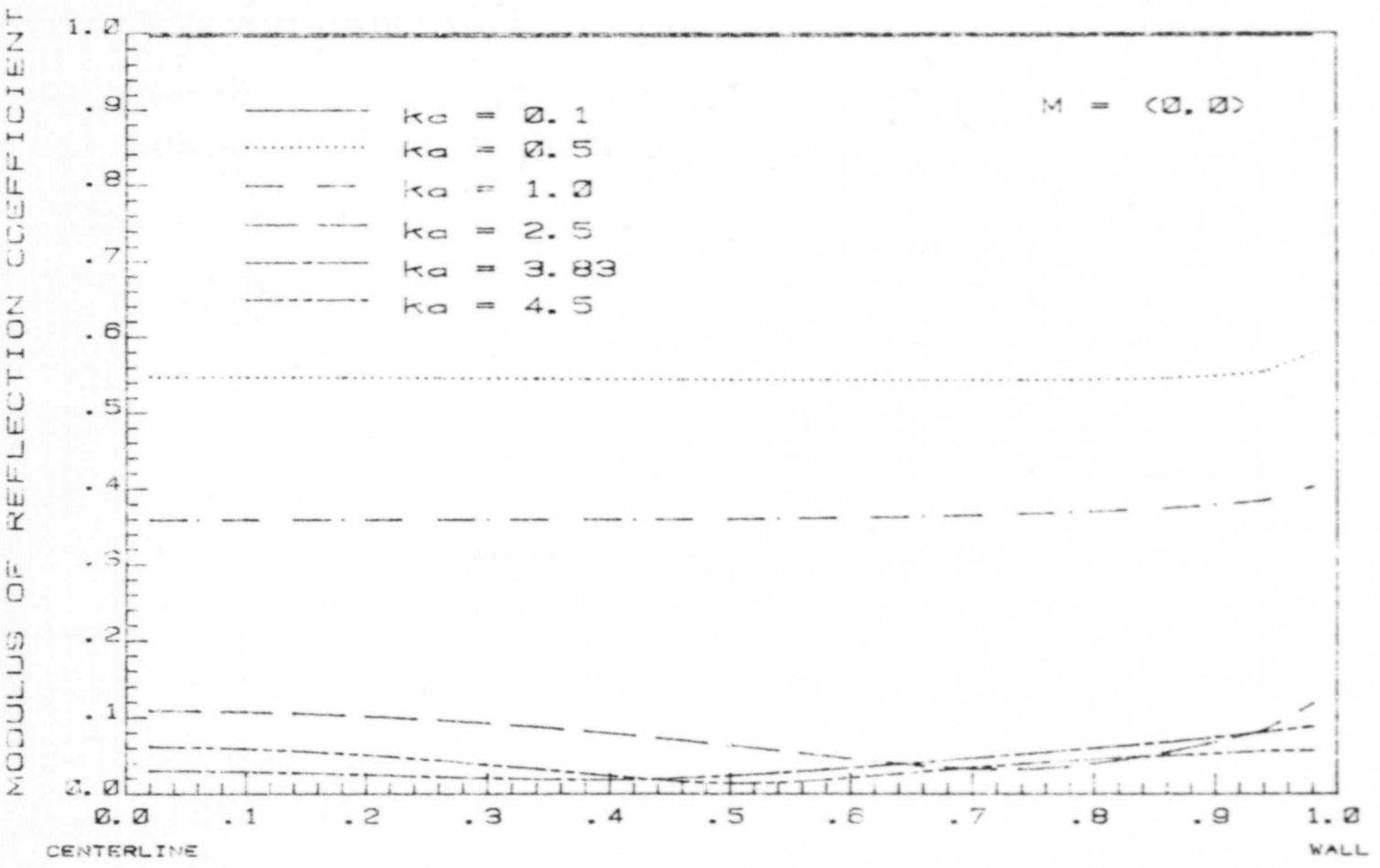

50° HYPERBOLOIDAL INLET (Exit Plane)

Fig. 55

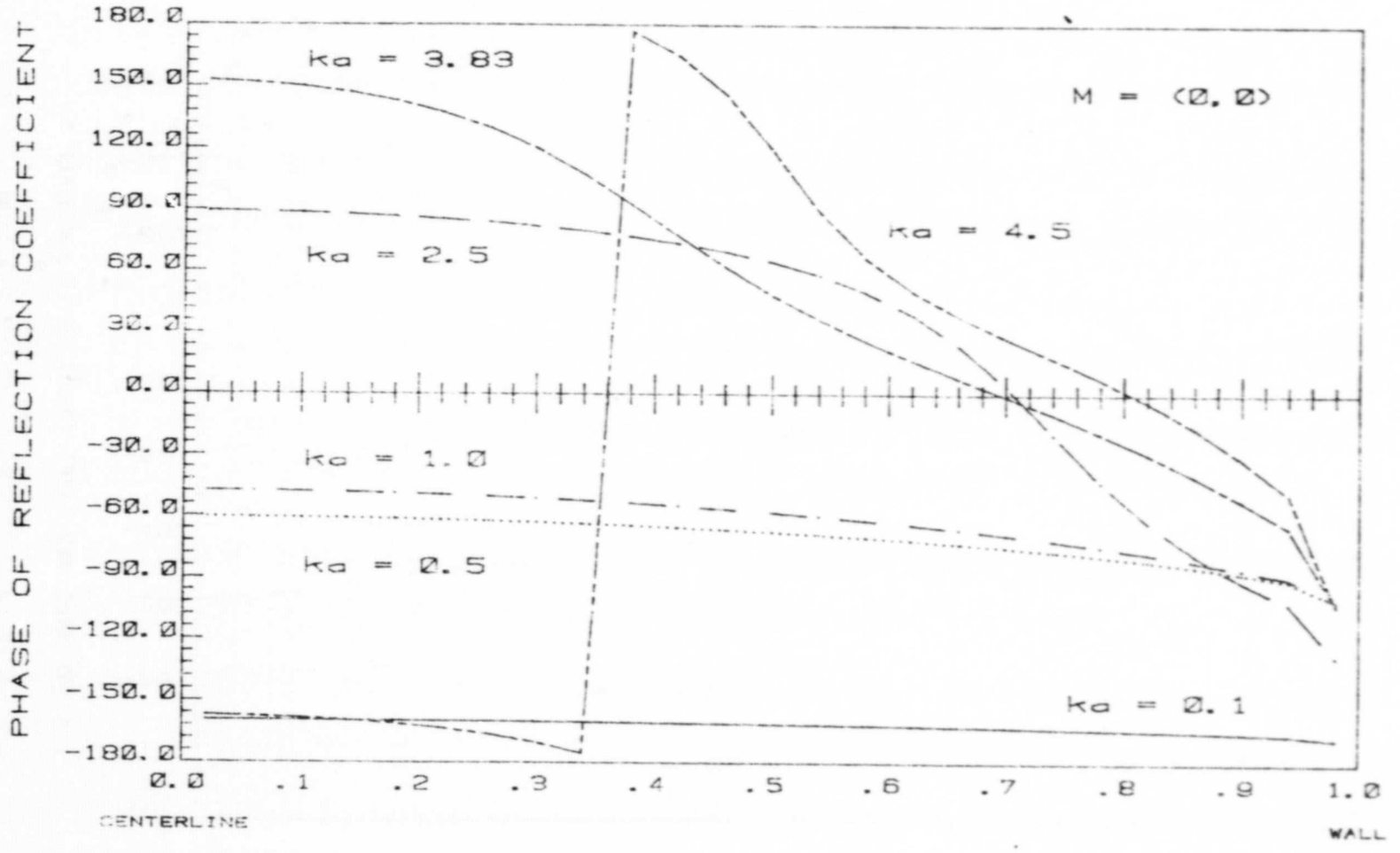

50° HYPERBOLOIDAL INLET (Exit Plane)

Fig. 56

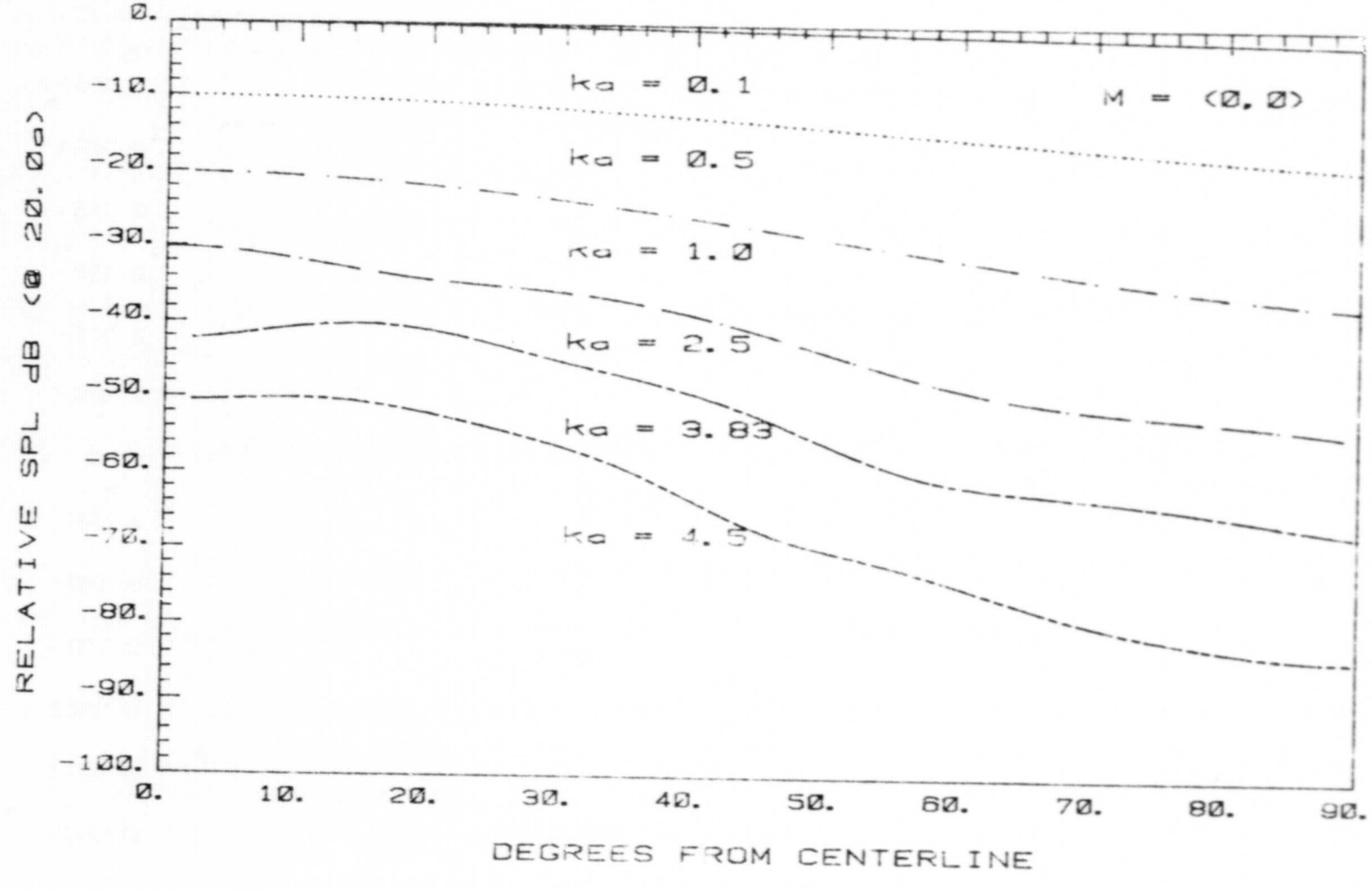

50° HYPERBOLOIDAL INLET

Fig. 57

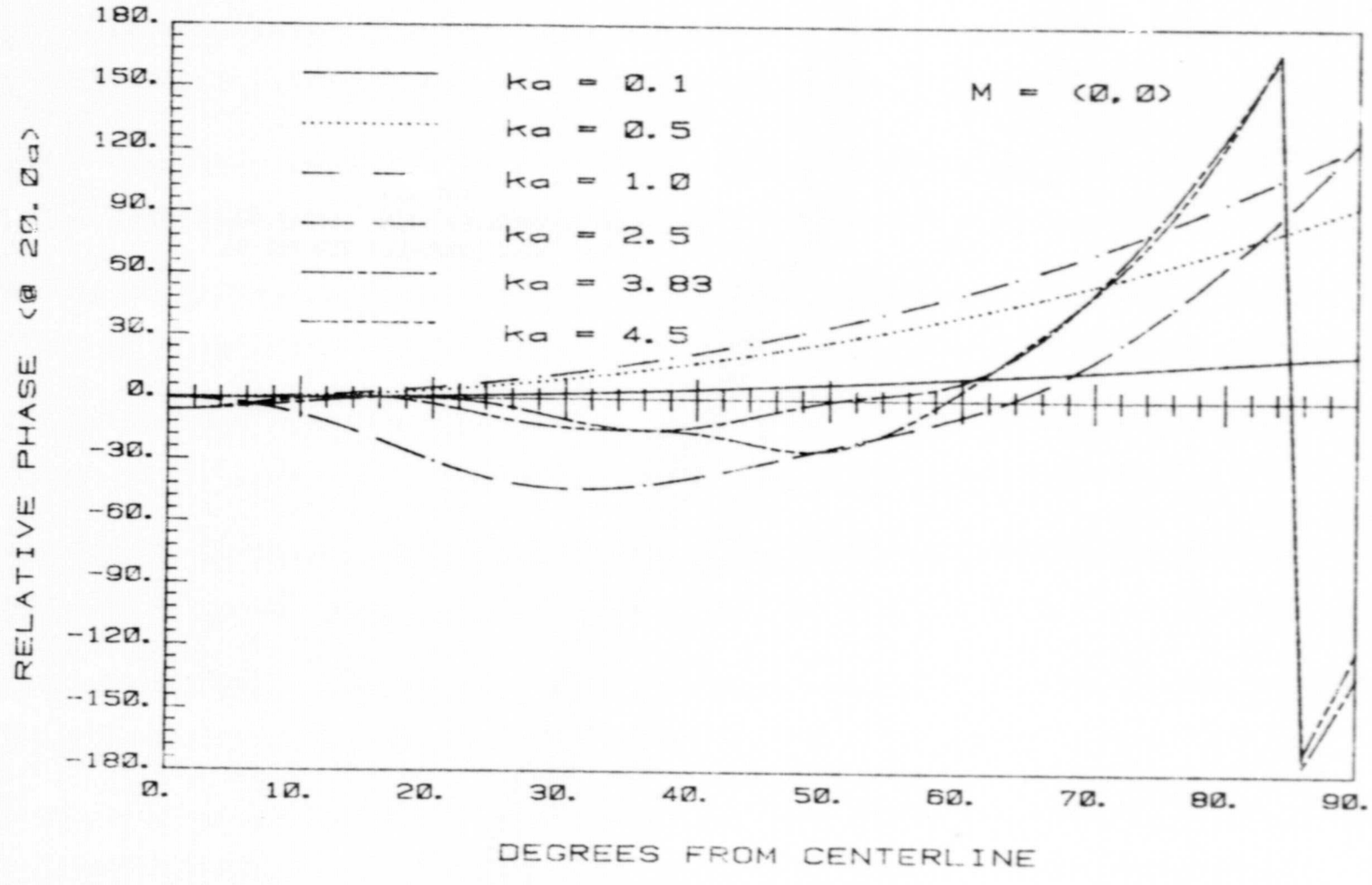

50° HYPERBOLOIDAL INLET

Fig. 58

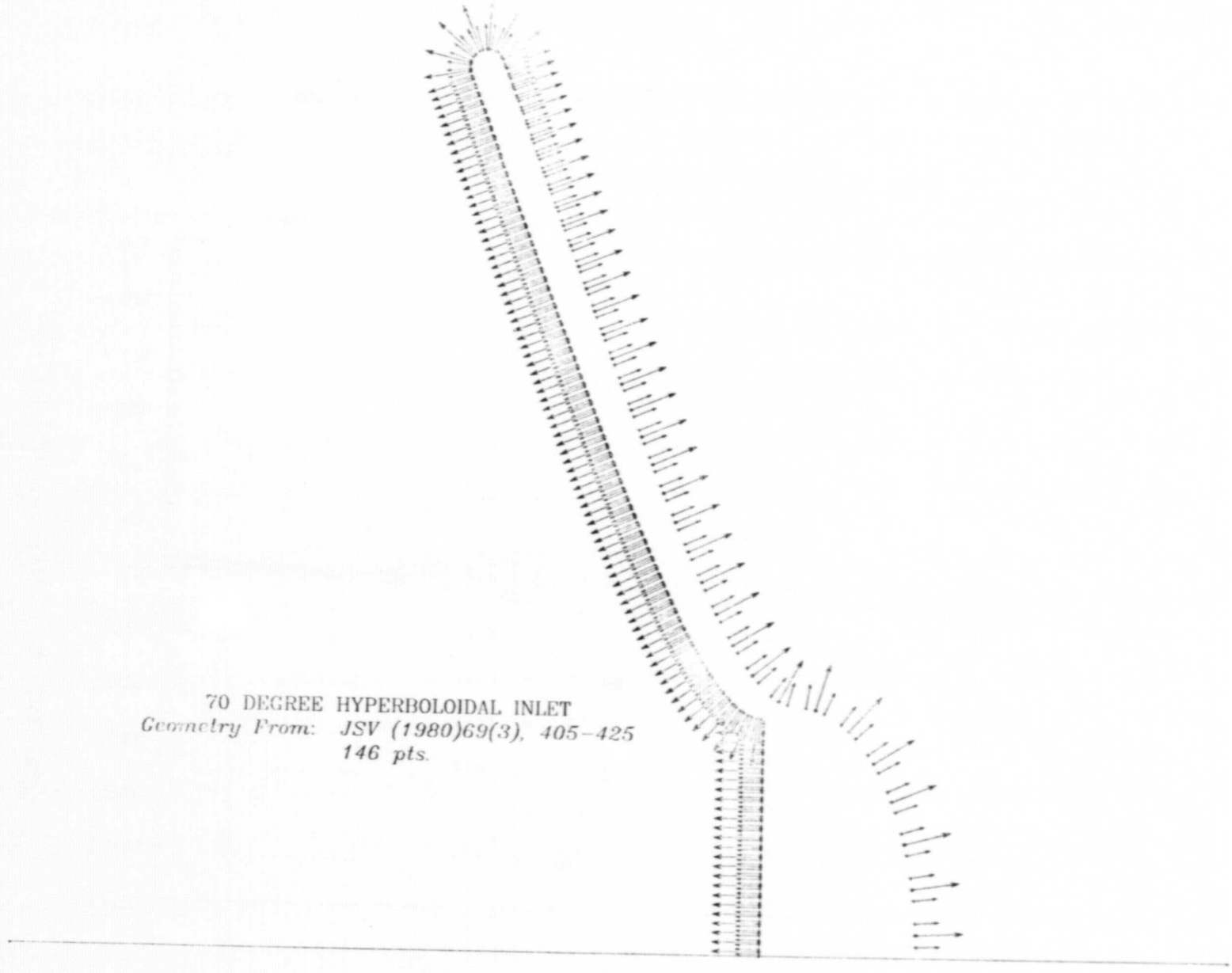

Fig. 59 70 Degree Hyperbolodial Inlet Geometry used for Computer Calculations.

70 DEGREE HYPERBOLOIDAL INLET

Deg	SPL	Deg	SPL
0	0	46	111
2	−8	48	113
4	38	50	115
6	64	52	116
8	81	54	116
10	92	56	117
12	99	58	117
14	102	60	116
16	101	62	115
18	93	64	114
20	97	66	113
22	101	68	112
24	96	70	112
26	93	72	111
28	97	74	110
30	95	76	109
32	102	78	108
34	106	80	107
36	105	82	106
38	104	84	105
40	102	86	104
42	103	88	103
44	108	90	101

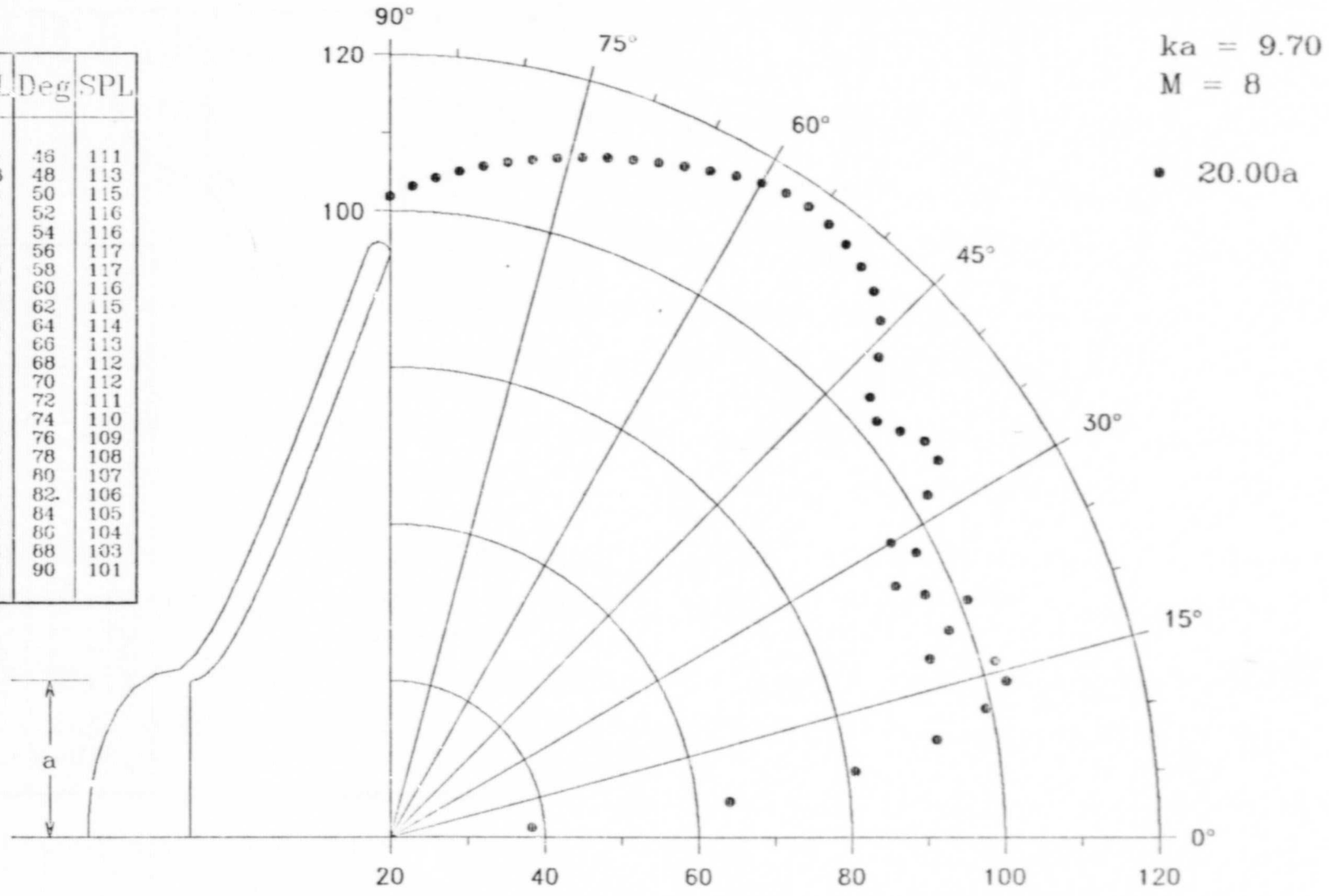

Fig. 60 SPL (dB)

70 DEGREE HYPERBOLOIDAL INLET

Deg	SPL	Deg	SPL
0	0	46	118
2	10	48	120
4	56	50	122
6	81	52	123
8	96	54	123
10	104	56	123
12	107	58	123
14	101	60	122
16	100	62	122
18	104	64	121
20	93	66	119
22	101	68	118
24	96	70	116
26	106	72	115
28	107	74	113
30	104	76	112
32	101	78	111
34	109	80	110
36	114	82	109
38	116	84	108
40	117	86	107
42	117	88	106
44	117	90	105

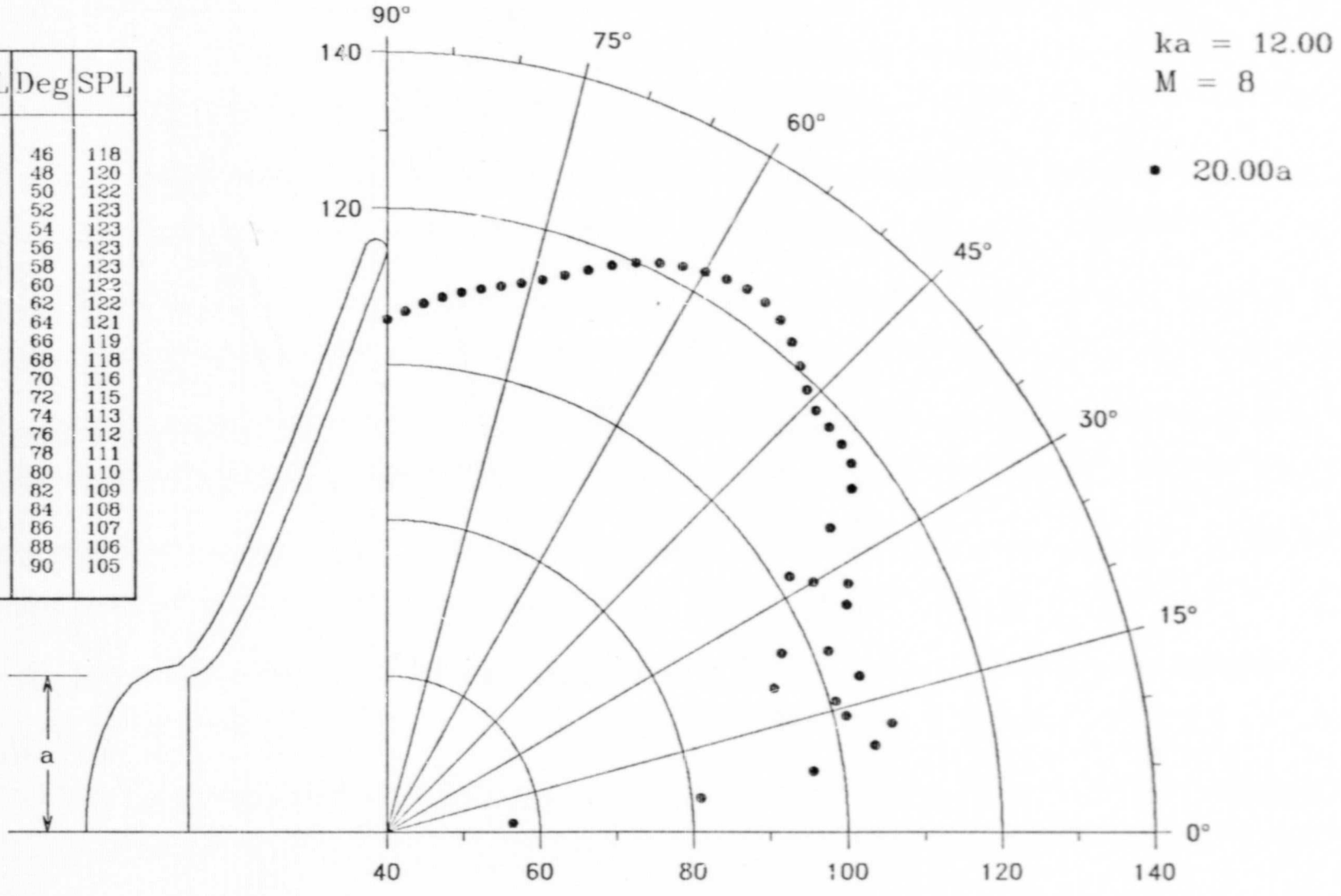

Fig. 61 SPL (dB)

70 DEGREE HYPERBOLOIDAL INLET

Deg	SPL	Deg	SPL
0	0	46	128
2	25	48	127
4	69	50	126
6	91	52	125
8	101	54	122
10	101	56	120
12	96	58	117
14	96	60	114
16	102	62	112
18	103	64	111
20	102	66	110
22	111	68	110
24	116	70	110
26	118	72	109
28	121	74	108
30	124	76	107
32	125	78	105
34	127	80	104
36	128	82	103
38	129	84	101
40	129	86	100
42	129	88	100
44	128	90	99

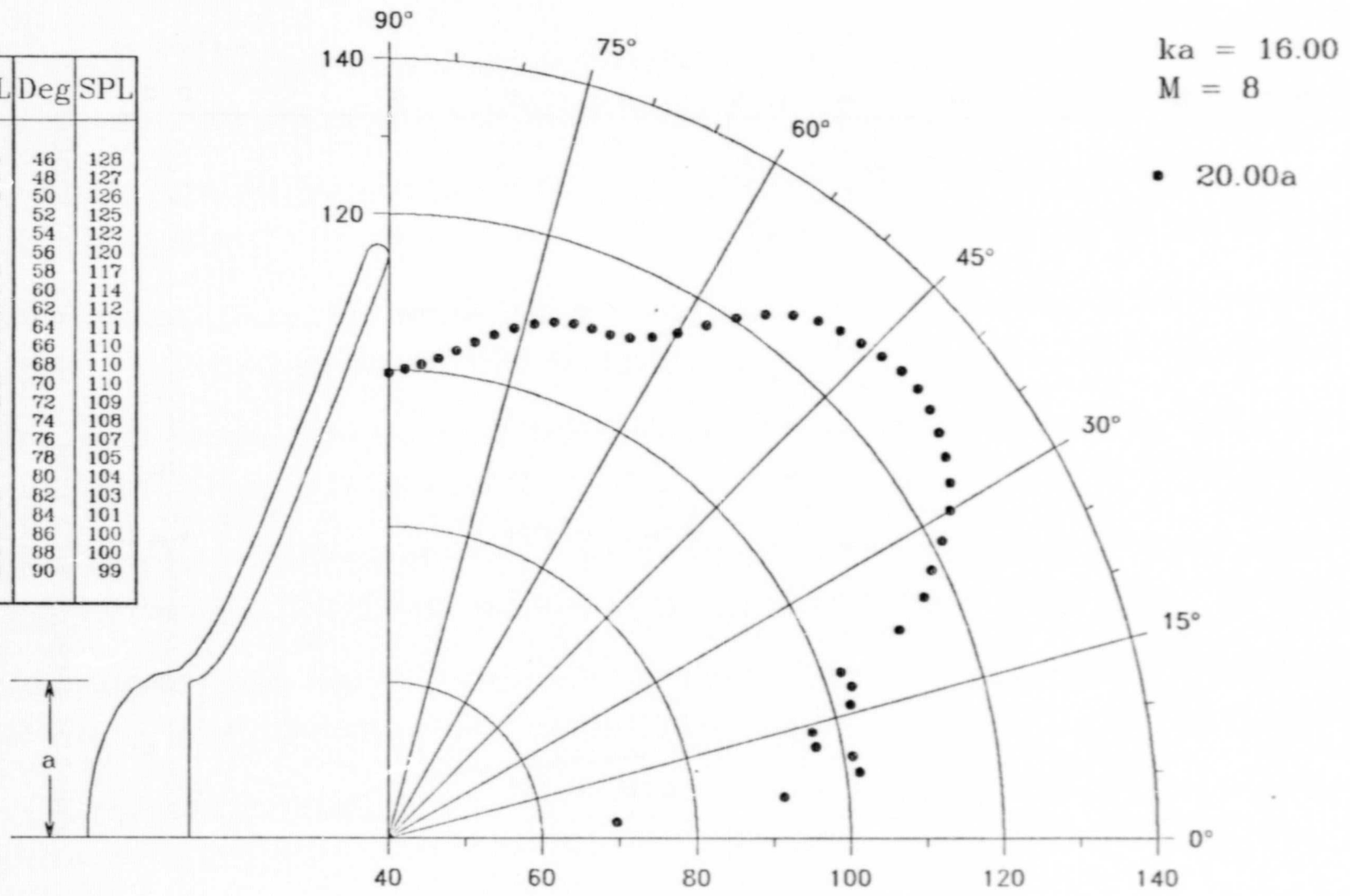

Fig. 62 SPL (dB)

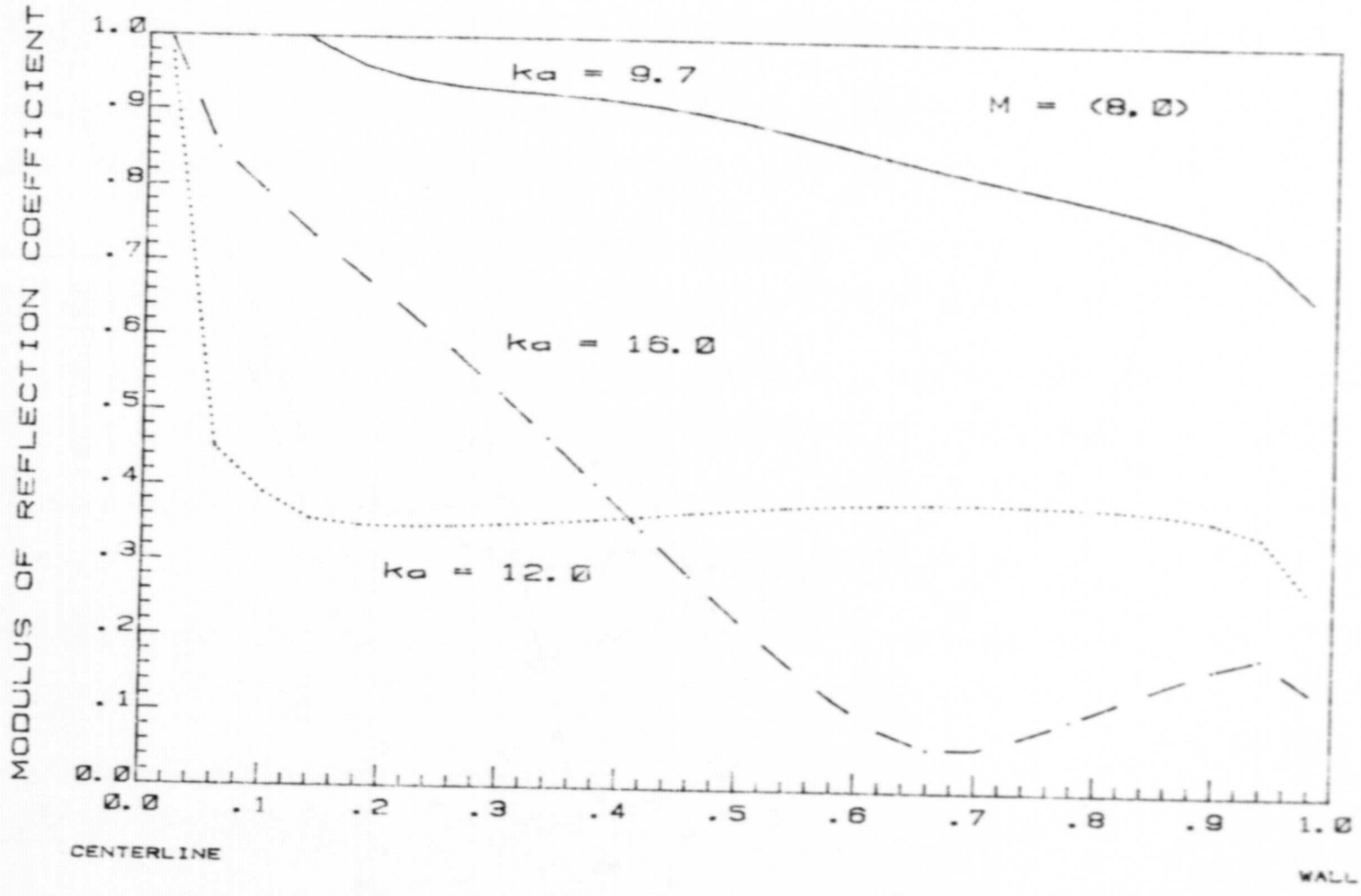

70° HYPERBOLOIDAL INLET (Exit Plane)

Fig. 63

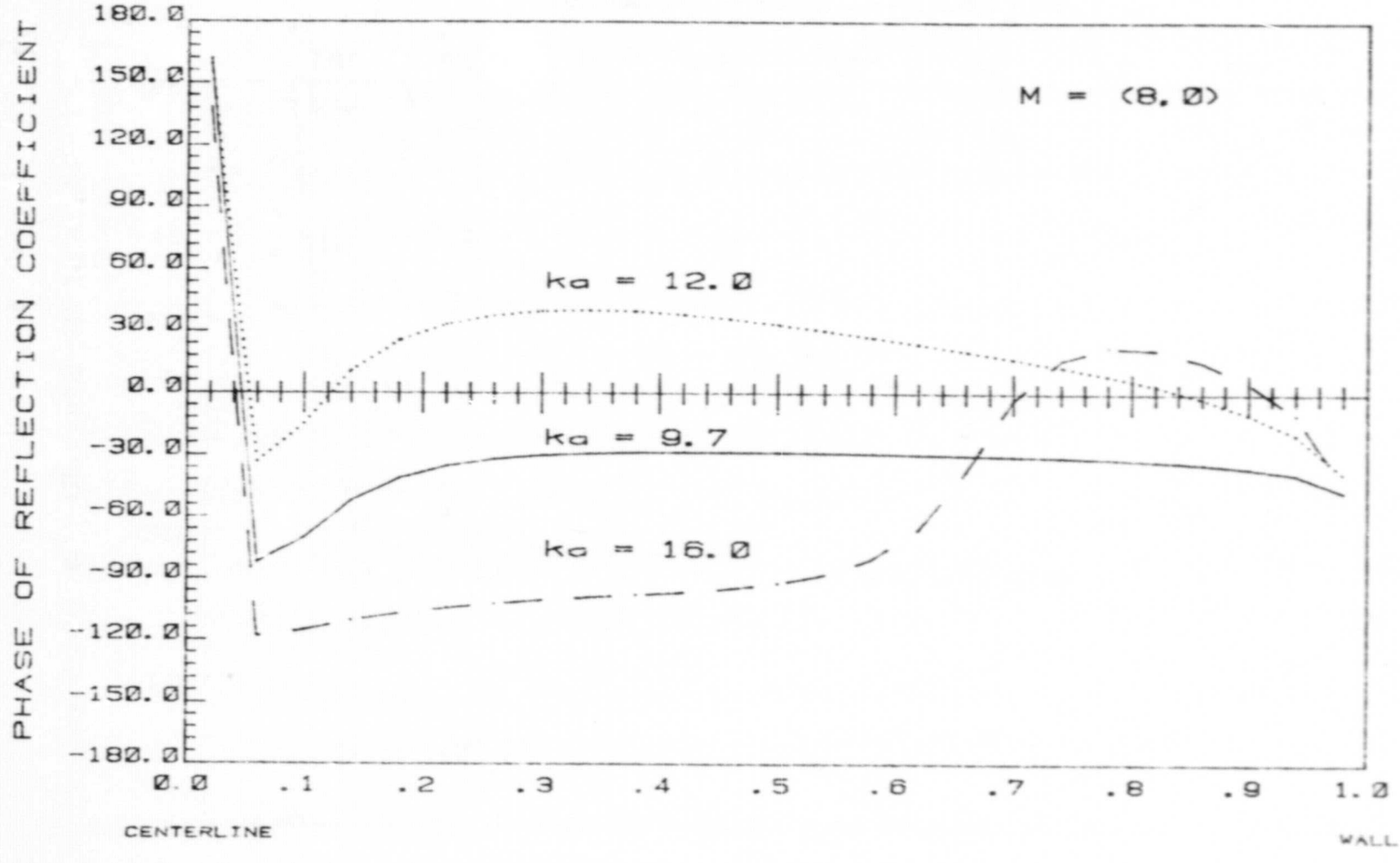

70° HYPERBOLOIDAL INLET (Exit Plane)

Fig. 64

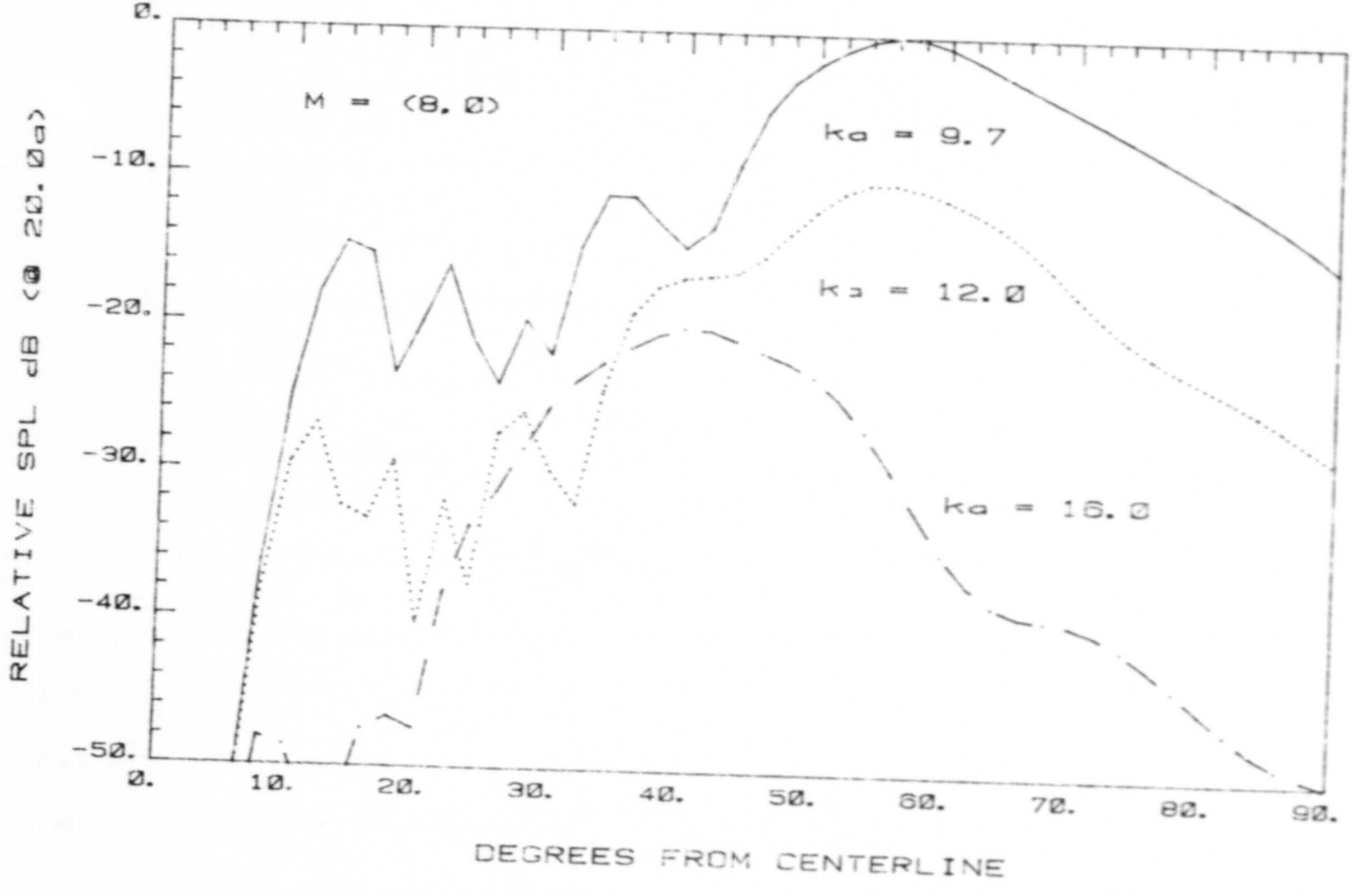

70° HYPERBOLOIDAL INLET

Fig. 65

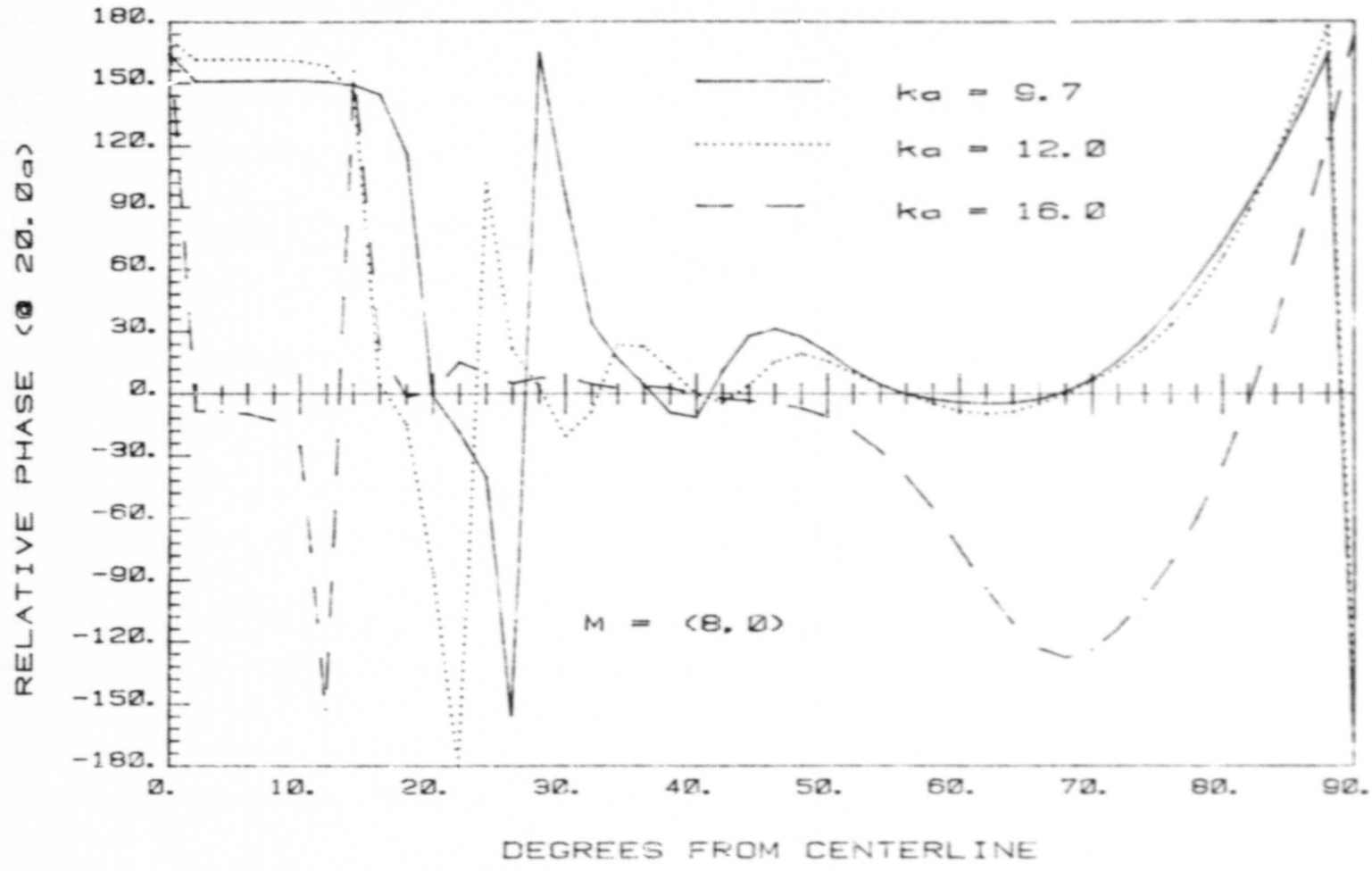

70° HYPERBOLOIDAL INLET

Fig. 66

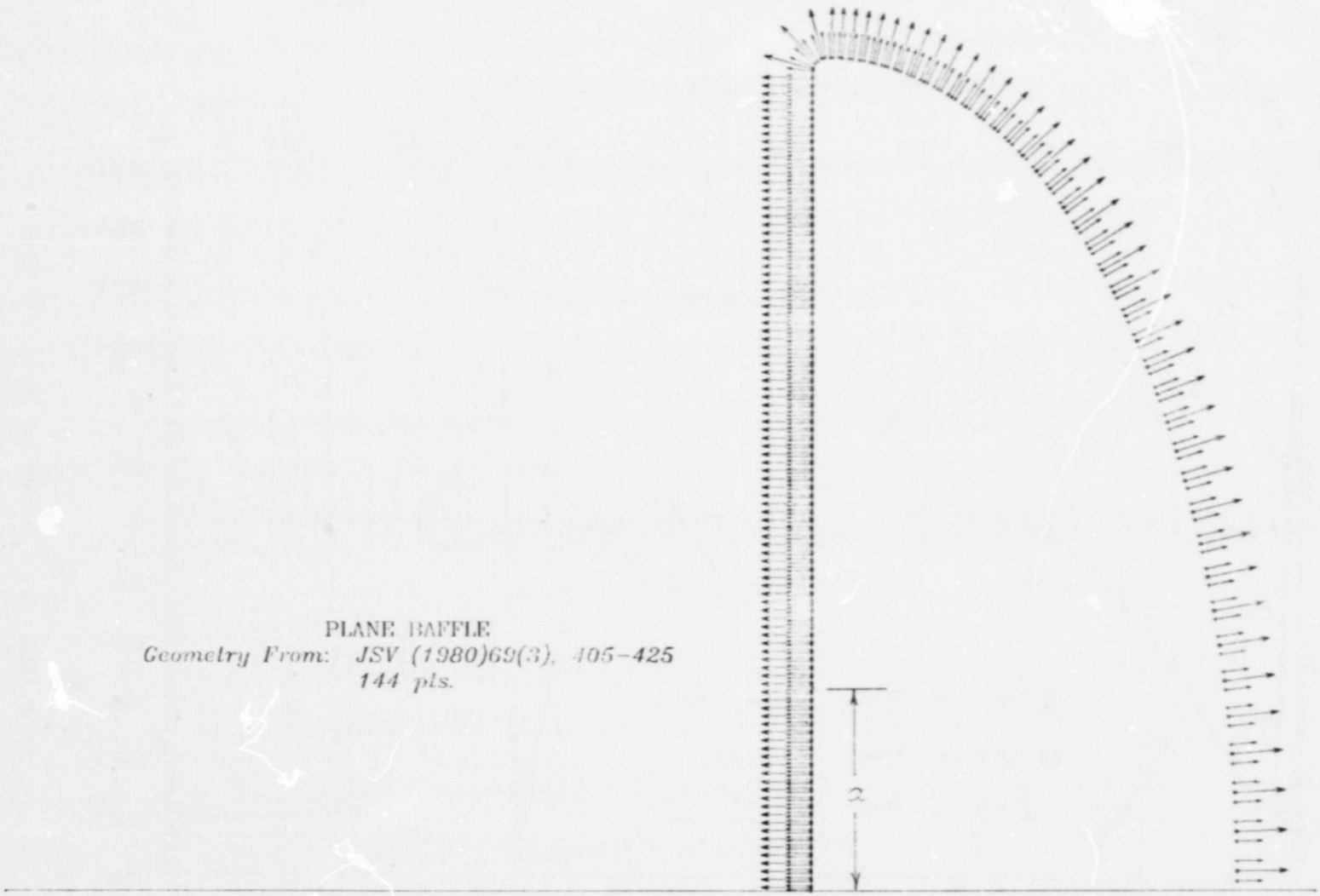

Fig. 67 Plane Baffle Geometry used for Computer Calculations.

PLANE BAFFLE

Deg	SPL	Deg	SPL
0	116	46	114
2	116	48	113
4	116	50	113
6	116	52	113
8	116	54	113
10	116	56	112
12	116	58	112
14	116	60	112
16	116	62	112
18	116	64	111
20	115	66	111
22	115	68	111
24	115	70	110
26	115	72	110
28	115	74	110
30	115	76	109
32	115	78	109
34	115	80	109
36	115	82	108
38	114	84	108
40	114	86	107
42	111	88	107
44	111	90	107

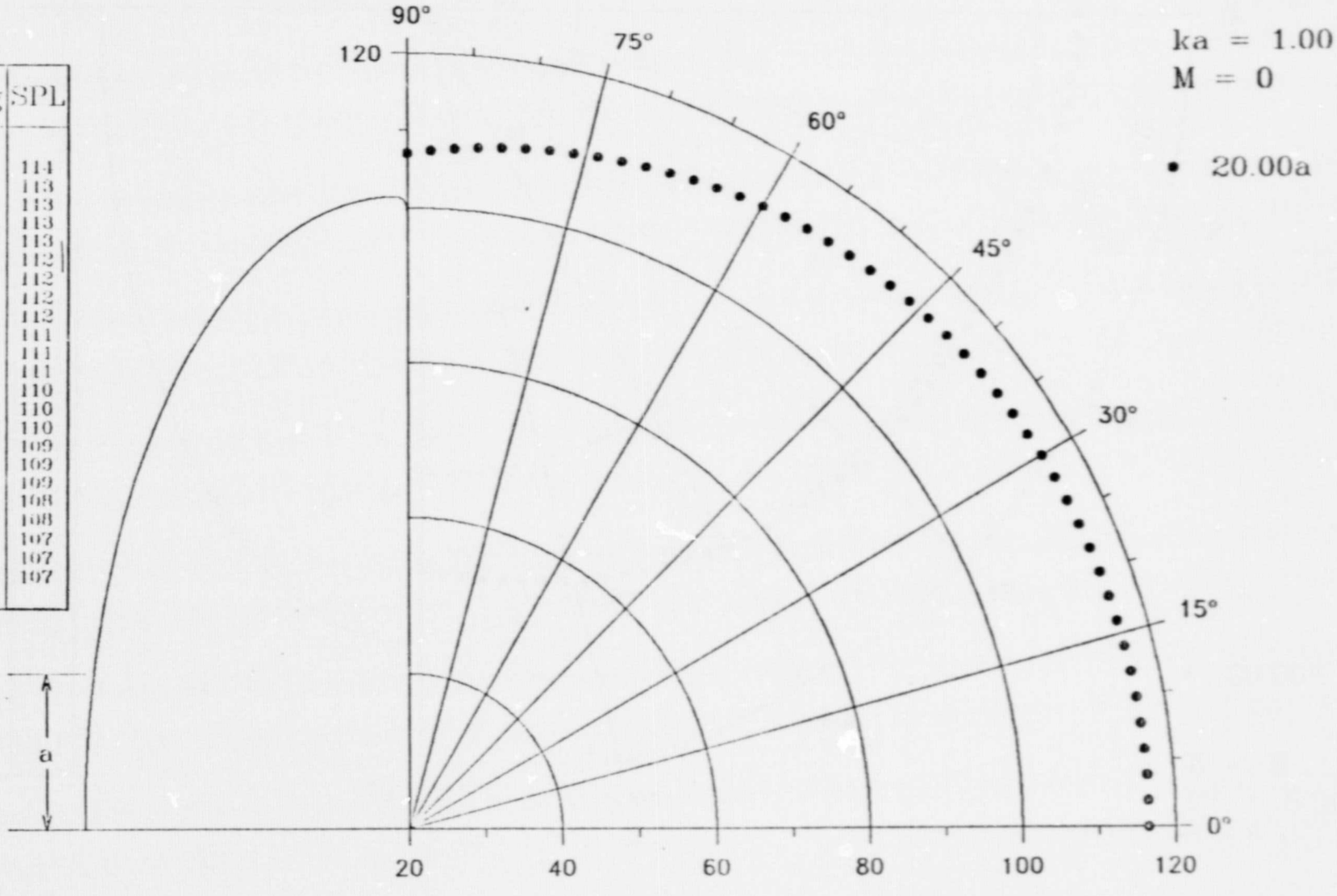

Fig. 68 SPL (dB)

PLANE BAFFLE

Deg.	SPL	Deg.	SPL
0	125	46	121
2	125	48	121
4	125	50	120
6	124	52	120
8	124	54	120
10	124	56	120
12	124	58	119
14	123	60	119
16	123	62	119
18	122	64	118
20	122	66	118
22	122	68	117
24	122	70	117
26	121	72	116
28	121	74	116
30	121	76	115
32	121	78	115
34	121	80	114
36	121	82	114
38	121	84	113
40	121	86	113
42	121	88	112
44	121	90	112

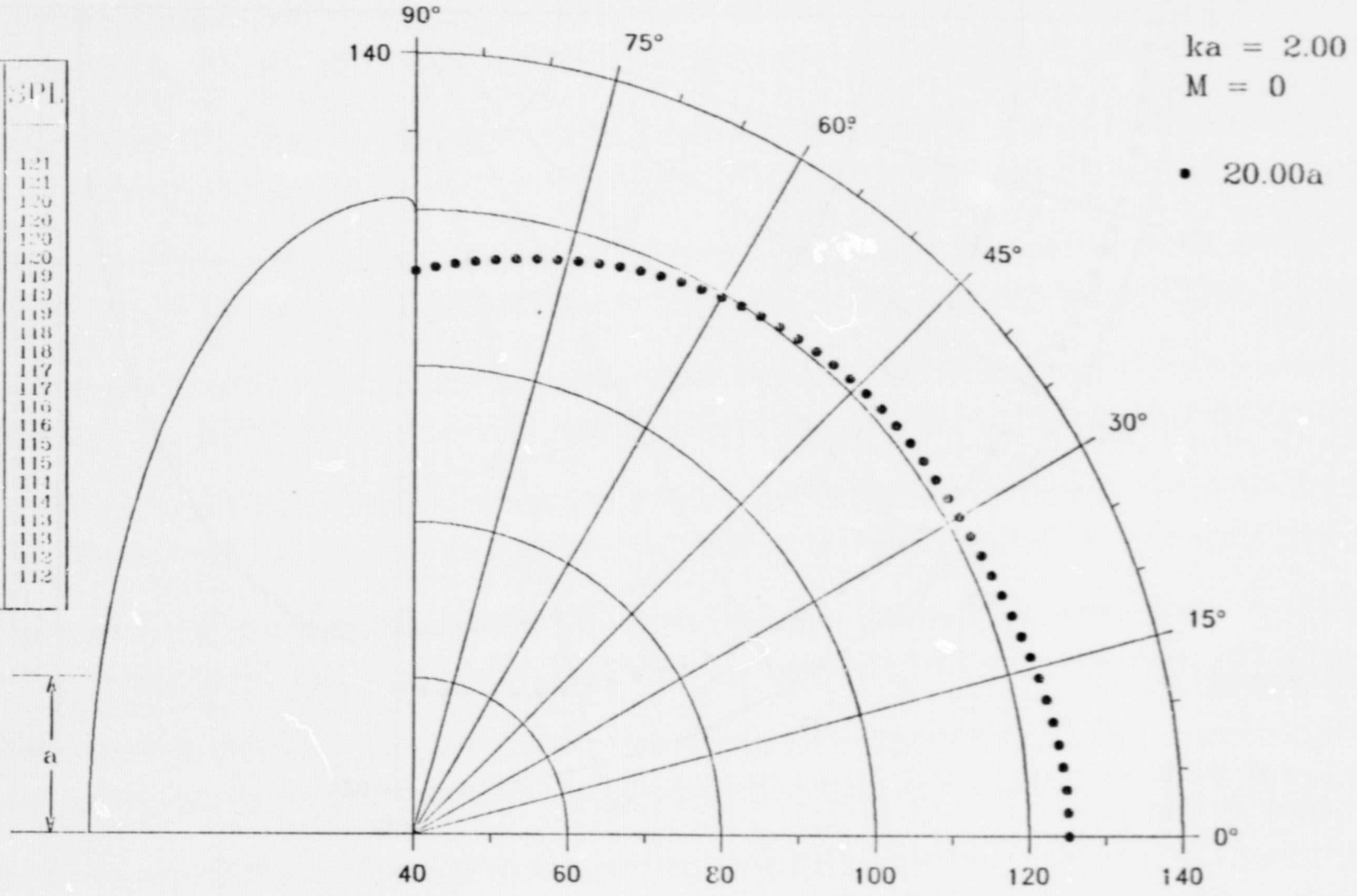

Fig. 69 SPL (dB)

PLANE BAFFLE

Deg	SPL	Deg	SPL
0	123	46	124
2	123	48	123
4	123	50	123
6	123	52	123
8	123	54	122
10	123	56	122
12	123	58	121
14	123	60	121
16	123	62	120
18	123	64	120
20	123	66	119
22	123	68	118
24	126	70	118
26	126	72	117
28	127	74	116
30	127	76	116
32	126	78	115
34	126	80	114
36	125	82	113
38	125	84	113
40	125	86	112
42	123	88	111
44	124	90	111

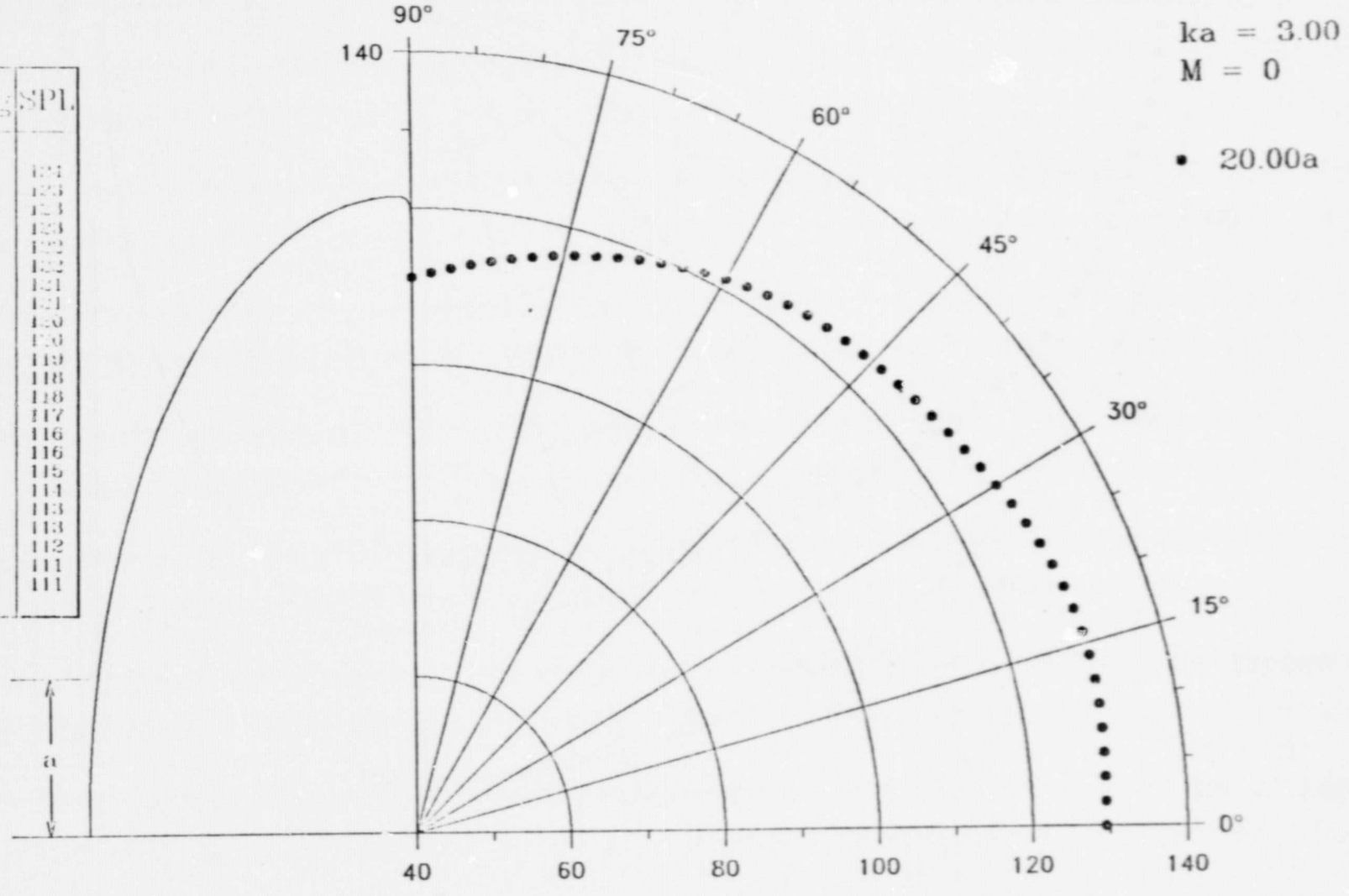

Fig. 70 SPL (dB)

PLANE BAFFLE

Deg	SPL	Deg	SPL
0	13[illegible]	[illegible]	[illegible]
2	13[illegible]	[illegible]	[illegible]
4	13[illegible]	[illegible]	[illegible]
6	131	[illegible]	[illegible]
8	131	[illegible]	[illegible]
10	13[illegible]	[illegible]	[illegible]
12	13[illegible]	[illegible]	[illegible]
14	13[illegible]	[illegible]	[illegible]
16	13[illegible]	[illegible]	[illegible]
18	13[illegible]	[illegible]	[illegible]
20	13[illegible]	[illegible]	[illegible]
22	13[illegible]	[illegible]	[illegible]
24	132	[illegible]	[illegible]
26	131	[illegible]	[illegible]
28	130	[illegible]	[illegible]
30	130	[illegible]	[illegible]
32	129	[illegible]	[illegible]
34	128	[illegible]	[illegible]
36	127	[illegible]	[illegible]
38	127	[illegible]	[illegible]
40	126	[illegible]	[illegible]
42	125	[illegible]	[illegible]
44	124	[illegible]	[illegible]

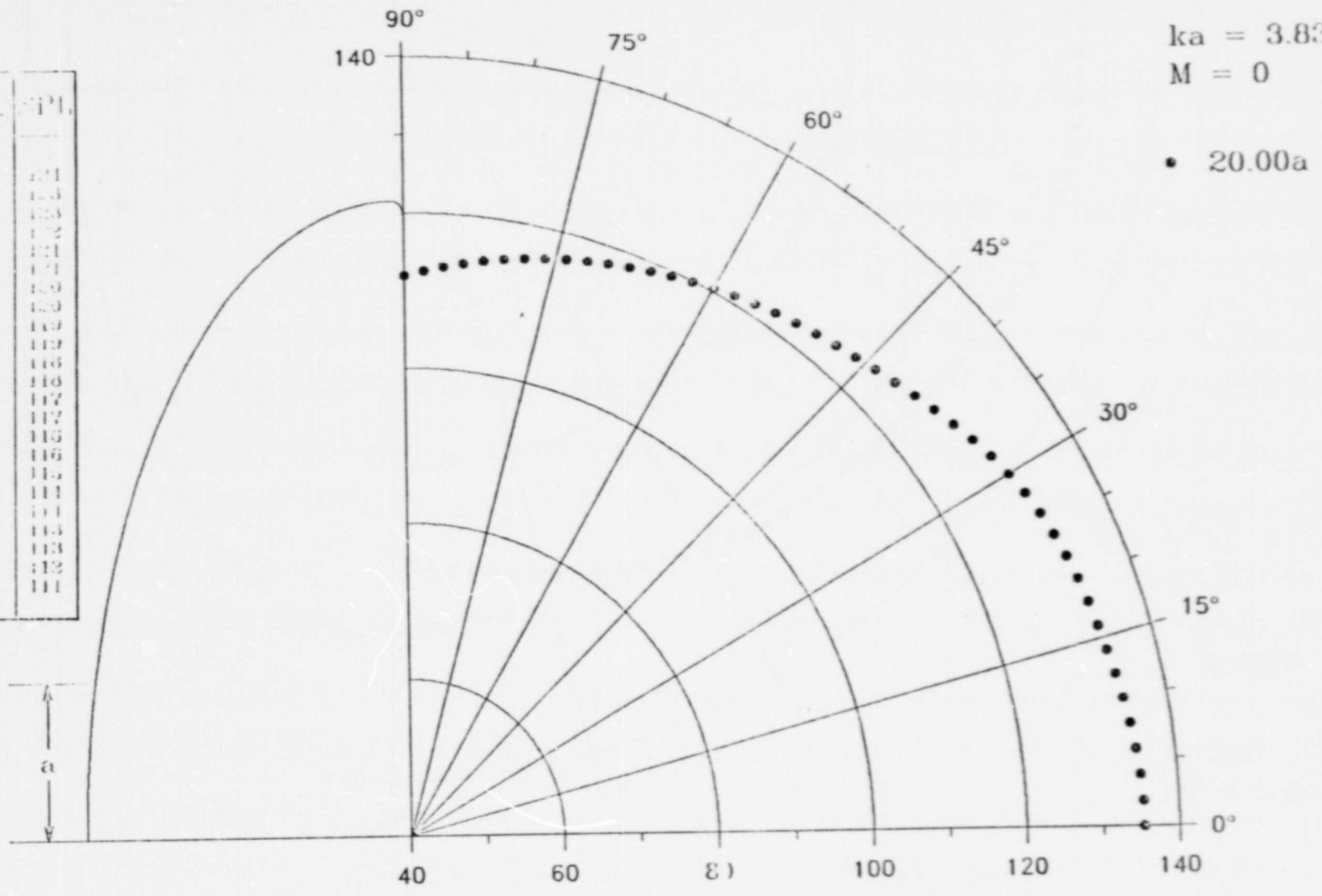

Fig. 71 SPL (dB)

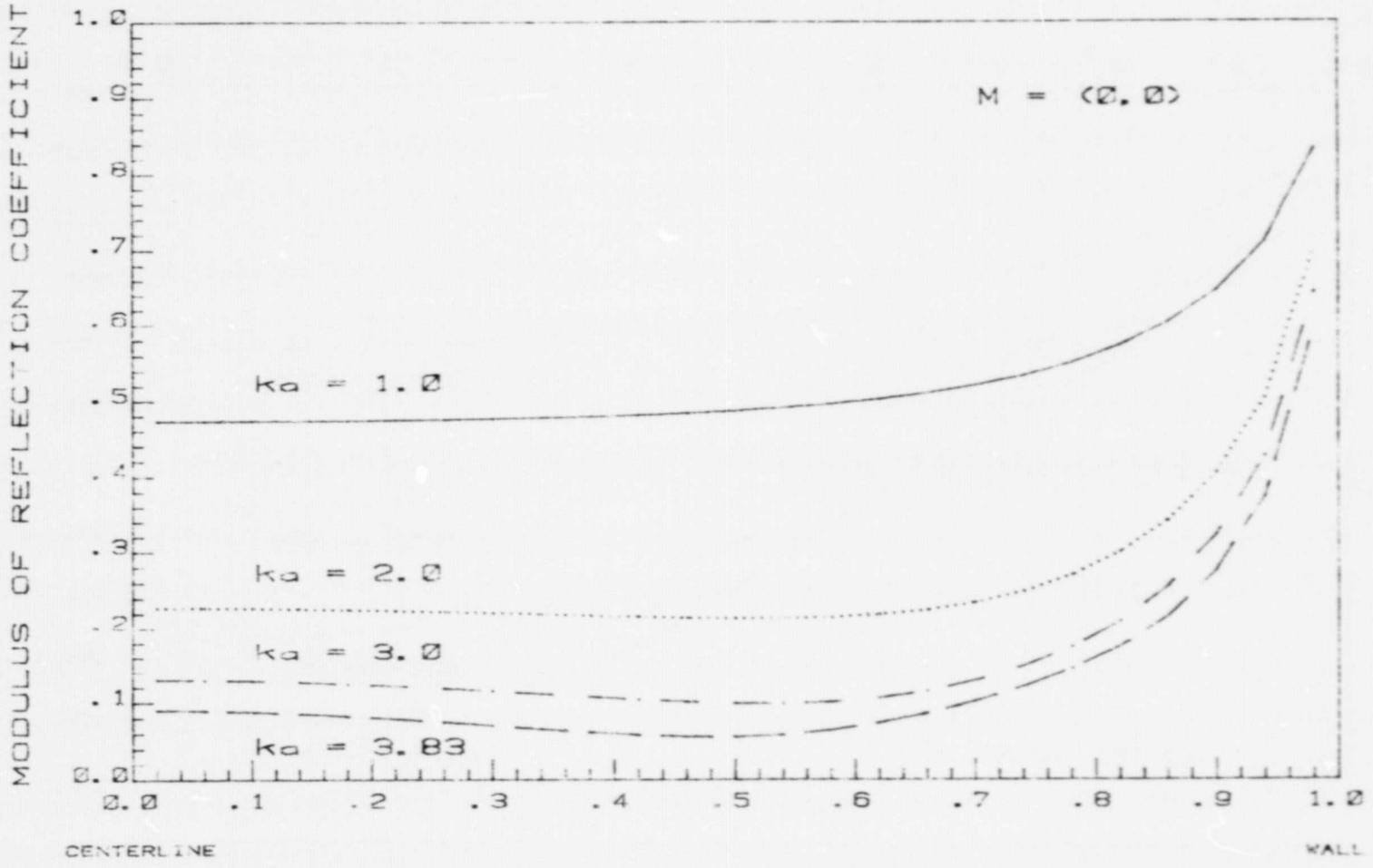

PLANE BAFFLE

Fig. 72

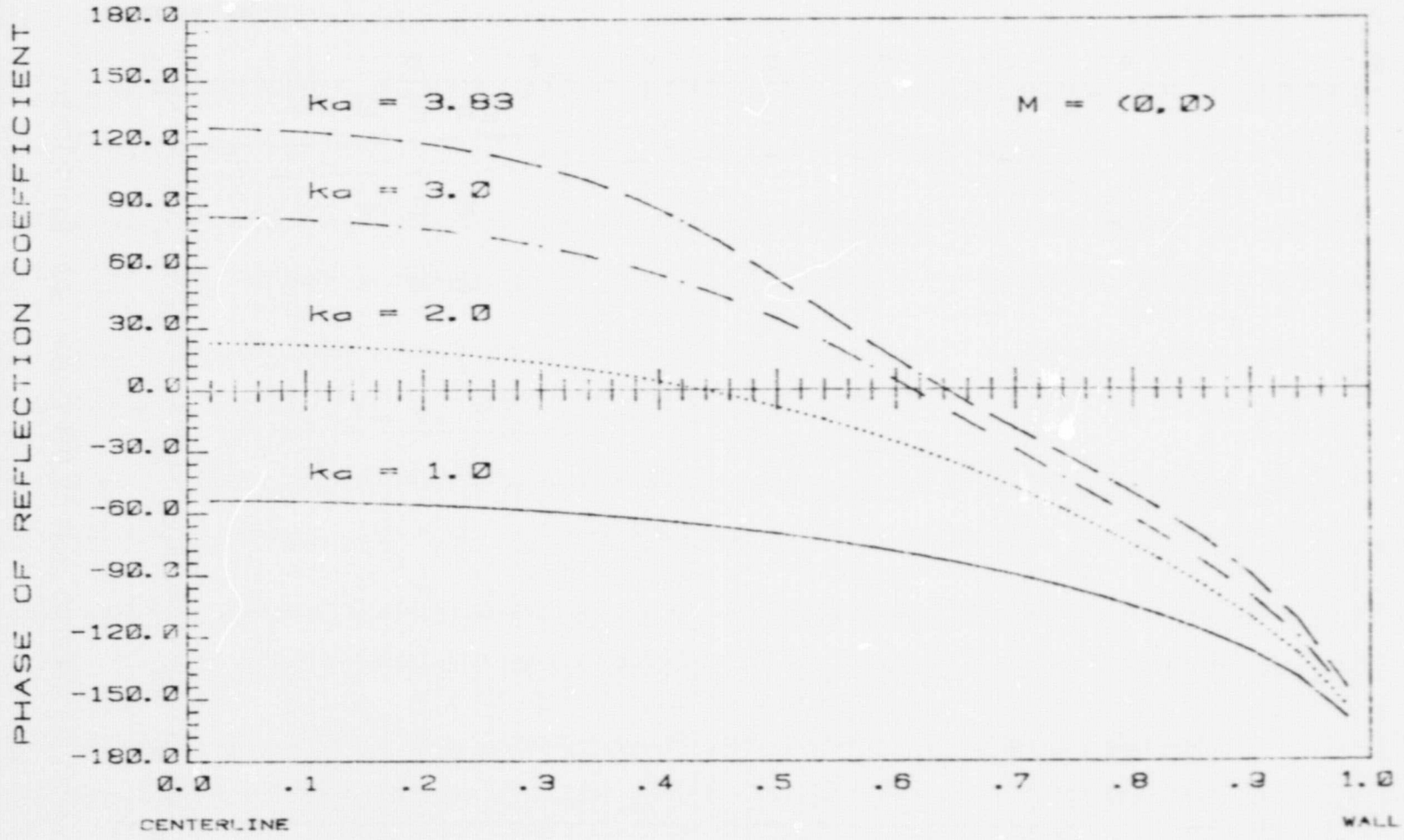

PLANE BAFFLE

Fig. 73

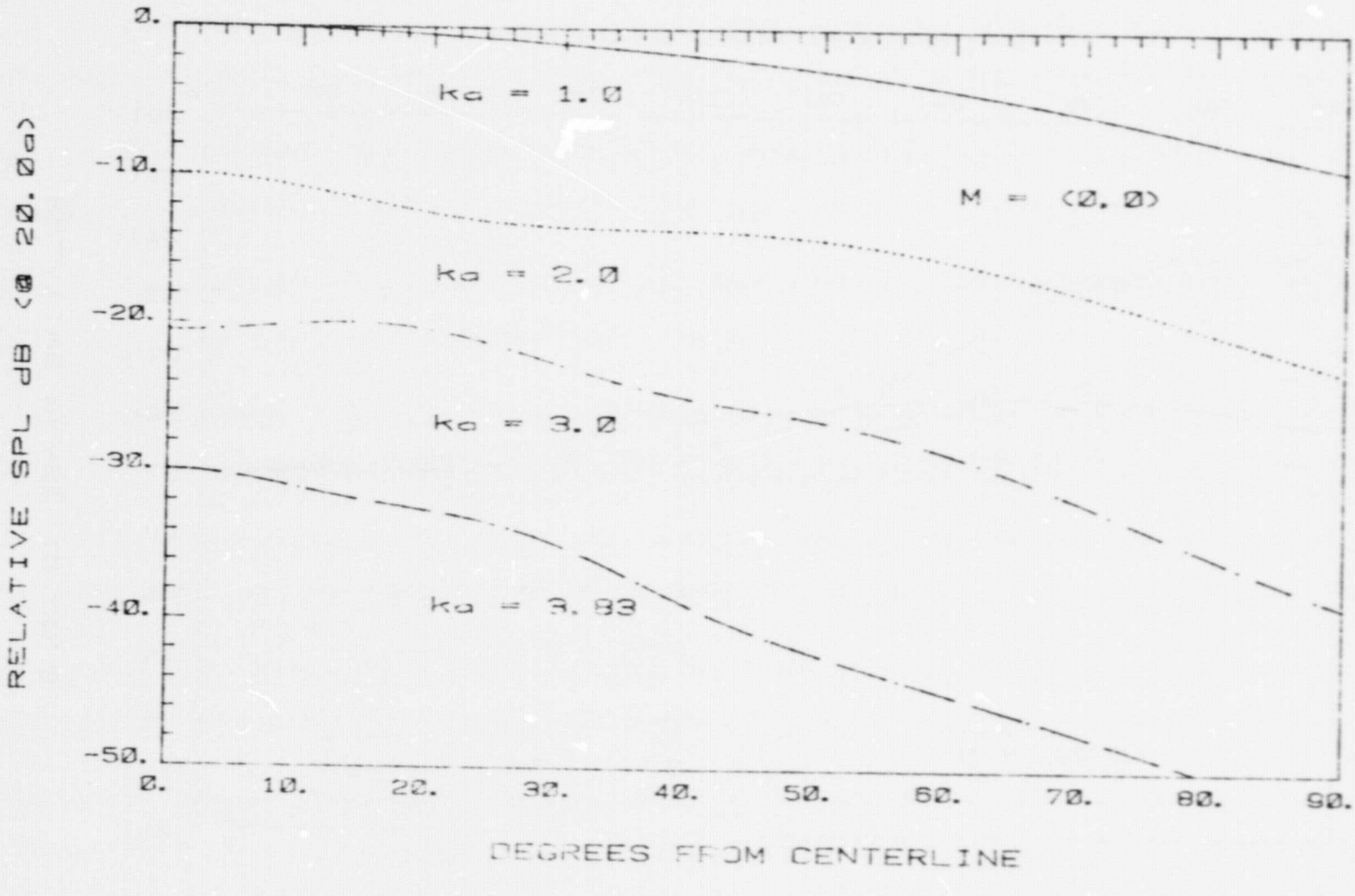

PLANE BAFFLE

Fig. 74

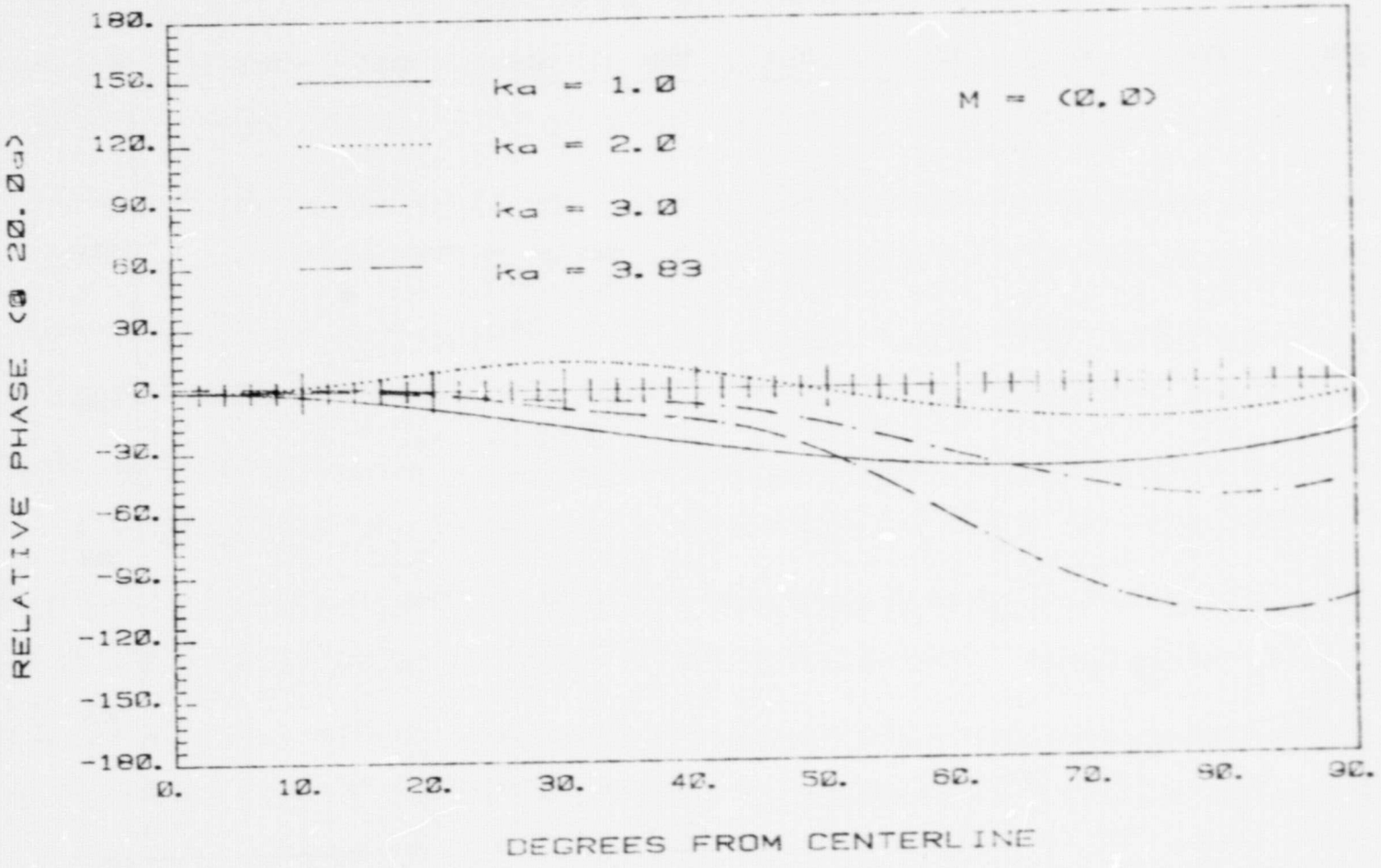

PLANE BAFFLE

Fig. 75

PLANE BAFFLE

Deg	SPL	Deg	SPL
0	117	46	94
2	117	48	100
4	116	50	103
6	116	52	105
8	115	54	107
10	115	56	108
12	114	58	109
14	113	60	110
16	112	62	110
18	111	64	110
20	110	66	110
22	110	68	110
24	109	70	110
26	109	72	110
28	108	74	109
30	108	76	109
32	107	78	109
34	106	80	108
36	105	82	108
38	103	84	107
40	100	86	106
42	95	88	106
44	78	90	105

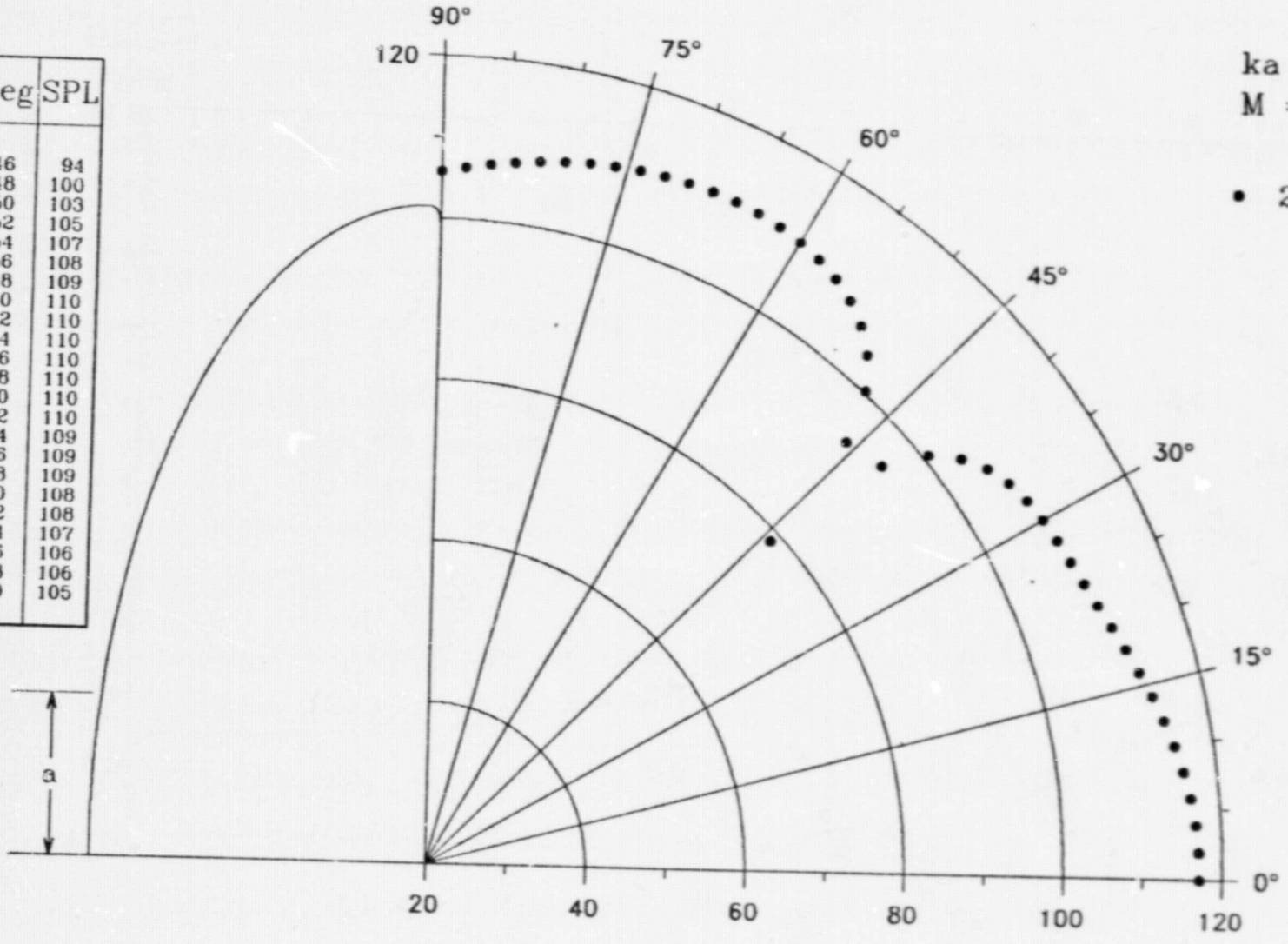

Fig. 76 SPL (dB)

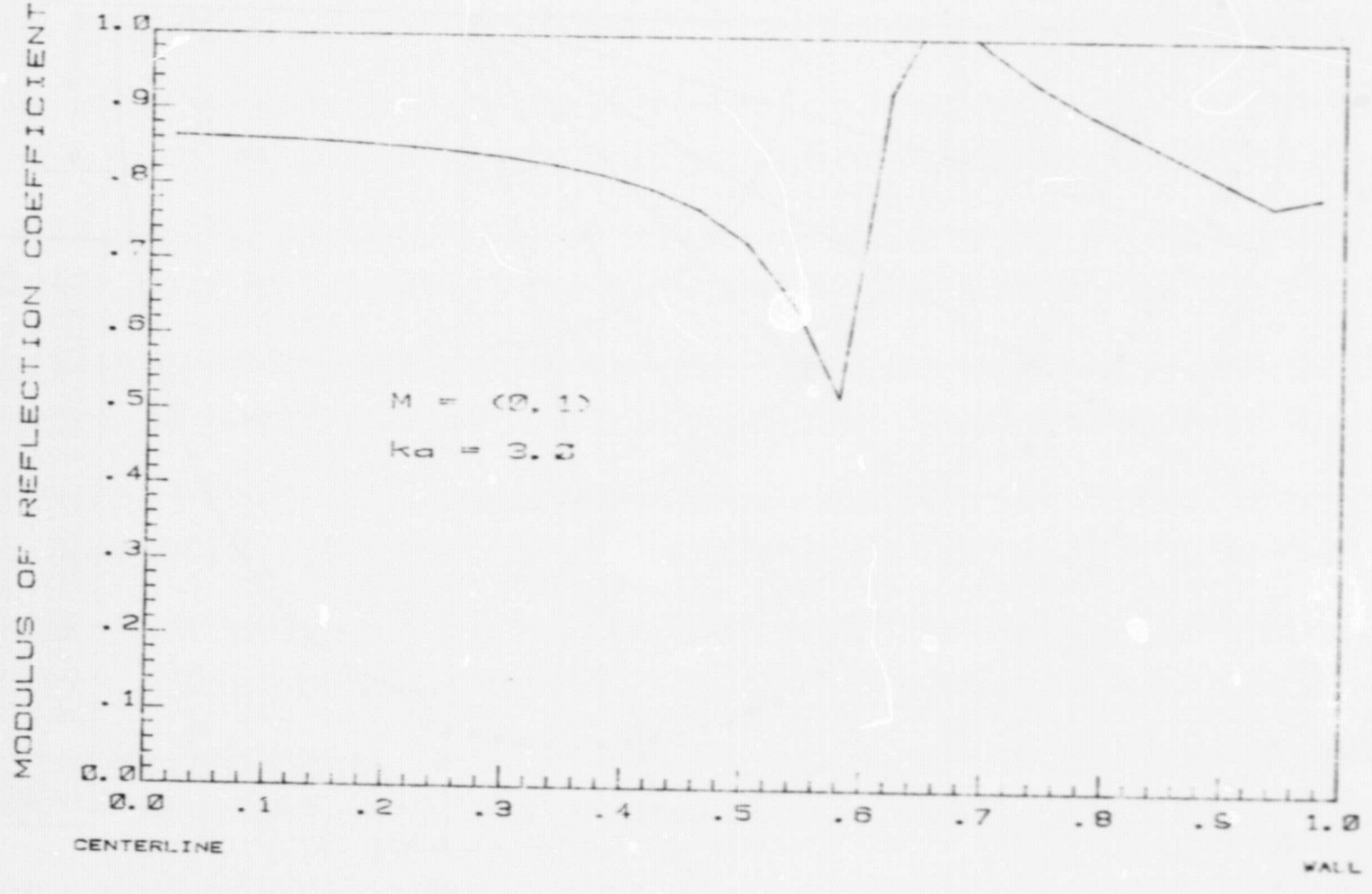

PLANE BAFFLE

Fig. 77

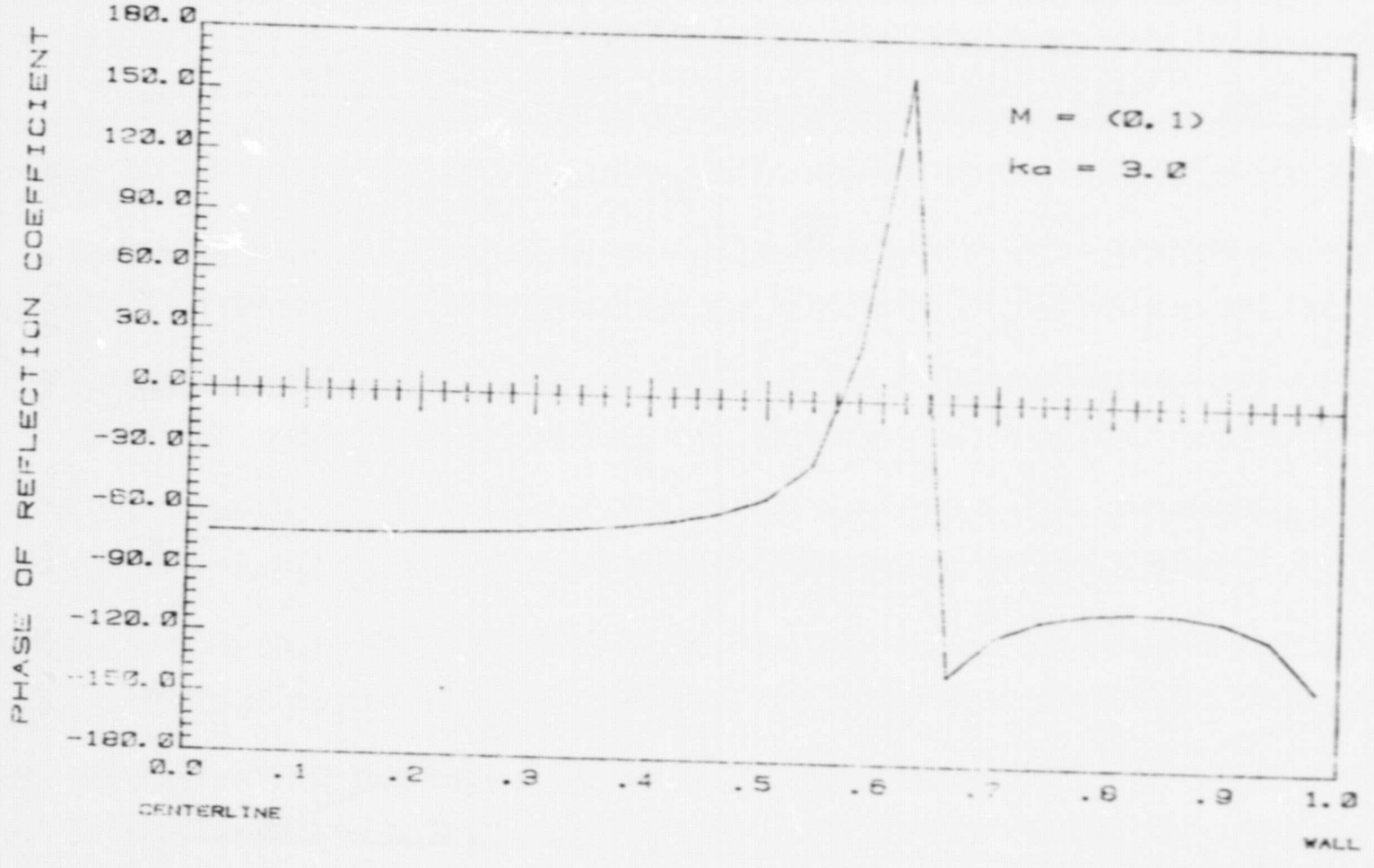

PLANE BAFFLE

Fig. 78

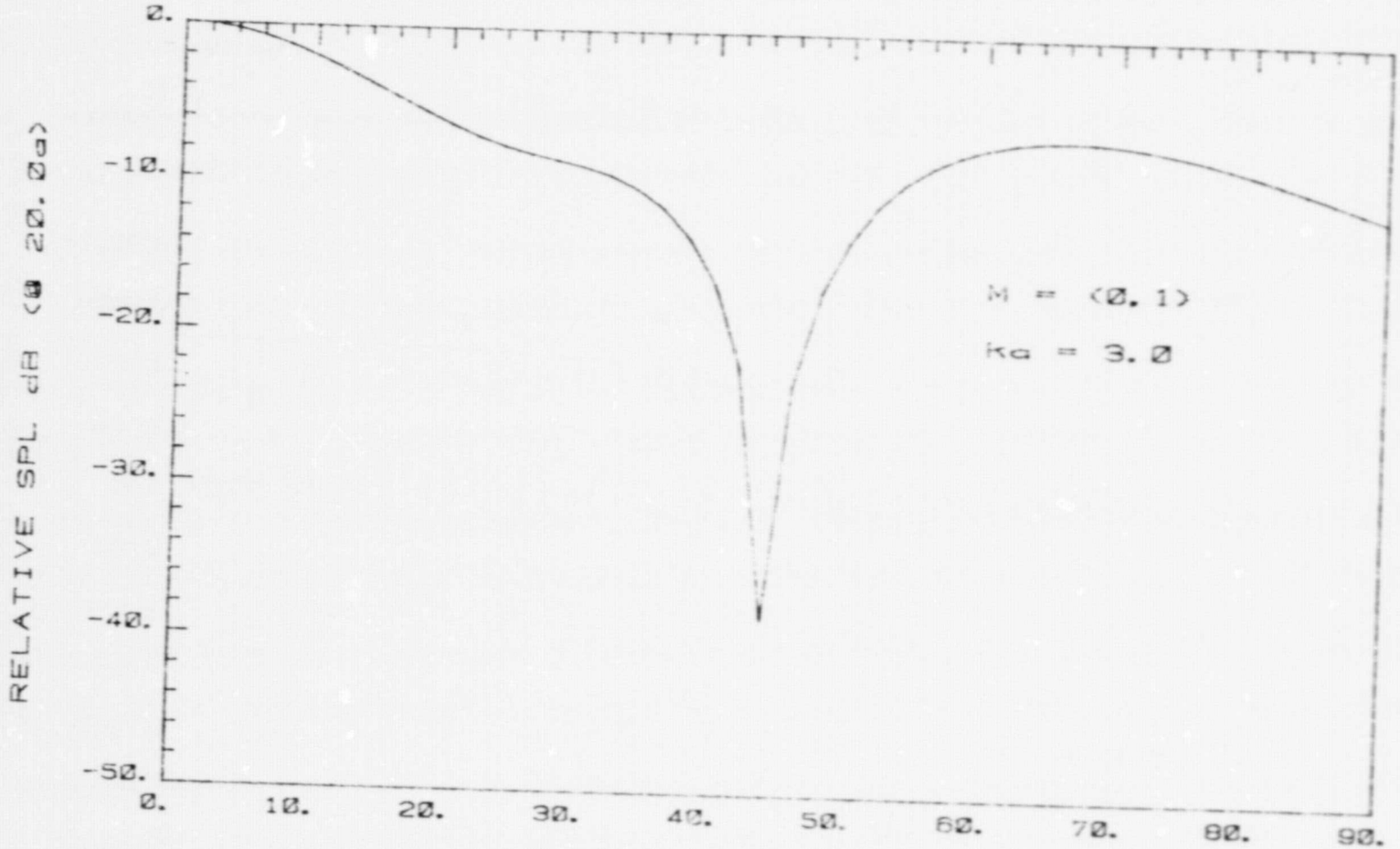

PLANE BAFFLE

Fig. 79

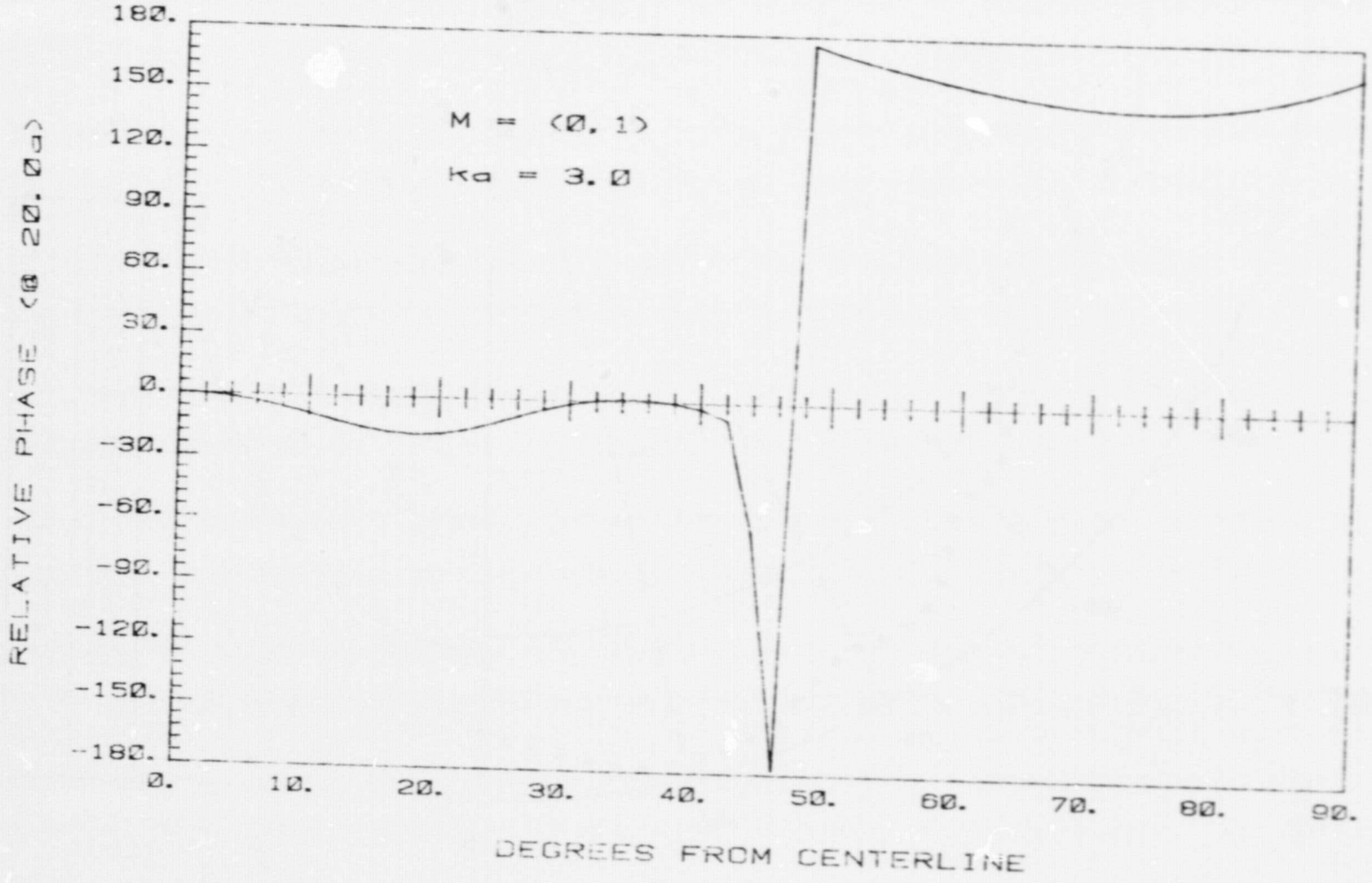

PLANE BAFFLE

Fig. 80

PLANE BAFFLE

Deg	SPL	Deg	SPL
0	8	46	105
2	−10	48	106
4	32	50	108
6	61	52	111
8	78	54	112
10	87	56	113
12	90	58	113
14	90	60	112
16	90	62	112
18	88	64	113
20	94	66	115
22	97	68	116
24	89	70	117
26	92	72	117
28	90	74	117
30	92	76	117
32	97	78	117
34	94	80	116
36	92	82	115
38	90	84	111
40	103	86	113
42	106	88	112
44	106	90	111

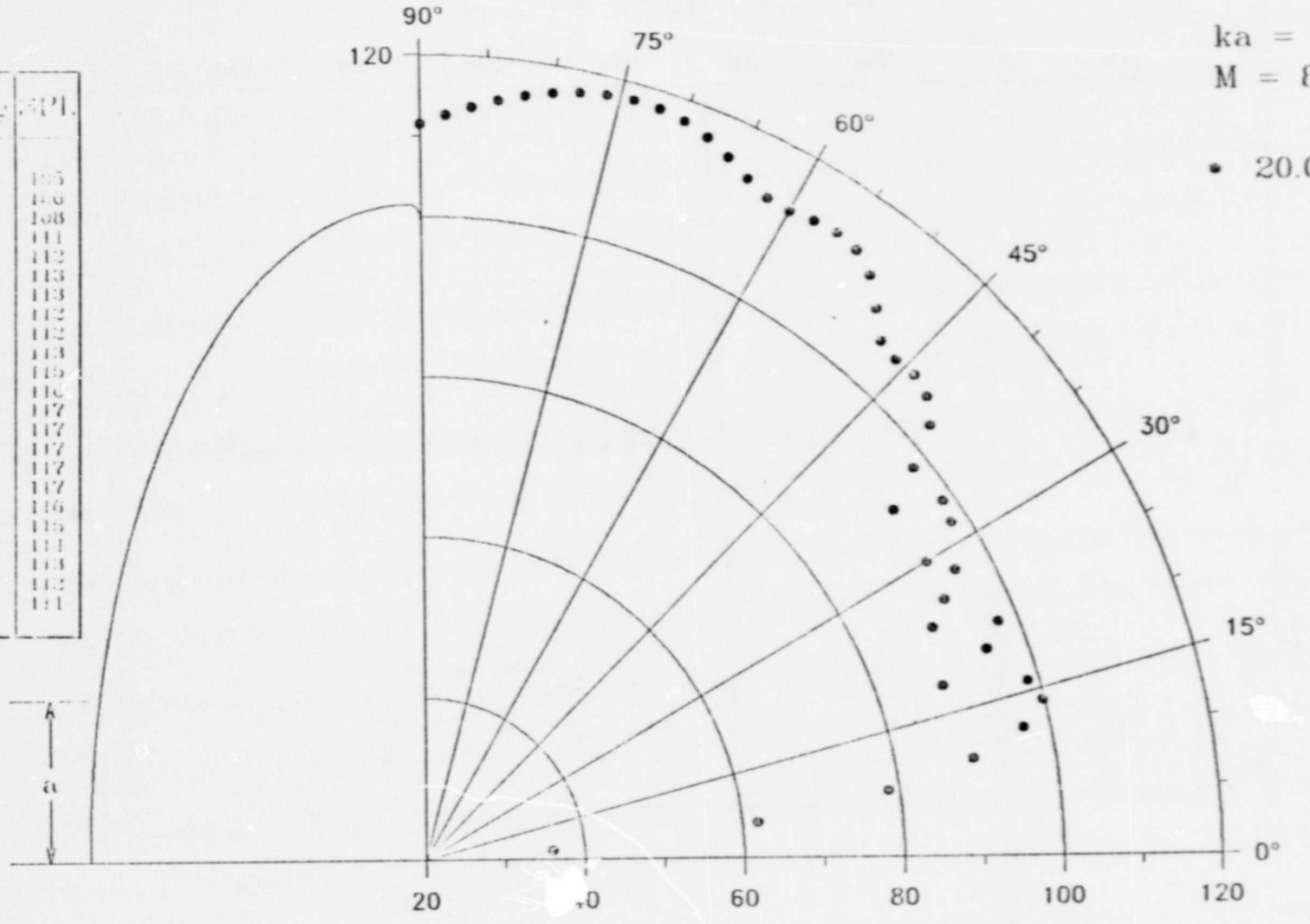

Fig. 81 SPL (dB)

PLANE BAFFLE

Deg	SPL	Deg	SPL
0	0	[illegible]	118
2	3	[illegible]	119
4	49	50	119
6	74	52	119
8	89	54	120
10	97	56	121
12	99	58	121
14	98	60	121
16	98	62	120
18	96	64	120
20	96	66	120
22	96	68	120
24	91	70	120
26	92	72	120
28	100	74	120
30	104	76	120
32	106	78	119
34	107	80	118
36	110	82	117
38	113	84	115
40	114	86	114
42	115	88	113
44	117	90	112

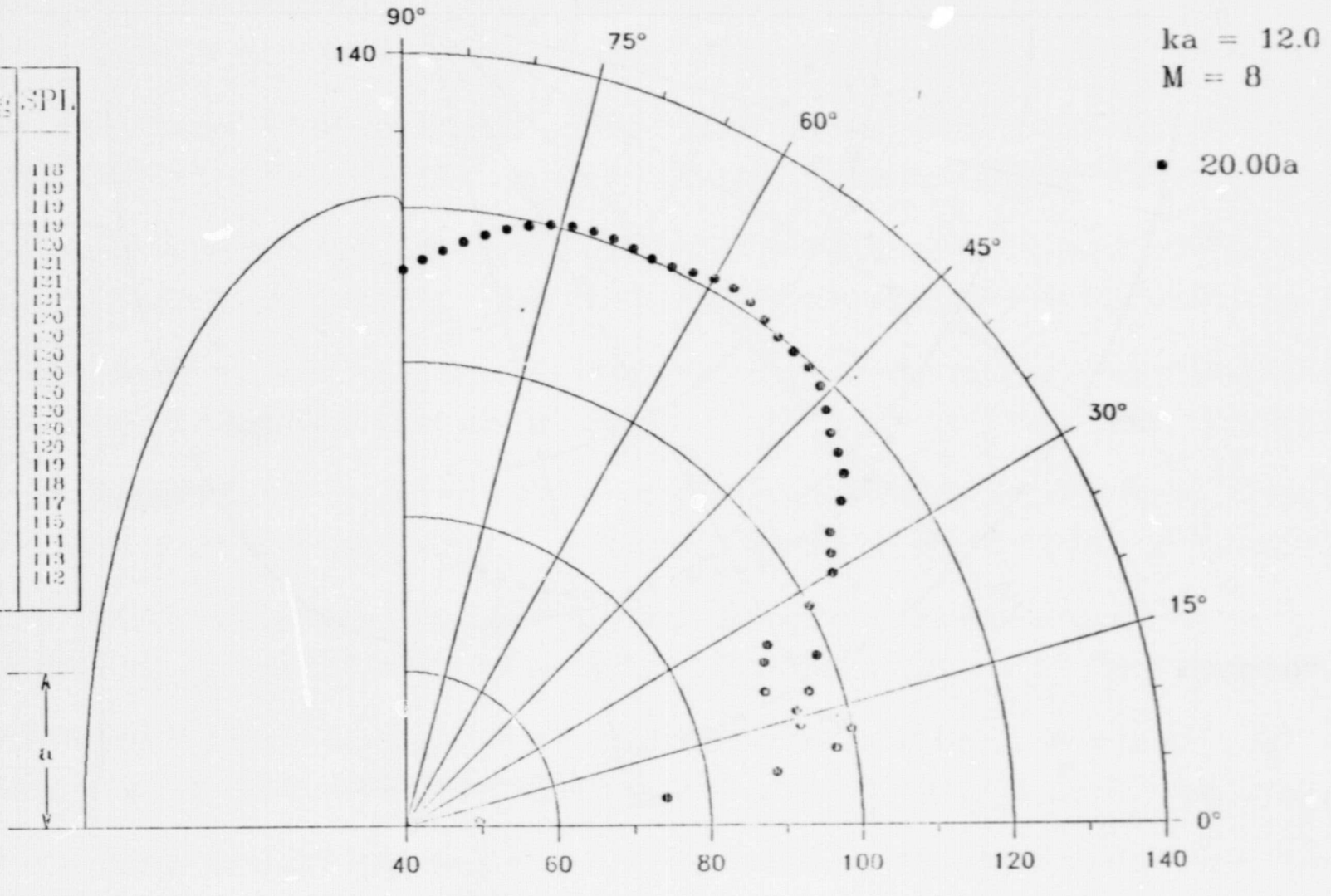

Fig. 82 SPL (dB)

PLANE BAFFLE

Deg	SPL	Deg	SPL
0	0	[illegible]	135
2	8	[illegible]	134
4	51	[illegible]	134
6	78	[illegible]	134
8	91	[illegible]	134
10	95	[illegible]	134
12	95	[illegible]	134
14	89	[illegible]	133
16	93	[illegible]	132
18	91	[illegible]	131
20	95	[illegible]	130
22	94	[illegible]	130
24	101	[illegible]	129
26	105	[illegible]	129
28	107	[illegible]	128
30	111	[illegible]	127
32	114	[illegible]	126
34	116	[illegible]	125
36	118	[illegible]	124
38	120	[illegible]	123
40	121	[illegible]	121
42	122	[illegible]	119
44	123	[illegible]	109

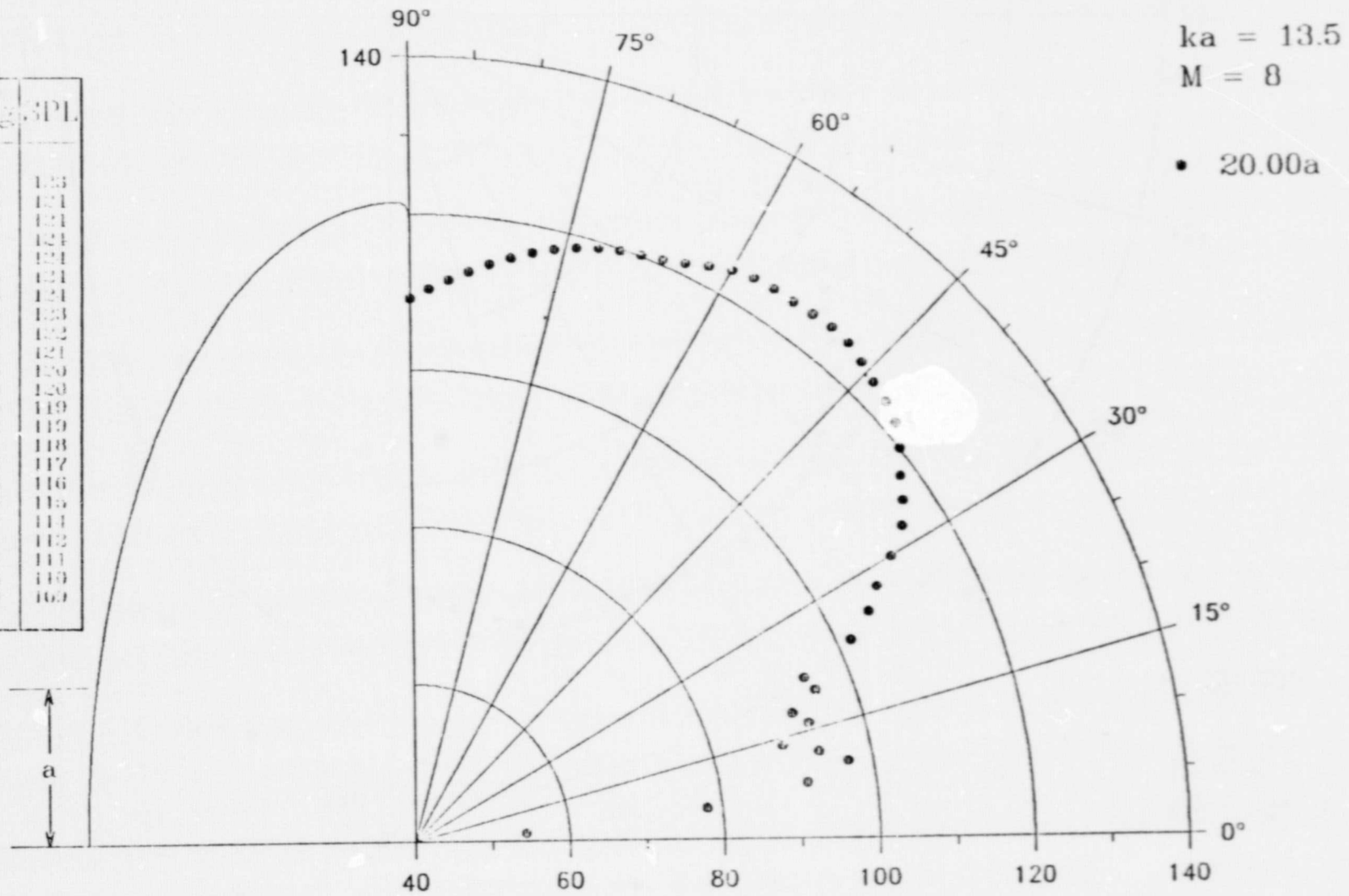

Fig. 83 SPL (dB)

PLANE BAFFLE

Deg	SPL	Deg	SPL
0	6	[illegible]	[illegible]
2	13	[illegible]	[illegible]
4	58	[illegible]	[illegible]
6	81	[illegible]	[illegible]
8	93	[illegible]	[illegible]
10	93	[illegible]	[illegible]
12	83	[illegible]	[illegible]
14	95	[illegible]	[illegible]
16	85	[illegible]	[illegible]
18	91	[illegible]	[illegible]
20	97	[illegible]	[illegible]
22	[illegible]	[illegible]	[illegible]
24	[illegible]	[illegible]	[illegible]
26	[illegible]	[illegible]	[illegible]
28	[illegible]	[illegible]	[illegible]
30	[illegible]	[illegible]	[illegible]
32	[illegible]	[illegible]	[illegible]
34	[illegible]	[illegible]	[illegible]
36	[illegible]	[illegible]	[illegible]
38	[illegible]	[illegible]	[illegible]
40	[illegible]	[illegible]	[illegible]
42	[illegible]	[illegible]	[illegible]
44	[illegible]	[illegible]	[illegible]

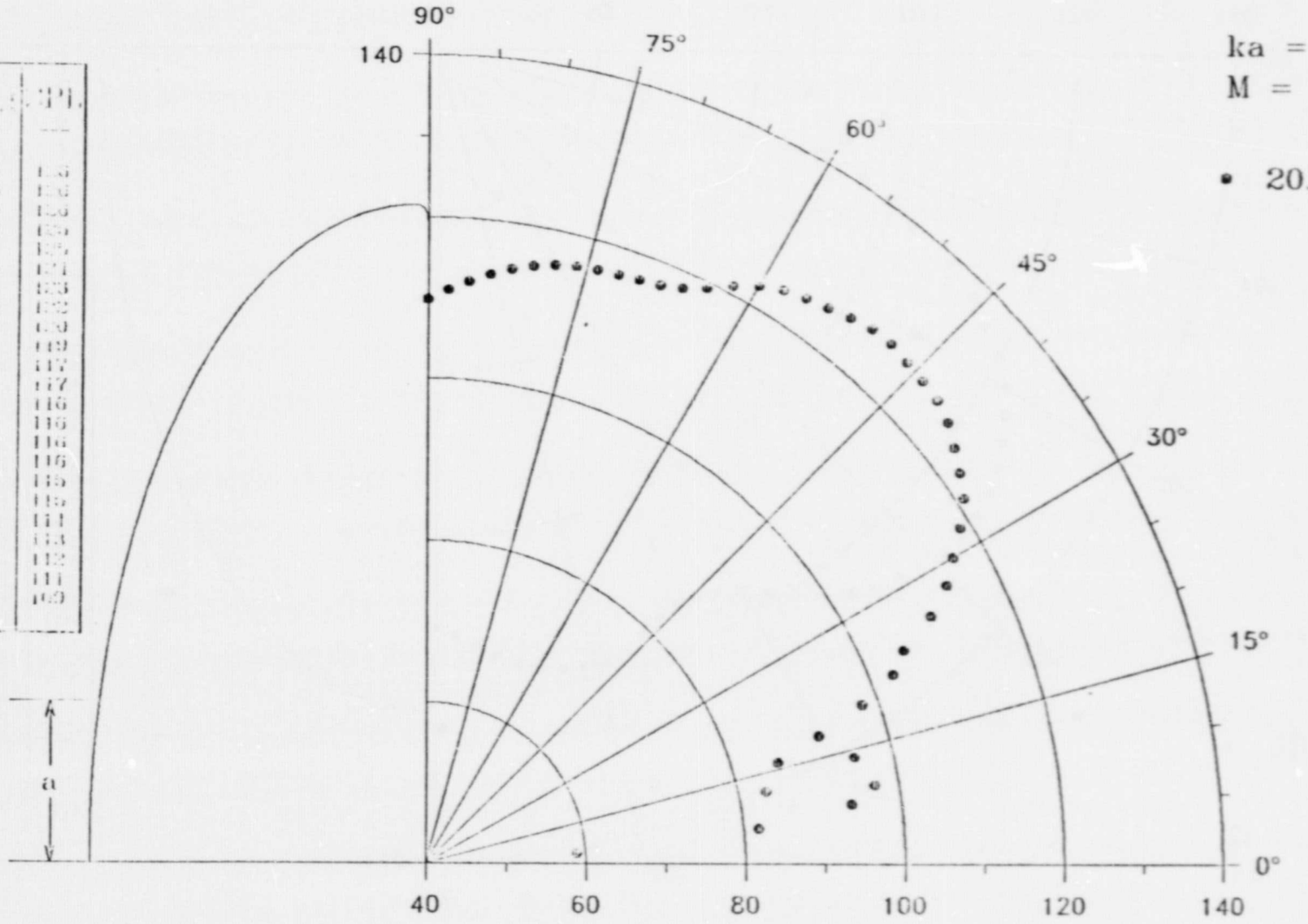

Fig. 84 SPL (dB)

PLANE BAFFLE

Deg	SPL	Deg	SPL
0	6	[illegible]	127
2	20	[illegible]	127
4	67	[illegible]	126
6	86	[illegible]	121
8	96	[illegible]	120
10	91	[illegible]	120
12	92	[illegible]	118
14	89	[illegible]	116
16	95	[illegible]	115
18	99	[illegible]	114
20	103	[illegible]	114
22	109	[illegible]	115
24	113	[illegible]	116
26	116	[illegible]	117
28	119	[illegible]	118
30	122	[illegible]	118
32	124	[illegible]	118
34	125	[illegible]	117
36	127	[illegible]	116
38	128	[illegible]	115
40	128	[illegible]	113
42	128	[illegible]	112
44	128	[illegible]	110

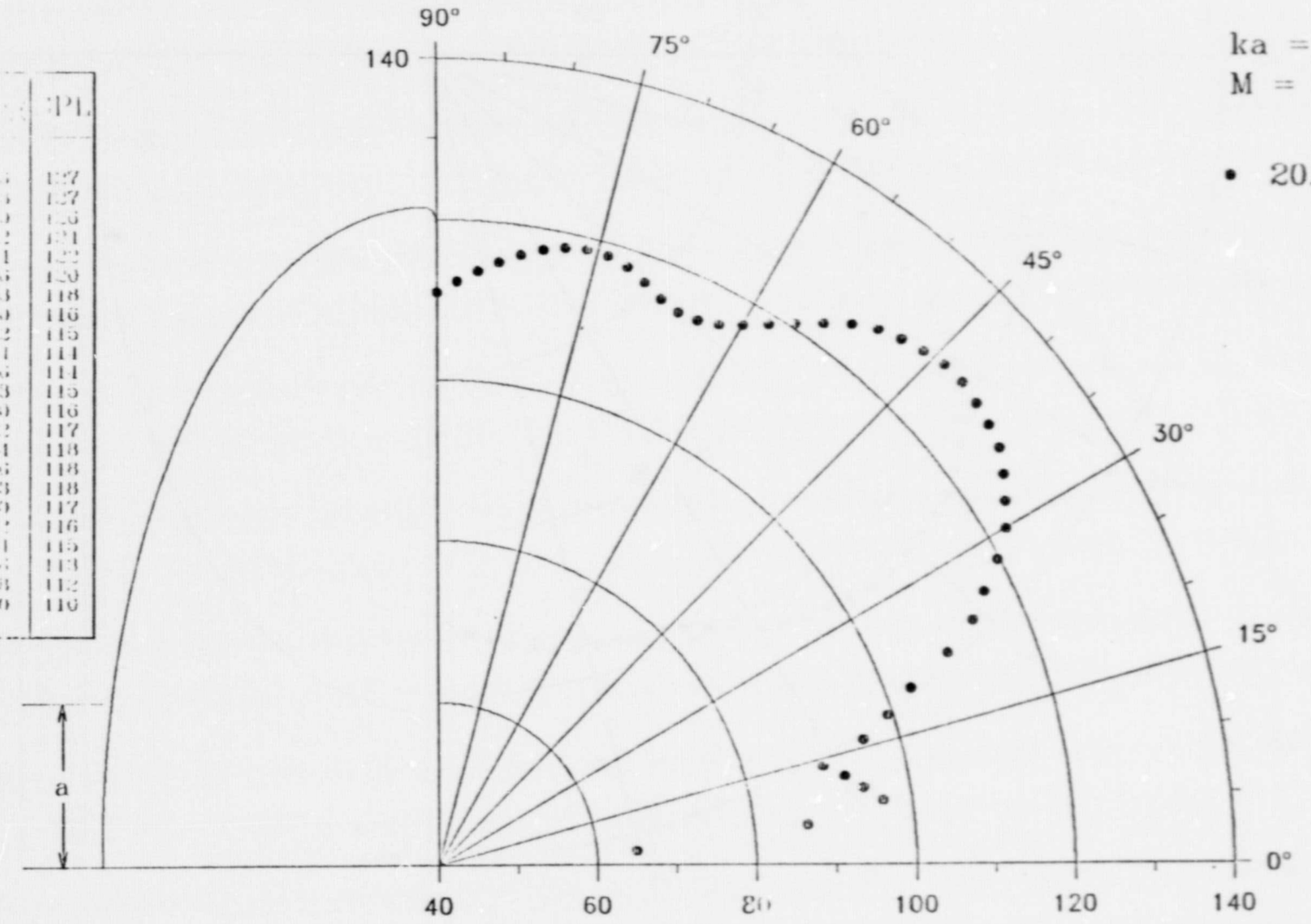

Fig. 85 SPL (dB)

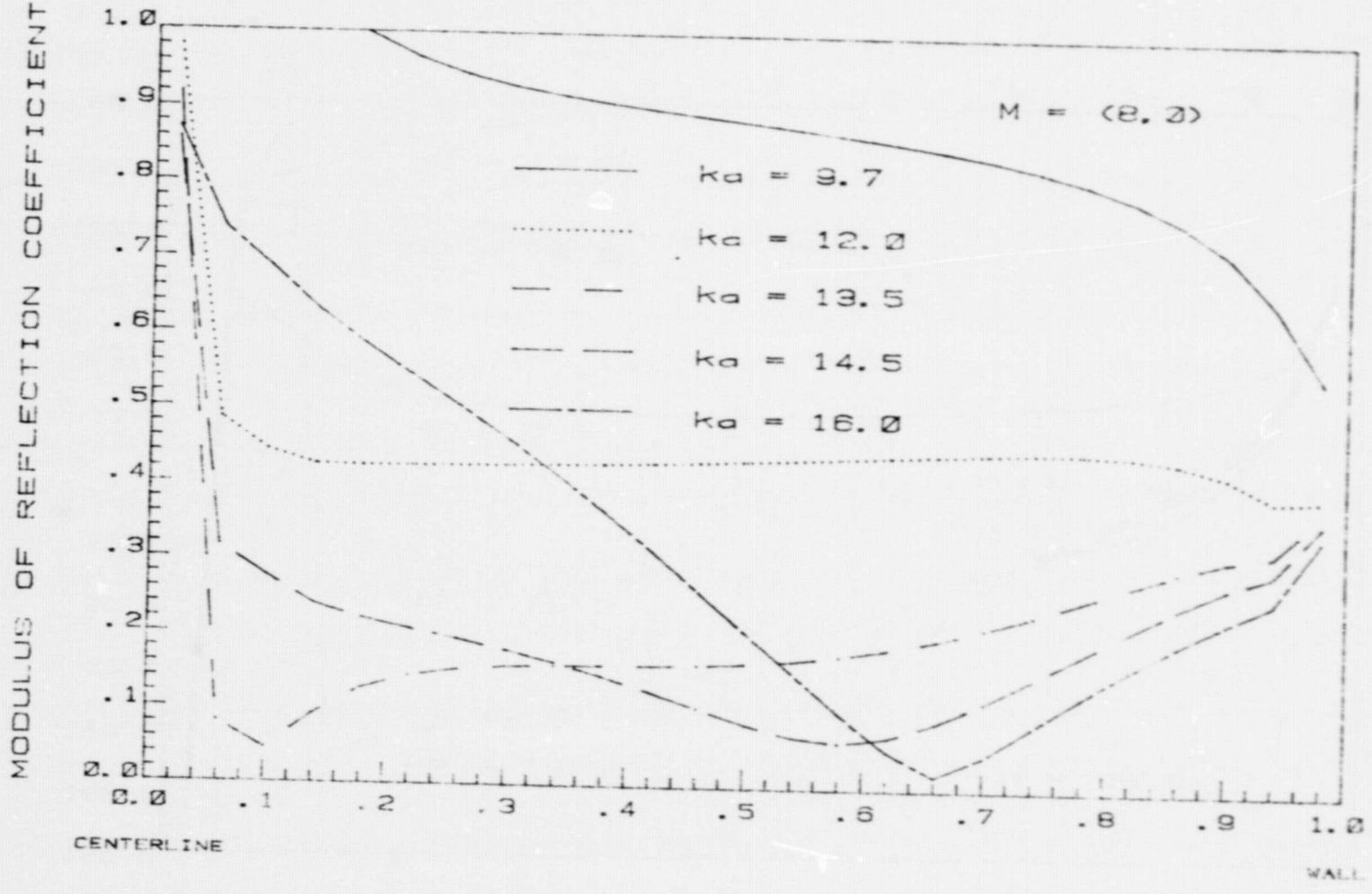

PLANE BAFFLE

Fig. 86

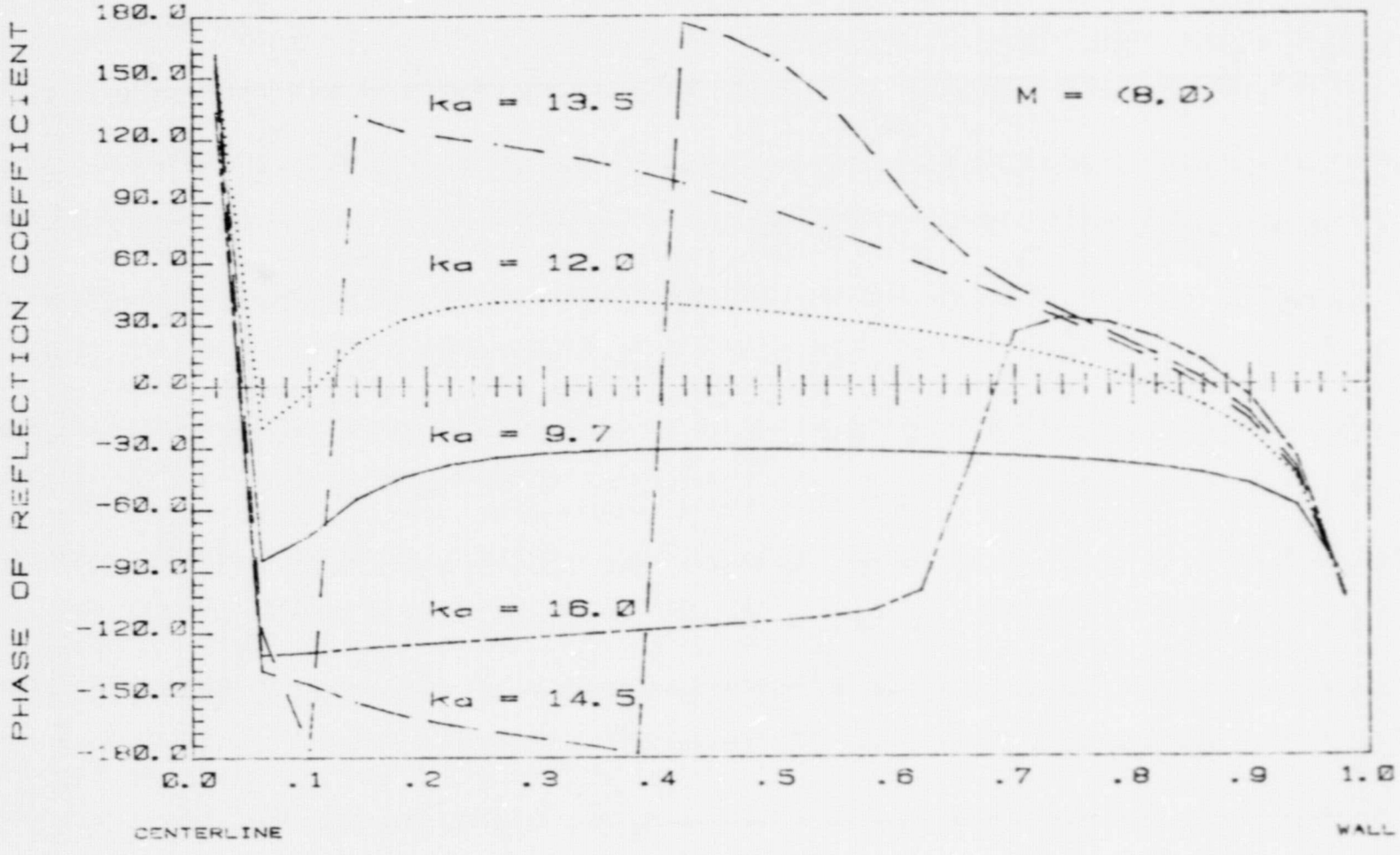

PLANE BAFFLE

Fig. 87

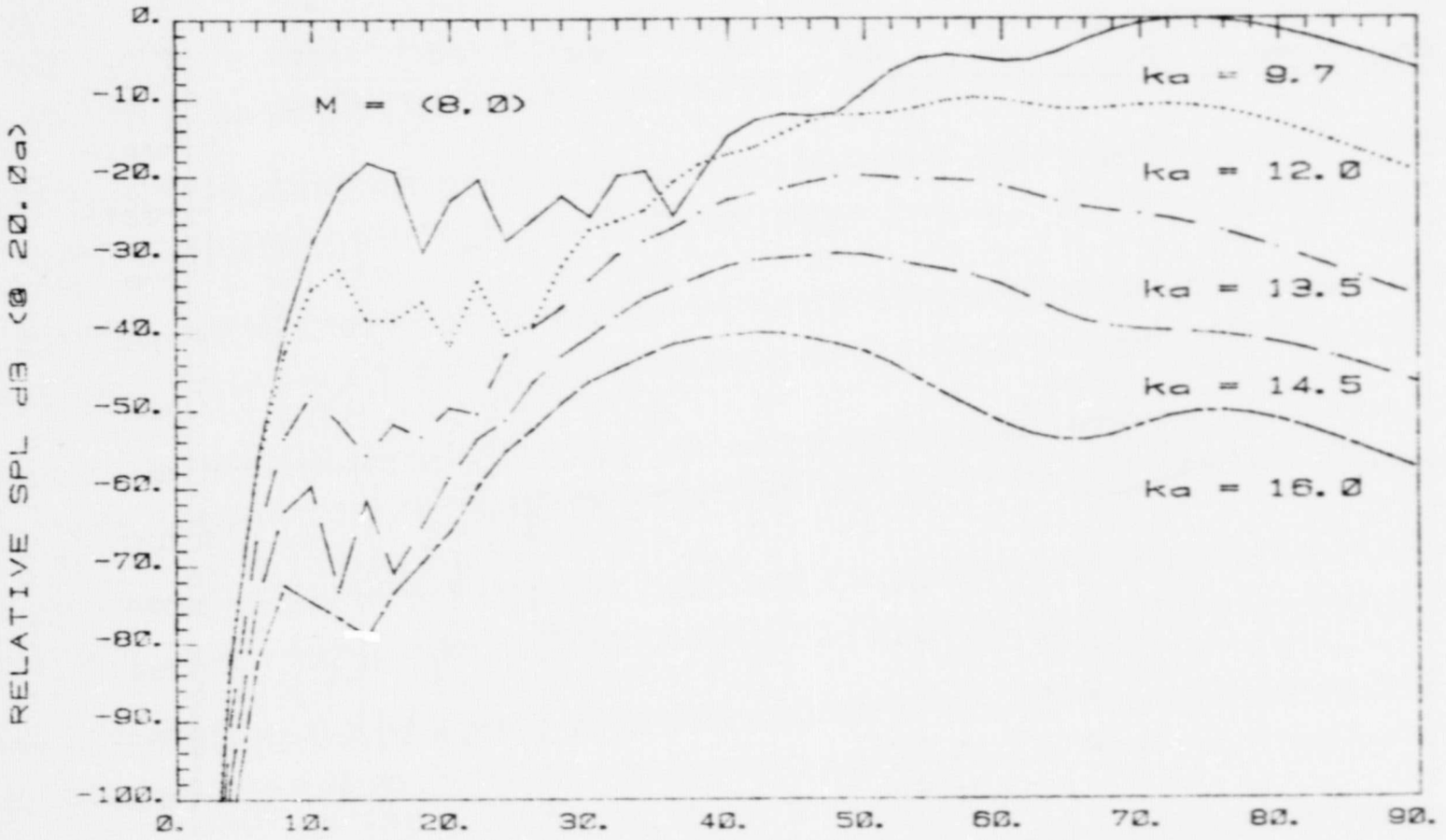

PLANE BAFFLE

Fig. 88

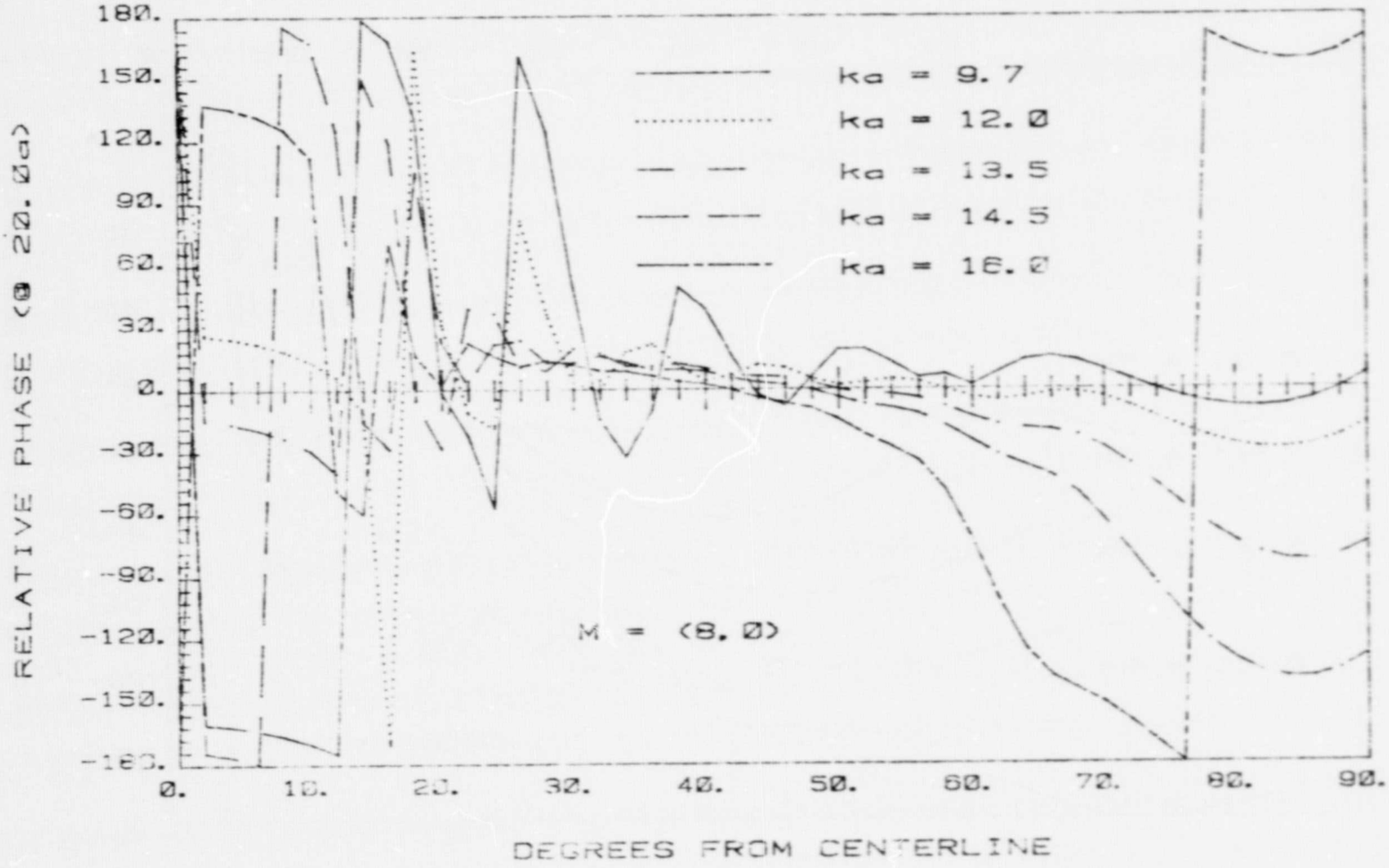

PLANE BAFFLE

Fig. 89

PLANE BAFFLE

Deg	SPL	Deg	SPL
0	0	46	112
2	-1	48	112
4	44	50	112
6	69	52	113
8	84	54	113
10	92	56	112
12	94	58	110
14	87	60	109
16	89	62	108
18	91	64	107
20	82	66	106
22	87	68	105
24	85	70	105
26	96	72	106
28	97	74	108
30	95	76	109
32	99	78	110
34	104	80	110
36	107	82	109
38	107	84	109
40	108	86	108
42	110	88	107
44	112	90	106

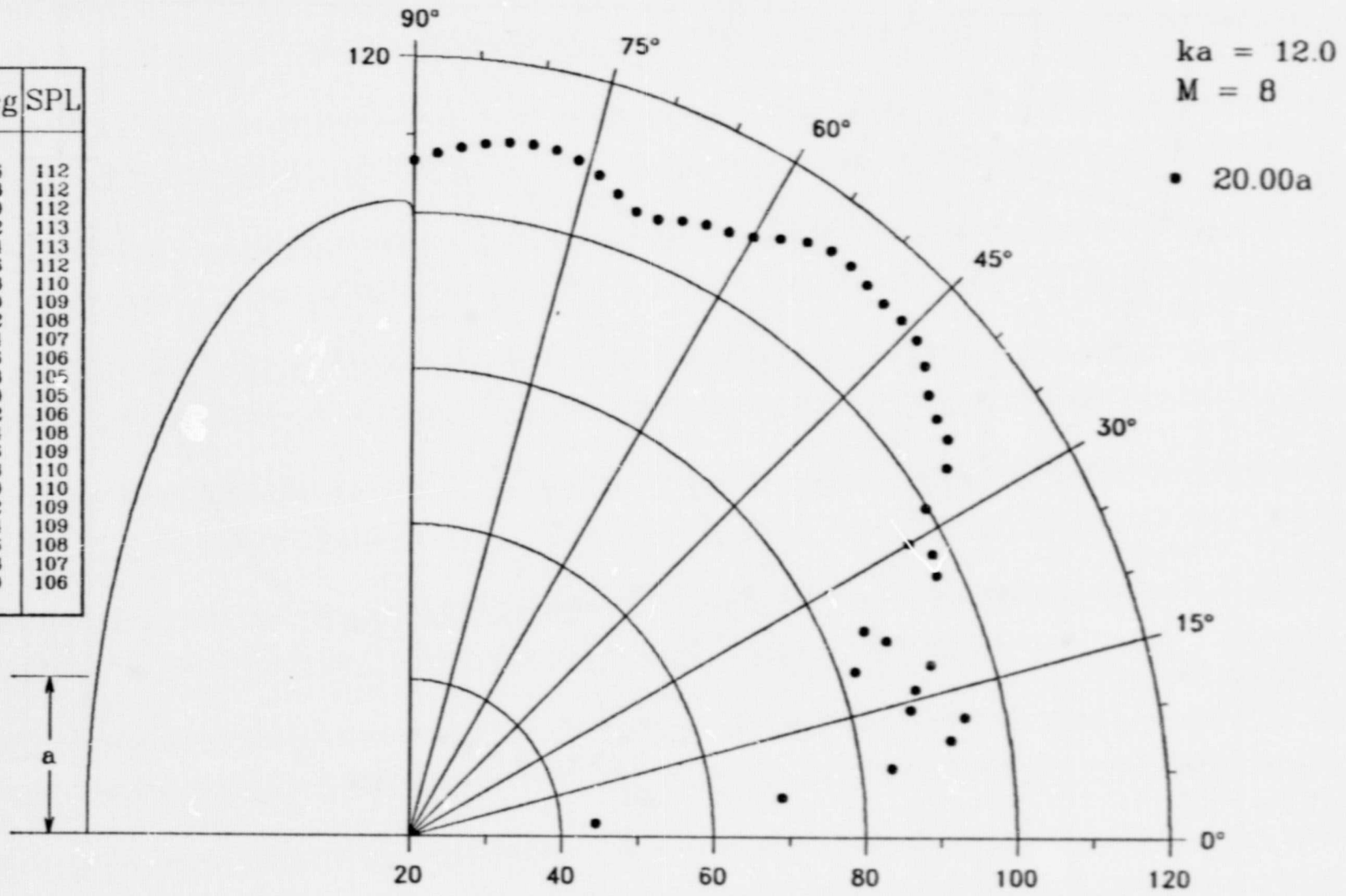

Fig. 90 SPL (dB)

PLANE BAFFLE

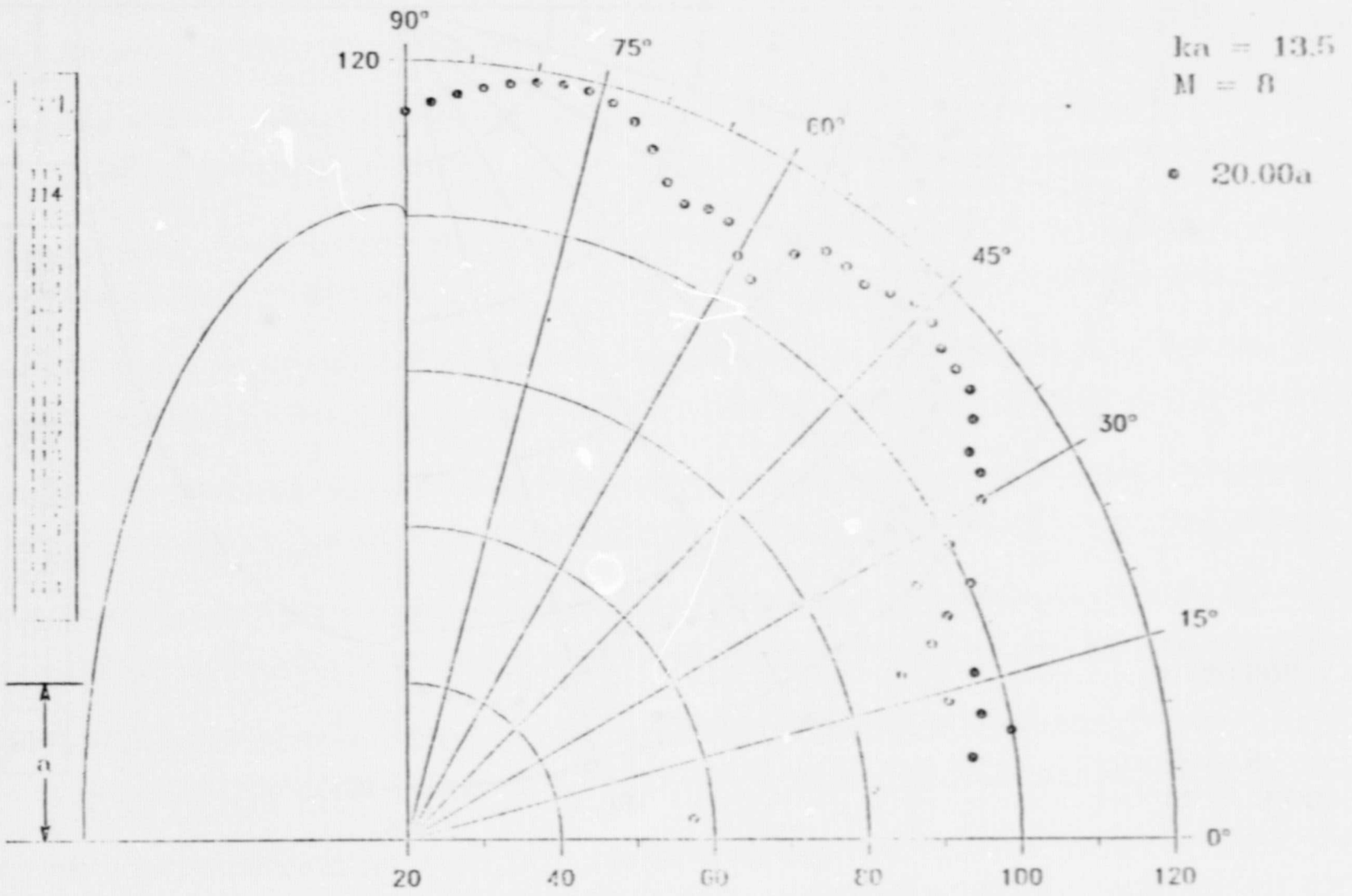

Deg	SPL
0	113
2	114
4	114
6	114
8	114
10	114
12	114
14	114
16	114
18	114
20	112
22	115
24	109
26	113
28	110
30	106
32	108
34	108
36	111
38	113
40	113
42	113
44	115

Fig. 91 SPL (dB)

PLANE BAFFLE

Deg	SPL	Deg	SPL
0	0	46	115
2	17	48	111
4	62	50	113
6	85	52	114
8	97	54	115
10	100	56	114
12	87	58	114
14	97	60	117
16	84	62	118
18	84	64	118
20	92	66	118
22	90	68	118
24	90	70	119
26	105	72	120
28	102	74	121
30	106	76	121
32	111	78	121
34	112	80	120
36	111	82	119
38	114	84	118
40	115	86	117
42	111	88	115
44	111	90	114

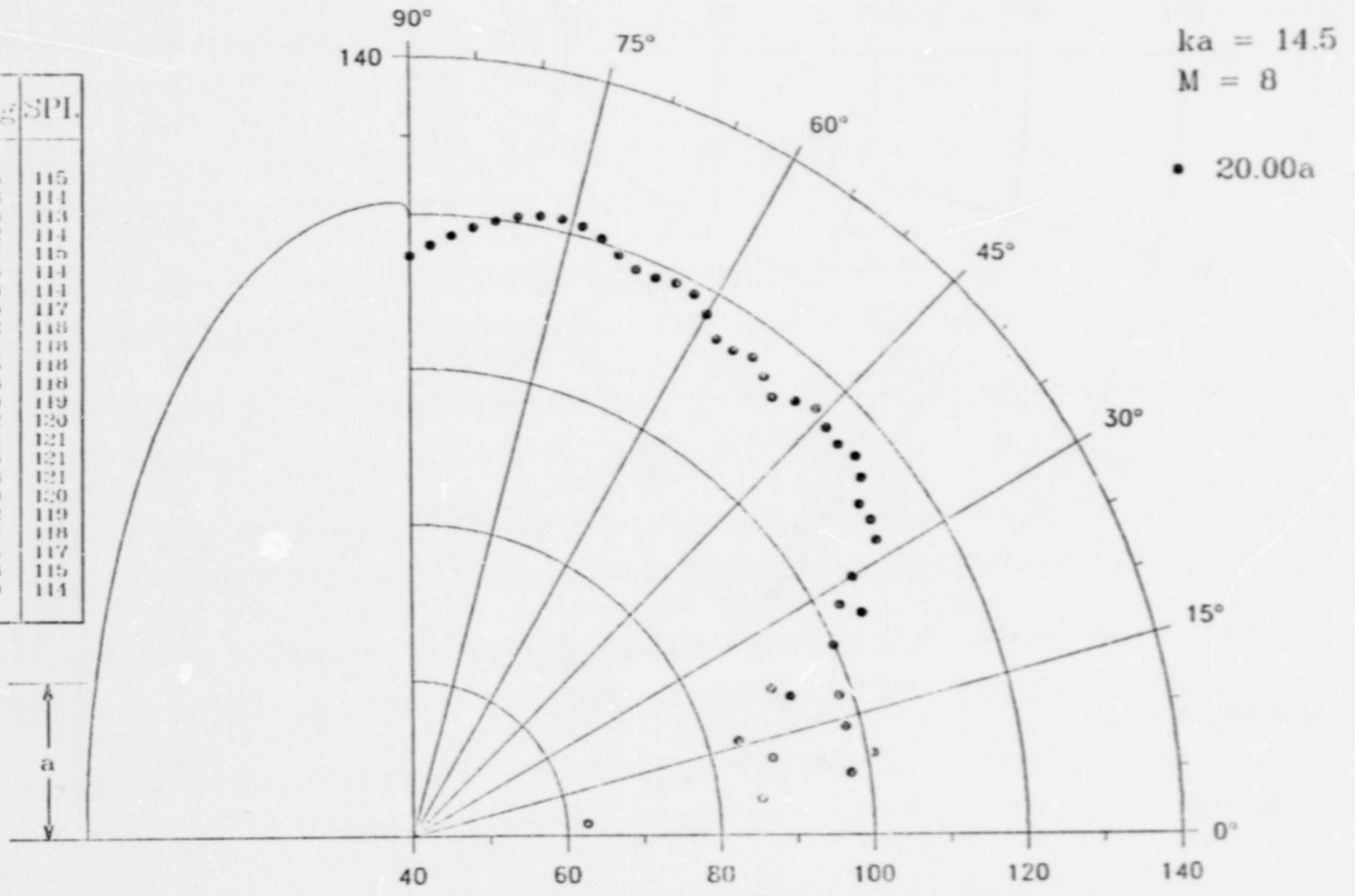

Fig. 92 SPL (dB)

PLANE BAFFLE

Deg	SPL	Deg	SPL
0	0	46	119
2	21	48	120
4	66	50	121
6	87	52	122
8	97	54	123
10	95	56	123
12	93	58	123
14	90	60	124
16	96	62	124
18	91	64	124
20	82	66	124
22	101	68	122
24	104	70	122
26	104	72	122
28	109	74	122
30	111	76	121
32	112	78	121
34	114	80	120
36	114	82	118
38	115	84	117
40	116	86	115
42	116	88	114
44	117	90	112

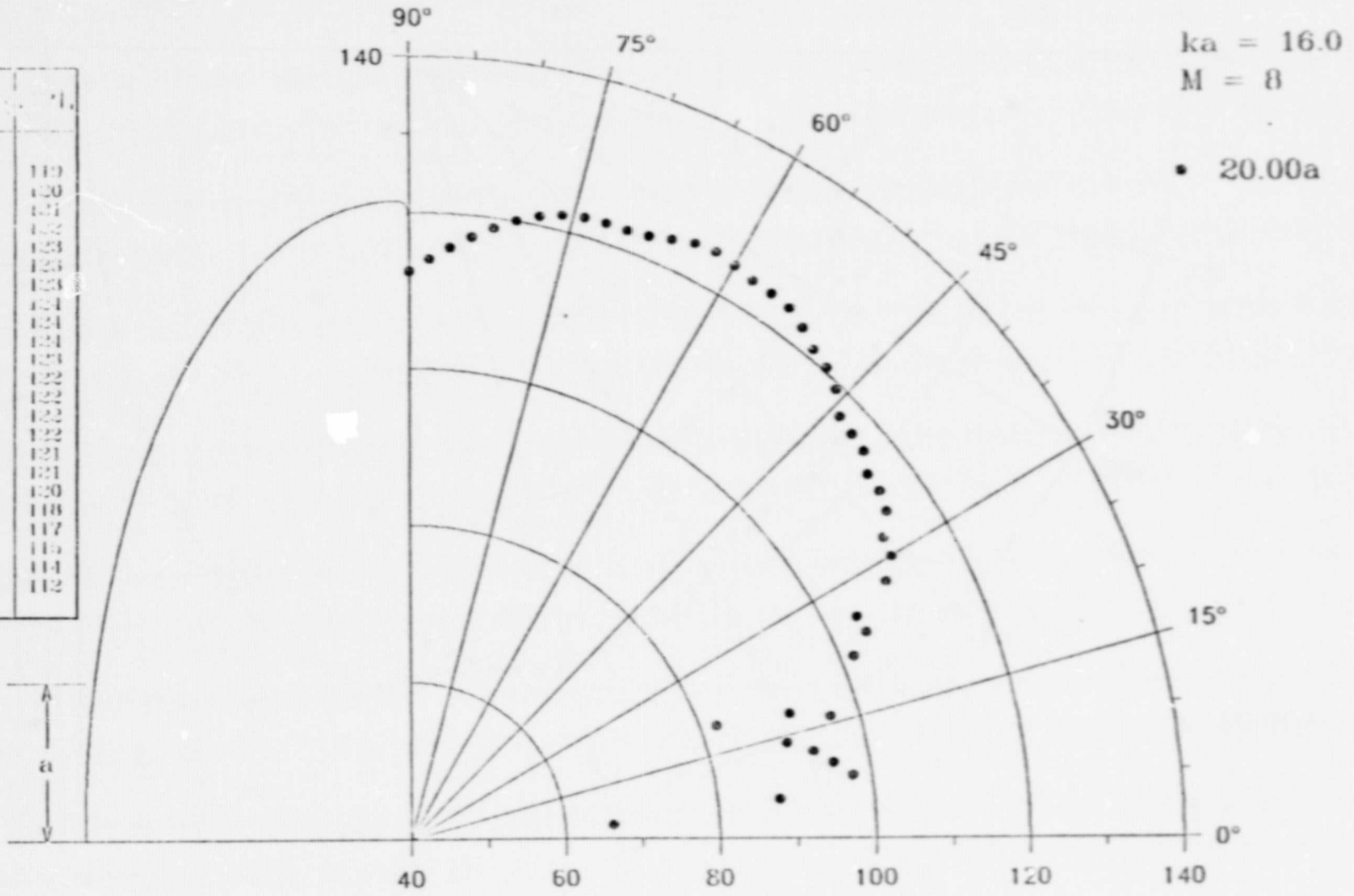

Fig. 93 SPL (dB)

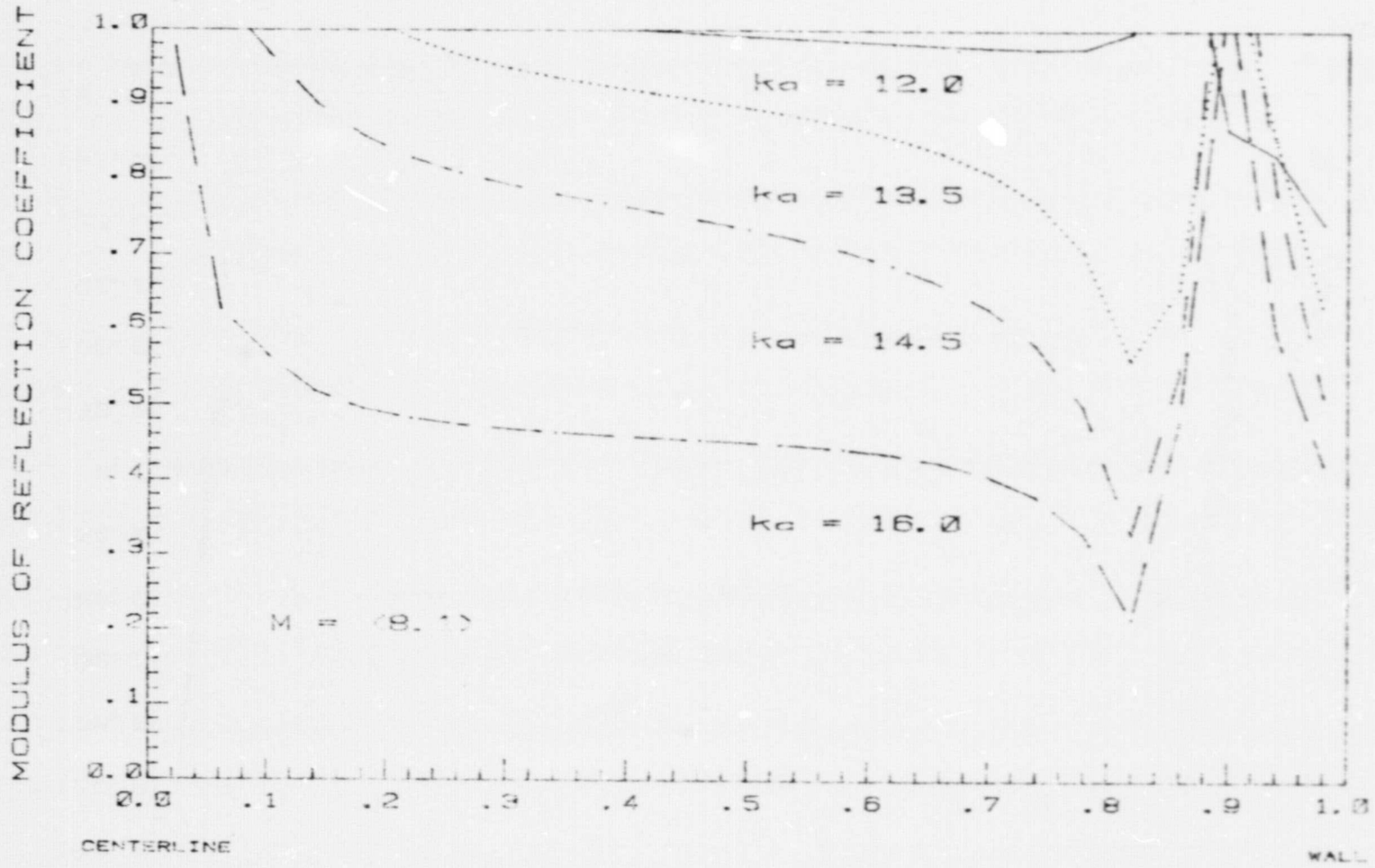

PLANE BAFFLE

Fig. 94

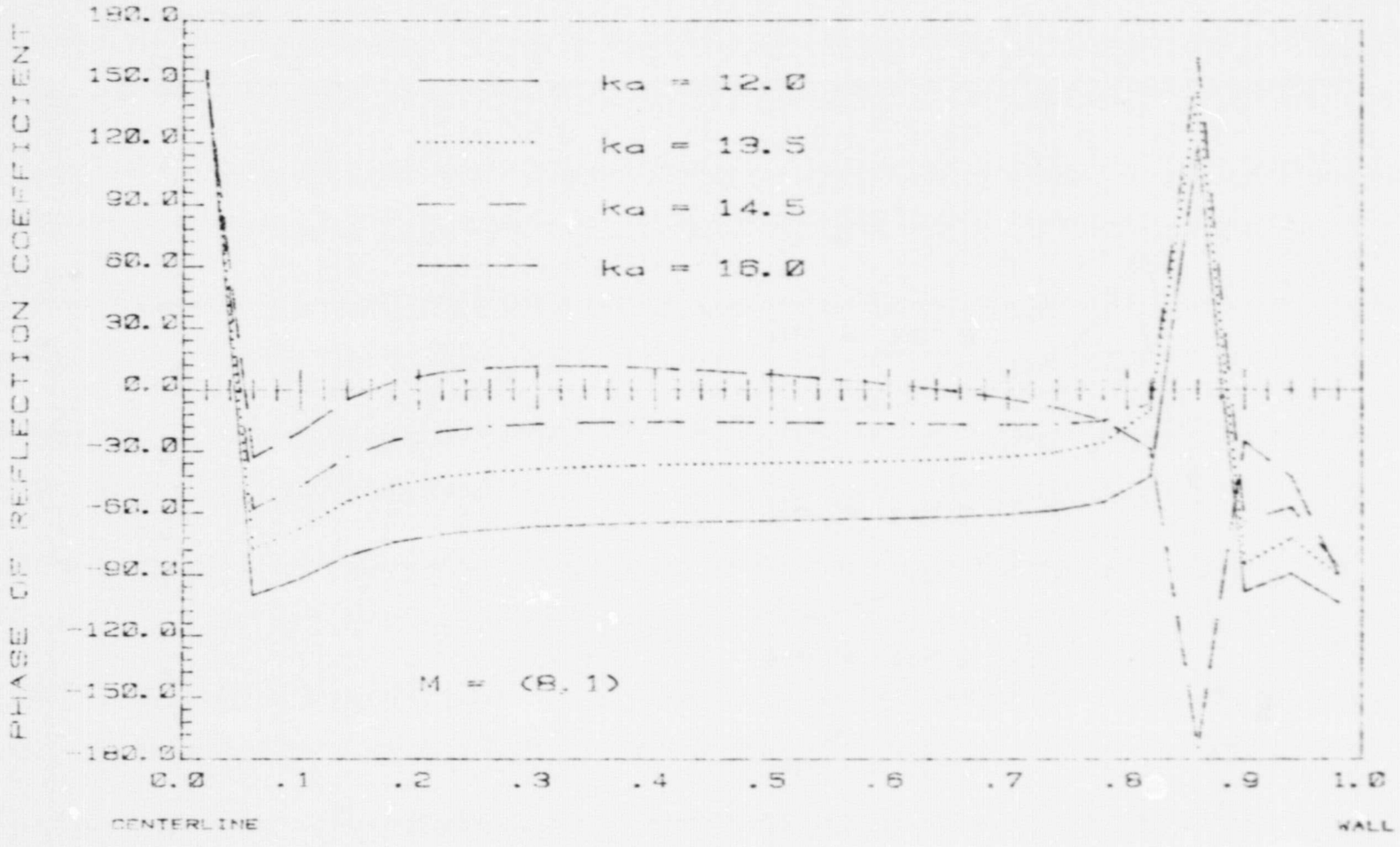

PLANE BAFFLE

Fig. 95

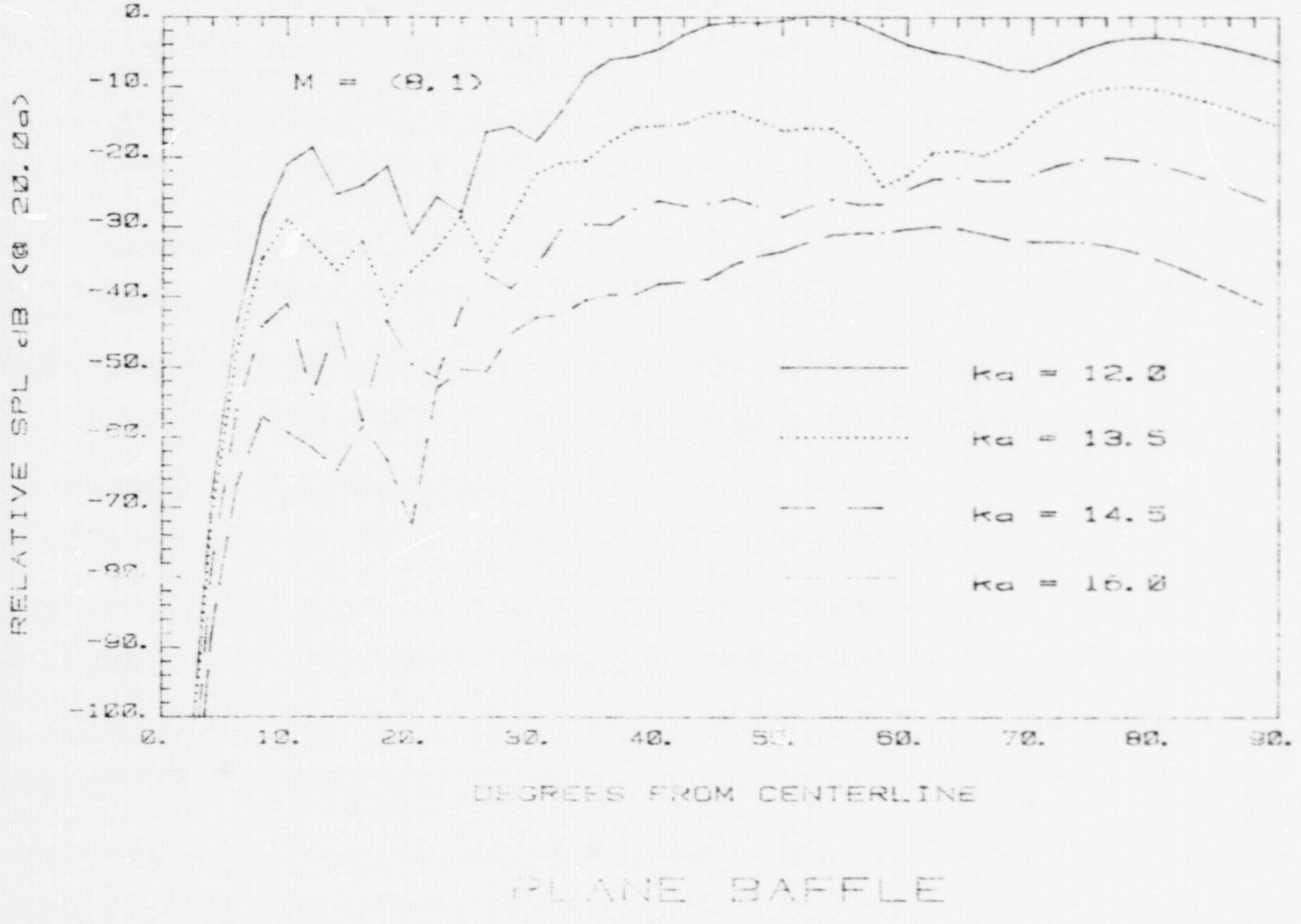
M = (8, 1)
Ka = 12.0
Ka = 13.5
Ka = 14.5
Ka = 16.0
RELATIVE SPL (dB (@ 20.0a)
0.
-10.
-20.
-30.
-40.
-50.
-70.
-90.
-100.
0.
10.
20.
30.
40.
60.
70.
80.
90.
DEGREES FROM CENTERLINE
PLANE BAFFLE

Fig. 96

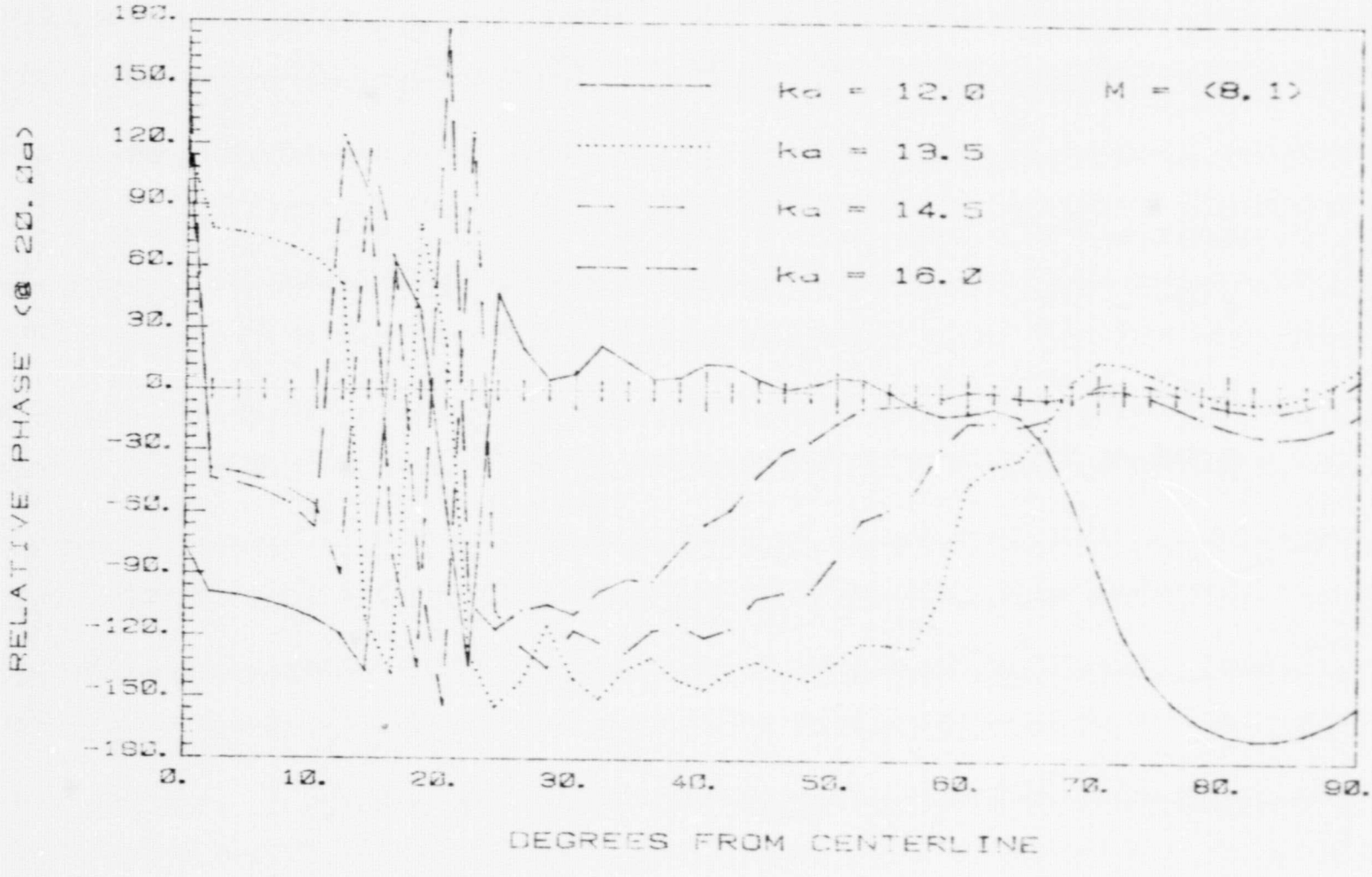
180.
150.
120.
90.
60.
30.
0.
-30.
-60.
-90.
-120.
-150.
-180.
RELATIVE PHASE (@ 20.0a)
ka = 12.0
ka = 13.5
ka = 14.5
ka = 16.2
M = (8.1)
0.
10.
20.
30.
40.
50.
60.
70.
80.
90.
DEGREES FROM CENTERLINE
PLANE BAFFLE

Fig. 97